

QUANTIFYING THE BIOGEOCHEMICAL IMPACT OF LAND PLANT  
EXPANSION IN THE MID DEVONIAN AND IMPLICATIONS IN MARINE  
ANOXIC EVENTS

Matthew Stephen Smart

Submitted to the faculty of the University Graduate School  
in partial fulfillment of the requirements  
for the degree  
Doctor of Philosophy  
in the Department of Earth Sciences,  
Indiana University

December 2022

Accepted by the Graduate Faculty of Indiana University, in partial fulfillment of the requirements for the degree of Doctor of Philosophy.

Doctoral Committee

---

Gabriel Filippelli, Ph.D., Chair

---

William Gilhooly III, Ph.D.

July 28, 2022

---

Andrew Barth, Ph.D.

---

Jeffrey Wilson, Ph.D.

© 2022

Matthew Stephen Smart

## DEDICATION

To my family who always encouraged me to reach for the stars. I hope they are not disappointed that I chose to explore the earth beneath me instead.

## ACKNOWLEDGEMENT

A special thank you to my research committee for guiding me over the years, especially Dr. Gabriel Filippelli for your mentorship and countless hours spent reviewing my draft manuscripts. Thank you also to the multiple undergraduate assistants who contributed greatly to this body of work and my fellow graduate students and post docs who shared their knowledge, time and friendship with me.

Matthew Stephen Smart

QUANTIFYING THE BIOGEOCHEMICAL IMPACT OF LAND PLANT  
EXPANSION IN THE MID DEVONIAN AND IMPLICATIONS IN MARINE  
ANOXIC EVENTS

The evolution of land plant root systems occurred stepwise throughout the Devonian, with the first evidence of complex root systems appearing in the mid-Givetian. This biological innovation provided an enhanced pathway for the transfer of terrestrial phosphorus (P) to the marine system via weathering and erosion. This enhancement is consistent with paleosol records and has led to hypotheses about the causes of marine eutrophication and mass extinctions during the Devonian. To gain insight into the transport of P between terrestrial and marine domains, presented here are geochemical records from a survey of Middle and Late Devonian lacustrine and near lacustrine sequences that span some of these key marine extinction intervals. Root innovation is hypothesized to have enhanced P delivery and results from multiple Devonian sequences from Euramerica show evidence of a net loss of P from terrestrial sources coincident with the appearance of early progymnosperms. Evidence from multiple Middle to Late Devonian sites (from Greenland and northern Scotland/Orkney), reveal a near-identical net loss of P. Nitrogen and Carbon isotopes from a subset of these lakes confirm elevated input of terrestrial plant material concurrent with P perturbations. Terrestrial P input appears to be episodic in nature, suggesting land plant expansion was driven by an external catalyst in the study region.

All sites analyzed are temporally proximal to significant marine extinctions, including precise correlation with the Kačák extinction event and the two pulses associated with the Frasnian-Famennian (F/F) mass extinction. The episodic expansion of terrestrial plants appears to be tied to variations in regional and global climate, and in the case of the F/F extinction, also to atmospheric changes associated with large scale volcanism. Using P data presented here as an input into an Earth system model of the coupled C-N-P-O<sub>2</sub>-S biogeochemical cycles shows that globally scaled riverine phosphorus export during the Frasnian-Famennian mass extinction generates widespread marine anoxia consistent with the geologic record. While timing precludes land plants as an initiating mechanism in the F/F extinction, these results suggest they are implicated in every marine extinction event in the Mid to Late Devonian.

Gabriel Filippelli, Ph.D., Chair

William Gilhooly, Ph.D.

Andrew Barth, Ph.D.

Jeffrey Wilson, Ph.D.

## TABLE OF CONTENTS

List of Tables .....	x
List of Figures.....	xi
List of Abbreviations .....	xii
Chapter 1. Introduction.....	1
1.1 Motivation and Objectives .....	1
1.2 Background.....	3
1.2.1 A CO <sub>2</sub> -Filled World .....	3
1.2.2 The Invasion of Vascular Land Plants.....	4
1.2.3 Devonian Biotic Crises.....	6
1.3 Research Questions, Hypotheses and Significance .....	8
1.4 Research Locations and Geologic Background.....	9
1.5 General Methodology .....	12
1.6 Summary of Findings .....	14
1.7 References .....	15
Chapter 2. Enhanced Terrestrial Nutrient Release During the Devonian Emergence and Expansion of Forests: Evidence from Lacustrine Phosphorus and Geochemical Records .....	23
2.1 Introduction .....	23
2.1.1 Importance of Phosphorus in Biogeochemical Cycling .....	24
2.1.2 The Land Plant Revolution.....	27
2.1.3 Sustainability of a Terrestrial Phosphorus Flush? .....	29
2.2 Materials and Methods .....	31
2.2.1 Site Selection .....	31
2.2.2 Geologic Setting .....	32
2.2.3 Age Constraints .....	35
2.2.4 Sample Preparation and Analysis.....	36
2.3 Results .....	42
2.3.1 Geanies .....	42
2.3.2 Hoxa Head .....	45
2.3.3 Ella Ø.....	47
2.3.4 Heggli Ber.....	48
2.3.5 Heintzbjerg .....	49
2.4 Discussion.....	52
2.4.1 Broad Observations .....	52
2.4.2 Climate and Weathering Interpretations.....	53
2.4.3 Redox Conditions .....	54
2.4.4 Evidence of Enhanced Terrestrial Phosphorus Flux .....	56
2.4.5 Model for Lake Response to Climate and Nutrient Perturbations .....	58
2.4.6 The Land Plant Connection .....	61
2.4.7 Global Implications .....	67
2.5 Conclusions .....	73
2.6 References .....	75
Chapter 3. Land Plant Evolution and Volcanism Led to the Late Devonian Mass Extinction .....	92



3.1 Introduction .....	92
3.2 Enhanced Phosphorus Export During the Late Devonian Mass Extinction.....	96
3.3 Materials and Methods .....	98
3.3.1 P/Al and Phosphorus Accumulation Data .....	98
3.3.2 Earth System Box Model.....	101
3.3.3 Enhanced Terrestrial Nutrient Export Model .....	103
3.3.4 Enhanced Volcanic Activity Model .....	104
3.4 Results and Discussion .....	105
3.5 A Multifaceted Extinction Mechanism .....	111
3.6 References .....	114
Chapter 4. Linking Land Plant Expansion to Episodic Anoxia in a Devonian Lake .....	124
4.1 Introduction .....	124
4.2 Materials and Methods .....	126
4.2.1 Sample Location and Background.....	126
4.2.2 Sample Preparation and Analysis.....	127
4.2.3 Utility of Isotopic and Elemental Data.....	128
4.3 Results .....	132
4.3.1 Isotopic and Elemental Analyses.....	132
4.3.2 Principal Component Analysis – Entire Sequence.....	135
4.3.3 Principal Component Analysis – Lower Geanies.....	137
4.3.4 Principal Component Analysis – Upper Geanies .....	139
4.3.5 Potential Influence on Elemental and Isotopic Data .....	140
4.4 Discussion.....	145
4.4.1 Evidence for the Presence of Vascular Land Plants .....	145
4.4.2 A Multi-proxy Approach.....	146
4.4.3 Integrating Principal Component Analysis .....	154
4.5 Conclusions .....	161
4.6 References .....	162
Chapter 5. Conclusions and Future Study .....	176
5.1 Land Plant Evolution as an Extinction Mechanism .....	176
5.2 Future Study .....	177
5.3 References .....	179
Appendices .....	180
Appendix A .....	180
Appendix B.....	182
Curriculum Vitae	

LIST OF TABLES

Appendix A: Elemental Correlations by Sample Location and Lake Cycle ..... 180  
Appendix B: Phosphorus Accumulation Rates ..... 182

## LIST OF FIGURES

Figure 1.1: Devonian Extinction Events .....	7
Figure 1.2: Area of Study .....	11
Figure 2.1: Sample Sites and Chronology of Significant Devonian Events.....	24
Figure 2.2: Depiction of Phosphorus Transitions with Landscape Evolution.....	26
Figure 2.3: Middle Devonian Stratigraphy.....	34
Figure 2.4: Geochemical Data from Geanies, Easter Ross, Scotland.....	44
Figure 2.5: Geochemical Data from Hoxa Head, South Ronaldsay, Orkney .....	46
Figure 2.6: Geochemical Data from Ella Ø, Greenland .....	47
Figure 2.7: Geochemical Data from Hegglic Ber, Sanday, Orkney .....	49
Figure 2.8: Geochemical Data from Heintzbjerg, Ymer Ø, Greenland.....	51
Figure 2.9: Model for Internal Geochemical Lake Response to Milankovitch-Driven Climatic Fluctuations and Terrestrial Nutrient Flux .....	60
Figure 2.10: Long Term Geochemical Changes Across all Sample Locations.....	70
Figure 3.1: Paleogeographic Reconstruction of the Heintzbjerg Study Location .....	95
Figure 3.2: Orbitally Tuned Heintzbjerg Phosphorus Data.....	97
Figure 3.3: Comparison of Phosphorus Accumulation Rate Estimates .....	101
Figure 3.4: Biogeochemical Dynamics Induced by Elevated Episodes of P Weathering On Land .....	106
Figure 3.5: Biogeochemical Dynamics Induced by Enhanced Volcanic Activity .....	108
Figure 3.6: Changes in Net Primary Production on Land as Predicted by the Enhanced Volcanic Activity Model .....	112
Figure 4.1: Location of the Geanies Sample Site.....	127
Figure 4.2: Results for EA-IRMS Analyses of the Geanies Sequence.....	134
Figure 4.3: Cross Plot of PCA Results for PC1 and PC2 for the Entire Geanies Sequence (Lakes 9-20) .....	136
Figure 4.4: Cross Plot of PCA Results for PC1 and PC2 for the Lower Lakes at Geanies (Lakes 9-13).....	138
Figure 4.5: Cross Plot of PCA Results for PC1 and PC2 for the Upper Lakes at Geanies (Lakes 14-20).....	140
Figure 4.6: Cross Plot of Organic Carbon and Total Nitrogen.....	142
Figure 4.7: Cross Plots of Isotopic Versus Elemental Data for the Geanies Sequence...	143
Figure 4.8: Cross Plot of Organic Carbon Isotope Values and Carbon/Nitrogen Ratios.....	148
Figure 4.9: Combined Plot Featuring Nitrogen and Carbon Isotopic and Elemental Data Combined with Previous Geochemical Data .....	151
Figure 4.10: Cross Plot of PCA Results for C/N Ratio >19.....	159
Figure 4.11: Cross Plot of PCA Results for C/N Ratio < 19 .....	160

## LIST OF ABBREVIATIONS

CAM: Crassulacean Acid Metabolism  
COPSE: Carbon Oxygen Phosphorus Sulfur Evolution Model  
DOA: Degree of Anoxia  
EA: Elemental Analyzer  
EF: Enrichment Factor  
Fm: Formation  
IAEA: International Atomic Energy Agency  
ICP-OES: Inductively Coupled Plasma-Optical Emission Spectrometry  
IRMS: Isotope Ratio Mass Spectrometer  
KW: Kellwasser Event  
kyr: Thousand Years  
LIP: Large Igneous Province  
LKW: Lower Kellwasser Event  
LOWESS: Locally Weighted Scatterplot Smoothing  
Ma: Million Years Ago  
MORS: Middle Old Red Sandstone  
Myr: Million Years  
NPP: Net Primary Production  
P/Me: Phosphorus to Metal Ion Ratio  
PAL: Present Atmospheric Level  
PC: Principal Component  
PCA: Principal Component Analysis  
PDD: Pripyat-Dnieper-Donets LIP  
PPM: Parts Per Million  
TC: Total Carbon  
TIC: Total Inorganic Carbon  
TN: Total Nitrogen  
TOC: Total Organic Carbon  
UKW: Upper Kellwasser Event  
USGS: United States Geologic Survey  
Wt. %: Weight Percent  
XRF: X-ray Fluorescence

## CHAPTER 1. INTRODUCTION

### 1.1. Motivation and Objectives

The Devonian Period marks what is perhaps one of the most critical segments of Earth's past. It was wrought with tremendous biological and ecological change and bounded by dramatic fluctuations in atmospheric composition and multiple marine extinctions. It was during this phase in geologic history that plants developed extensive root systems, diversified and expanded into continental interiors, and modern processes of soil formation were initiated. Prior to the Devonian, continental interiors were relatively bereft of vegetation, save near bodies of water (Algeo et al., 1995). The first vascular land plants only evolved during the Ordovician and it wasn't until the Devonian that Earth's landscape was colonized by the first trees (Algeo et al., 1995; Murphy, 2005). Atmospheric composition also differed greatly, having CO<sub>2</sub> concentrations orders of magnitude greater than modern values (Royer et al., 2007; Franks et al., 2014; Lenton et al., 2016). Indeed, the early Devonian was an Earth one would not readily recognize, but the dynamic changes which occurred to plant life over the roughly 60-million-year span would have significant implications to all life on the planet. The expansion and radiation of land plants during the Devonian brought about one of the most significant changes to the terrestrial biosphere in geologic history. This expansion is thought to have resulted in a tremendous increase in soil development and weathering, initiating contemporary soil formation processes and thus resulting in significant changes to terrestrial and ocean nutrient and carbon cycling (Racki, 2005; Berry and Wang, 2006; Wicander et al., 2011; Stein et al., 2012; Giesen and Berry, 2013; Hao and Xue, 2013;

Carmichael et al., 2014; Berry and Marshall, 2015; Morris et al., 2015; Becker et al., 2016; Lenton et al., 2016). It has been hypothesized that this rapid radiation of land plants drove an unprecedented nutrient flux into Devonian oceans causing eutrophication and the subsequent development of vast anoxic zones characteristic of the period (Algeo et al., 1995; Algeo and Scheckler, 1998). To support this hypothesis and link nutrient-driven eutrophication pulses from land plant expansion to ocean anoxia, attempts have been made in the past utilizing nutrient signals from marine records, however due to profound changes in the marine phosphorus cycle caused by ocean stratification and these large anoxia zones during this period, this approach is problematic (Racki, 2005; Becker et al., 2016). Subsequently, there are still many questions surrounding the role of enhanced phosphorus input to ancient oceans. It is widely agreed that for these vast ocean anoxic zones to form, there had to have been an external eutrophication pulse of some sort (Meyer and Kump, 2008). Thus, to definitively prove the intimate connection between the evolution and expansion of land plants and nutrient loading to ancient oceans, another approach is needed.

Lacustrine sequences have long been used to study nutrient dynamics and can record vital information about weathering, nutrient flux and a host of other important parameters. Although depositional environments vary greatly, lake environments are generally low energy in nature and thus can provide a high-resolution sediment record with fine-scale laminations that can be narrowed down to specific decadal, and even sometimes annual and seasonal, variations. This project will capitalize on the archive-bearing potential in ancient lacustrine sequences to develop land-based measures of phosphorus weathering and mobilization in the Devonian. The aim is to assess the global

role of plant and soil evolution and at last provide the final evidence linking the extraordinary events in the Devonian, the expansion of land plants and the external eutrophication pulse needed to drive the formation of vast ocean anoxic zones. Utilizing these lacustrine and other near-lacustrine sequences, this project aims to test the hypotheses that (1) the expansion, radiation and diversification of land plants in the Devonian is directly linked to terrestrial phosphorus loss which drove extensive environmental change; (2) this phosphorus loss effected measurable changes on lacustrine nitrogen and carbon dynamics; and (3) this phosphorus pulse was not a singular event, but rather dynamic and variable, potentially explaining the multiple eutrophication pulses and subsequent biotic crises in Mid to Late Devonian.

## 1.2. Background

### 1.2.1. A CO<sub>2</sub>-Filled World

Land plants, both vascular and non-vascular, appeared first during the Paleozoic era. The atmospheric composition of the Earth varied drastically during the Paleozoic, and at the dawn of the Devonian the atmospheric composition was quite unlike that of the contemporary world. CO<sub>2</sub> concentration reconstructions from deep time periods largely rely on carbon isotope ratios (<sup>13</sup>C/<sup>12</sup>C) derived from pedogenic carbonates (Cronin, 2010), although these proxies are generally only reliable back through the Devonian (Royer et al., 2004). Due to limitations inherent in using proxies, current records of early Paleozoic climate are very coarse in nature, nevertheless, Royer et al., (2004) estimated global CO<sub>2</sub> concentrations as high as 7000 ppm during the early Cambrian and around

2500 ppm leading into the Devonian, in contrast to pre-industrial levels of 270 ppm (see also Franks et al., 2014). Oxygen concentrations were also quite different than modern-day and were likely much lower at the dawn of the Devonian and only approaching modern levels closer to the Mid to Late Devonian (Lenton et al., 2016). As one can infer from the large concentration of greenhouse gases, the climate of the early Paleozoic was particularly warm; though this may not be a true measure of global climate as there is a hypothesized decoupling of CO<sub>2</sub> and climate during the late Ordovician glaciation (Veizer et al., 2000). The high CO<sub>2</sub> concentration is possibly a result of widespread rifting and volcanism (Martin, 2013), but regardless of the initial cause, CO<sub>2</sub> levels began to rapidly draw down by the end of the Devonian as an unprecedented diversification and radiation of land plants literally changed the face of Earth's continents.

### 1.2.2. The Invasion of Vascular Land Plants

Beginning with the Cambrian explosion, the Paleozoic is marked by a vast increase in the complexity of earth's biosphere, particularly in the marine realm. This diversification included plankton, benthos and nekton as well as a general increase in complexity of food webs and the eventual appearance of large predators (Martin, 2013). Most relevant to the topic of nutrient dynamics of the period, was the evolution of semi-aquatic and terrestrial tracheophytes, or vascular plants, first appearing in the middle Ordovician (Murphy, 2005). What little terrestrial vegetation existed prior to this was confined to low-lying plants inhabiting the water-land interface (Algeo et al., 1995; Murphy, 2005). By the middle to late Devonian, land plants began to diversify and spread into continental interiors and uplands, populating a once mostly empty landscape with



vegetation (Algeo et al., 1995; Algeo and Scheckler, 1998; Piombino, 2016). The diversification and expansion of plants led to the first appearance of trees (arborescence) and the widespread propensity of plants to produce seeds (Algeo et al., 1995). The earliest of these trees appeared in the Eifelian and looked very little like contemporary trees (Giesen and Berry, 2013). The most notable, due to its size and significant root structure, of these early trees was *Archaeopteris*, a large progymnosperm which grew up to 30m in height (Algeo et al., 1995). Although not a seed-bearing plant, *Archaeopteris* was the dominant large plant until well into the Late Devonian when it was displaced by the more advanced seed-bearing plants which proliferated towards the end of the Famennian (Algeo et al., 1995). Occurring simultaneously with the expansion of land plants was the development of extensive root systems. The earliest evidence of roots associated with vascular land plants appeared in late Pragian, or Early Devonian, but were primitive in comparison to modern root systems (Algeo et al., 2001; Algeo and Scheckler, 1998). More substantial root systems did not appear until the Mid to Late Devonian and were generally associated with species such as *Archaeopteris* (Algeo et al., 2001; Algeo and Scheckler, 1998). Whereas prior to the Devonian there existed primarily shallow root structures and thus, only minimal soil development (Algeo et al., 2001; Algeo and Scheckler, 1998), these species were likely long-lived and thus established significant soil profiles and would have had a measurable impact on local biogeochemical cycling and resultant nutrient loads into the oceans. Indeed, many studies have shown that roots dramatically alter soil formation, and thus the soil biogeochemistry (e.g., Filippelli and Souch, 1999; Filippelli, 2008). The development of extensive root systems, stress-resistant seeds and an overall increase in size subsequently contributed to the

expansion of land plants into continental interiors and uplands (Algeo and Scheckler, 2010). The vast increase in land plants played a critical role in the drawdown of atmospheric CO<sub>2</sub> through photosynthesis and has also been linked to increased rates of silicate rock weathering by increasing soil residence times (Algeo et al., 1995; Algeo and Scheckler, 1998; Berry and Marshall, 2015; Murphy, 2005). Furthermore, this expansion likely led to vastly increased nutrient export to the oceans of the Period, potentially driving algal blooms and subsequently anoxia (Algeo et al., 1995; Algeo and Scheckler, 1998; Algeo and Scheckler, 2010; Falkowski et al., 2011).

### 1.2.3. Devonian Biotic Crises

Although the Devonian is characterized as a rather profound period for biological evolution and diversity, it is also known for numerous extinction events (Fig. 1.1). The first of which, the Choteč Event, occurred in the early Eifelian and the first extinction event with associated widespread marine anoxia that would later become a Devonian hallmark (House, 2002; Vodráčková et al., 2012; Becker et al., 2020). At the Eifelian/Givetian boundary was the Kačák event, a smaller extinction affecting mostly marine invertebrates, but also characterized by black shale formations characteristic of marine anoxia (House, 1985; House, 2002; Marshall et al., 2016; Becker et al., 2020). The Taghanic Event (also known as the Taghanic Crisis, among other names), occurred in three distinct phases, but was characterized by only local anoxic events rather than widespread and global anoxia found in other Devonian events (House, 1985; House, 2002; Aboussalam and Becker, 2011; Marshall et al., 2011; Becker et al., 2020). Finally, in the Late Devonian occurred two of the most biologically catastrophic events in Earth's

history, both significantly impacting the marine realm. The first of which was the Kellwasser Event (alternatively called the Late Devonian extinction or Frasnian-Famennian extinction). It is considered one of Earth’s “Big Five” mass extinctions and was characterized by a decrease of up to 40% of marine species families and 60% of genera and occurred at the Frasnian-Famennian boundary, about 374 Ma (Sallan and Coates, 2010; Becker et al., 2016; Percival et al., 2018; Da Silva et al, 2020). The second,

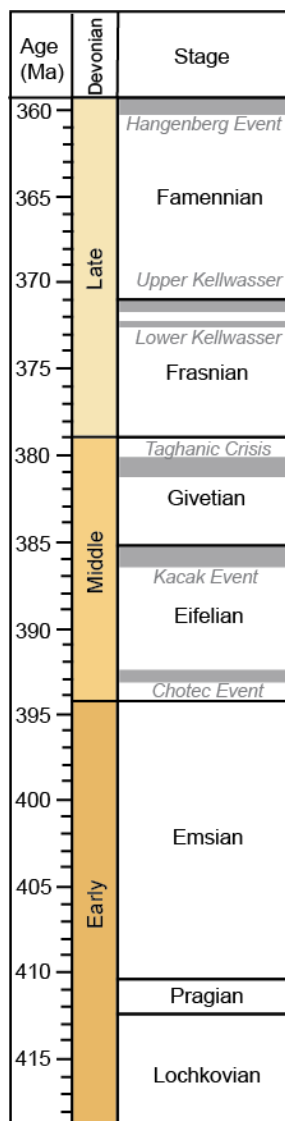


Figure 1.1. Distribution of significant extinction events in the Devonian characterized by either local or widespread ocean anoxia (House, 1985; House, 2002; Becker et al., 2016; Becker et al., 2020). Timescale utilized is from Becker et al., 2020.

and the smaller of the two, the Hangenberg event occurred about 15 million years later at the Devonian-Carboniferous boundary (House, 1985; House, 2002; Sallen and Coates, 2010; Becker et al., 2016; Becker et al., 2020). The Hangenberg event has been studied far less than the Kellwasser event, but it is estimated that this extinction event resulted in the loss of 50% of vertebrate species diversity in both the marine and non-marine realms (Sallen and Coates, 2010; Becker et al., 2016). While some of these above events had terrestrial extinction components, they were all primarily marine catastrophes. However, a common theme tying every one of these Devonian extinctions is the characteristic deposition of black shales indicative of ocean anoxia.

### 1.3. Research Questions, Hypotheses and Significance

Many questions remain regarding terrestrial phosphorus dynamics in the Devonian. Not least of these is the timing of terrestrial land plant proliferation as well as the magnitude and timing of associated nutrient release. Specifically, questions remain regarding how long weathering changes occurred during terrestrialization, quantification of phosphorus flux from land to ocean and the global extent of this flux. In addition to questions regarding the phosphorus dynamics during this critical period, there has yet to be sufficient work done on the coupling of phosphorus with nitrogen and carbon dynamics during soil development. Finally, there have not been sufficient studies exploring the overall mass balance of nutrient weathering and subsequent export to the oceans.

This project aims to address these shortcomings and perhaps finally answer many of these long-standing questions. Whereas previous work has centered around studying

marine sediments to infer information on terrestrial nutrient flux, lacustrine sequences may be able to provide a far more unambiguous record of these events. Thus, it is hypothesized that a temporal record of soil phosphorus transformations can be resolved utilizing such lacustrine sequences from the Mid to Late Devonian and can provide; evidence either supporting or refuting the following hypotheses:

- a. Colonization of continental interiors and subsequent root development was directly tied to terrestrial phosphorus loss, resulting in ecosystem instability and potentially driving biotic crises associated with the Late and End Devonian.
  
- b. Land plant-driven transformations in the terrestrial phosphorus cycle also impacted nitrogen and carbon dynamics within lacustrine systems.
  
- c. Unlike current theories which favor a simplistic roots-off, roots-on approach, the net mobilization and subsequent export of phosphorus from terrestrial landscapes was variable in light of ecosystem dynamics, thus explaining the multiple eutrophication pulses seen in late/end Devonian

#### 1.4. Research Locations and Geologic Background

The Devonian is temporally located in the Mid Paleozoic Era and spans a period between approximately 419 million years ago (Ma) and 355 Ma. It is bounded by periods of significant climatological, geological, biological and ecological changes. During the early stages of the Paleozoic, the planet was dominated by the supercontinent Gondwana

(Martin, 2013). Through the Cambrian and Ordovician, rifting began to tear apart Gondwana, with the resulting land masses drifting apart but primarily remaining in the southern hemisphere (Martin, 2013). This rifting also resulted in the creation of multiple ocean basins interconnecting the remnants of Gondwana (Martin, 2013). Seafloor spreading centers associated with rifting began to displace large volumes of water, gradually pushing it onto the local continents and creating large epicontinental seas in the continental interiors (Martin, 2013). These events resulted in a marine environment in the Devonian dramatically different than that of today. The vast epicontinental seas were characterized by widespread bottom anoxia and large rates of organic carbon burial (Algeo and Scheckler, 2010). This anoxia and subsequent carbon burial resulted in the formation of Devonian black shales, formations common in the mid to late Devonian (Tuite and Macko, 2013).

It is within this general geologic backdrop that the areas of study reside, the Orcadian Basin and the Devonian Basin in East Greenland (Fig. 1.2). Throughout much of the Devonian, the Orcadian Basin was the site of a large lake occupying what is now modern-day Scotland and the Moray Firth (a large inlet in the North Sea in northeastern Scotland) and extending as far north as the Shetland Islands (Fig. 1.2). Most of the deposits in this region belong to the Caithness Flagstone lithostratigraphic group laid down during the Eifelian and contain mostly mudstone-limestones, siltstones and sandstones (Donovan et al., 1974). The Caithness Flagstone Group is itself part of a larger outcrop known as Old Red Sandstone, which is comprised of lower, middle and upper subgroups. Sediments from the Caithness Flagstone Group make up the Middle Old Red Sandstone (MORS). Although mainly lacustrine in origin, the MORS also

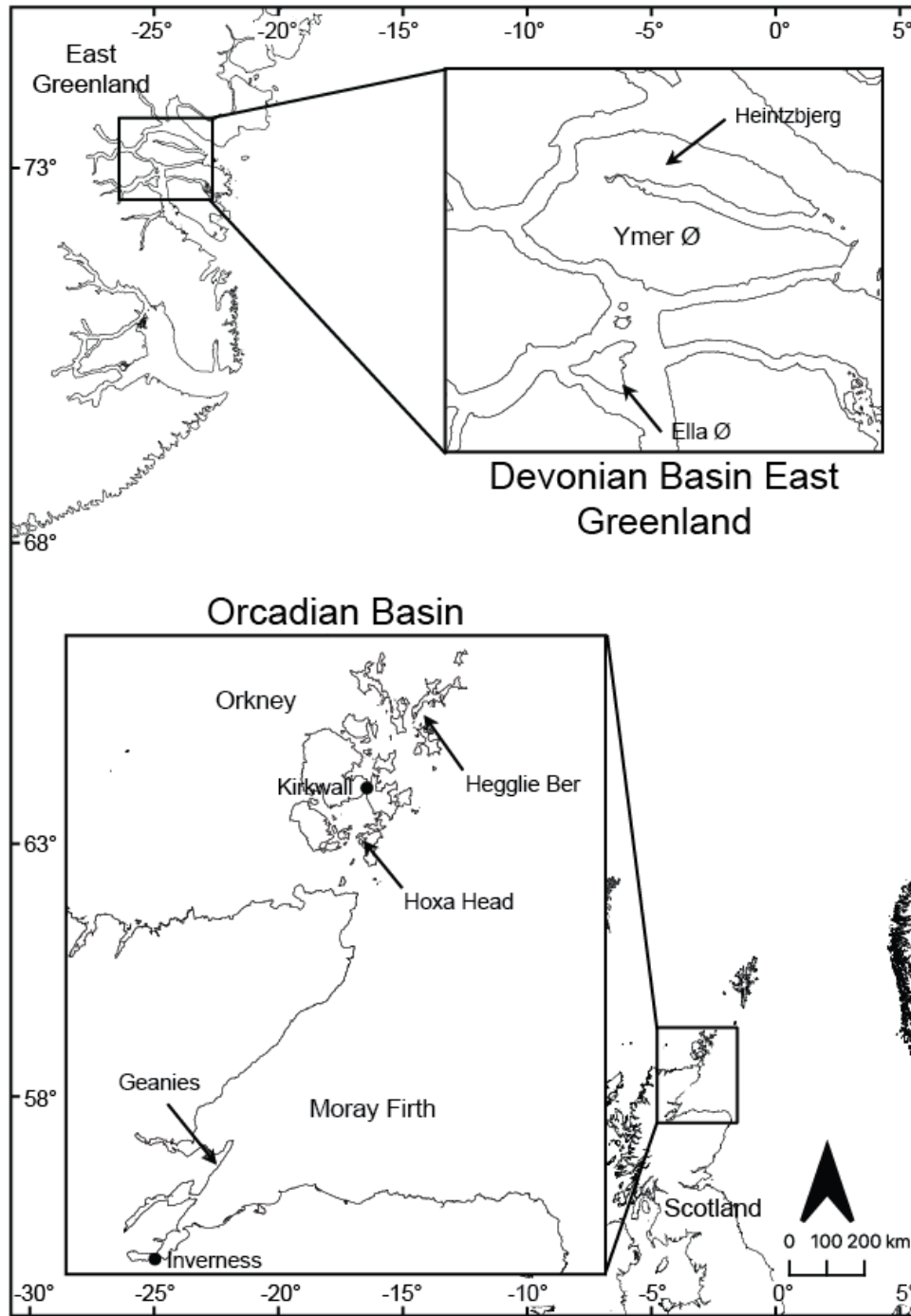


Figure 1.2. Location of study area in the Devonian Basin in East Greenland and the Orcadian Basin in Northern Scotland/Orkney and the Moray Firth. Selected study sites are marked with arrows and will be discussed in later sections.

contains fluvial sandstones and conglomerates near the margins of the Orcadian Basin and hosts several fossil fish beds which have been used to help constrain the age of the

sequences (Andrews and Hartley, 2015; Johnstone and Mykura, 1989; Trewin and Thirlwall, 2002). Although there are numerous Devonian lacustrine sequences throughout the globe, the Orcadian Basin is perhaps one of the most thoroughly studied considering its proximity to rich hydrocarbon resources in the North Sea (Stephenson et al., 2006). The Devonian Basin in East Greenland is similar in many respects and formed under similar conditions as the Orcadian Basin (McClay et al., 1986; Marshall and Stephenson, 1997; Trewin and Thirlwall, 2002). Both basins contain numerous lakes which formed in extensional basins resulting from the collapse of overthickened crust associated with the Caledonian orogen (McClay et al., 1986). Their paleolatitude was approximately between 20°S and 30°S and in an arid to semi-arid region (Andrews and Hartley, 2015; Tarling, 1985). Perhaps most significantly, although both areas saw many phases of transgression and regression throughout their existence as lacustrine basins (most likely due to climatic forcings), in general the depositional environment is characterized as low energy, ripe with fine-grained facies providing the potential for high resolution data collection and analyses (Andrews and Hartley, 2015).

### 1.5. General Methodology

This study utilizes a multi-tiered approach to analyze both terrestrial and lacustrine nutrient dynamics (P/N/C). To present the strongest possible data to support the study, lacustrine sequences from multiple sites within each of the study basins are utilized. These study sites cover a span of approximately 15 Myr beginning in the Eifelian and continuing into the Famennian. At each location, the terrestrial weathering history of P in relation to other weathering proxies was determined. The role that



dissolved P input to lacustrine systems had on C and N cycling in the mid-late Devonian as well as the quantification of P mobilization from land and export to marine systems was also studied. More specifically, the research is broken into four main objectives:

a. Characterization of P weathering dynamics based on temporal records of P in lacustrine sediments (Ch. 2). This was accomplished through sequential extraction analysis of P geochemical fractions in lacustrine sediments, total digestion analysis of P normalized to refractory components (such as P/Ti, P/Al), and total digestion analysis of P normalized to labile and active soil components (such as P/Ca, P/Fe).

b. Multi-proxy analyses to address redox cycling within Devonian lacustrine systems, chemical weathering extent, physical weathering extent and climate variations (Ch. 2). This was accomplished primarily through x-ray fluorescence analysis and involved the comparison of numerous elemental ratios utilized for chemical weathering, physical weathering and climate.

c. Determination of P weathering changes over time. P loss due to weathering was estimated for each outcrop sampled and the timing compared between outcrops. P loss values were then used as variable inputs in an Earth system model of the coupled C-N-P-O<sub>2</sub>-S biogeochemical cycles in order to evaluate whether recorded changes to P fluxes would be adequate to sustain Devonian marine biogeochemical perturbations and extinction dynamics (Ch. 3).

d. Quantification of N and C cycle dynamics during soil formation (Ch 4). This included N and C isotopic analyses of organic matter in lacustrine sequences to provide insight into nutrient dynamics in paleo-lacustrine systems and serve as a further tracer of terrestrial organic matter input into such systems.

#### 1.6. Summary of Findings

Evidence from multiple Middle to Late Devonian sites from Greenland and northern Scotland/Orkney reveal an episodic and near identical net loss of P over the entire 15 Myr study period. Additionally, while all study sites are temporally proximal to one or more Devonian extinction events, net loss of P was noted in precise correlation with the Kačák extinction event, and the two pulses associated with the Frasnian/Famennian mass extinction. Unexpectedly, weathering, climate and redox proxy data coupled with nutrient input variability for all sites reveal similar geochemical responses as seen in extant lacustrine systems. It is likely that orbitally forced climatic cyclicity was the catalyst for all significant terrestrial nutrient pulses, suggesting expansion of terrestrial plants may be tied to variations in regional and global climate. These conclusions are further reinforced based on results of C and N elemental and isotopic analyses for a series of late Eifelian lakes in the Orcadian Basin which confirm elevated input of terrestrial land plant derived organic matter concurrent with the largest episodes of P weathering. Using these episodes of P weathering as variable inputs in an Earth system model of the coupled C-N-P-O<sub>2</sub>-S biogeochemical cycles, globally scaled riverine P export during the Kellwasser Event generates widespread marine anoxia and produces C isotope, temperature, O<sub>2</sub>, and CO<sub>2</sub> perturbations generally consistent with the

geologic record. These results implicate land plant evolution and expansion in at least two of the marine extinction events in the Devonian, but leave open the possibility that they were directly involved in all of them.

### 1.7. References

Aboussalam, Z. S., & Becker, R. T. (2011). The global Taghanic Biocrisis (Givetian) in the eastern Anti-Atlas, Morocco. *Palaeogeography, Palaeoclimatology, Palaeoecology*, 304(1-2), 136-164.

Algeo, T. J., Berner, R. A., Maynard, J. B., & Scheckler, S. E. (1995). Late Devonian oceanic anoxic events and biotic crises: “rooted” in the evolution of vascular land plants. *GSA today*, 5(3), 45-66.

Algeo, T. J., & Scheckler, S. E. (1998). Terrestrial-marine teleconnections in the Devonian: links between the evolution of land plants, weathering processes, and marine anoxic events. *Philosophical Transactions of the Royal Society B: Biological Sciences*, 353(1365), 113-130.

Algeo, T. J., Scheckler, S. E., & Maynard, J. B. (2001). Effects of the Middle to Late Devonian spread of vascular land plants on weathering regimes, marine biotas, and global climate. *Plants invade the land: evolutionary and environmental perspectives*. Columbia University Press, New York, 213-236.

Algeo, T. J., & Scheckler, S. E. (2010). Land plant evolution and weathering rate changes in the Devonian. *Journal of Earth Science*, 21(1), 75-78.

Andrews, S. D., & Hartley, A. J. (2015). The response of lake margin sedimentary systems to climatically driven lake level fluctuations: Middle Devonian, Orcadian Basin, Scotland. *Sedimentology*, 62(6), 1693-1716.

Becker, R. T., Königshof, P., & Brett, C. E. (2016). Devonian climate, sea level and evolutionary events: an introduction. Geological Society, London, Special Publications, 423(1), 1-10.

Becker, R. T., Marshall, J. E. A., Da Silva, A. C., Agterberg, F. P., Gradstein, F. M., & Ogg, J. G. (2020). The Devonian Period. In *Geologic time scale 2020* (pp. 733-810). Elsevier.

Berry, C. M., & Wang, Y. (2006). A new plant attributed to Cladoxylopsida from the Middle Devonian of Yunnan Province, China. *Review of Palaeobotany and Palynology*, 142(3-4), 63-78.

Berry, C. M., & Marshall, J. E. (2015). Lycopsid forests in the early Late Devonian paleoequatorial zone of Svalbard. *Geology*, 43(12), 1043-1046.

Carmichael, S. K., Waters, J. A., Suttner, T. J., Kido, E., & DeReuil, A. A. (2014). A new model for the Kellwasser Anoxia Events (Late Devonian): shallow water anoxia in an open oceanic setting in the Central Asian Orogenic Belt. *Palaeogeography, Palaeoclimatology, Palaeoecology*, 399, 394-403.

Cronin, T. M. (2010). *Paleoclimates: Understanding climate change past and present*. New York, NY: Columbia University Press.

Da Silva, A. C., Sinnesael, M., Claeys, P., Davies, J. H., de Winter, N. J., Percival, L. M. E., ... & De Vleeschouwer, D. (2020). Anchoring the Late Devonian mass extinction in absolute time by integrating climatic controls and radio-isotopic dating. *Scientific reports*, 10(1), 1-12.

Donovan, R N, Foster, R J and Westoll, T S, 1974. A stratigraphical revision of the Old Red Sandstone of north-eastern Caithness. *Transactions of the Royal Society of Edinburgh*, Vol.69, p.167-201.

Franks, P. J., Royer, D. L., Beerling, D. J., Van de Water, P. K., Cantrill, D. J., Barbour, M. M., & Berry, J. A. (2014). New constraints on atmospheric CO<sub>2</sub> concentration for the Phanerozoic. *Geophysical Research Letters*, 41(13), 4685-4694.

Falkowski, P. G., Algeo, T., Codispoti, L., Deutsch, C., Emerson, S., Hales, B., ... & Pilcher, C. B. (2011). Ocean deoxygenation: past, present, and future. *Eos, Transactions American Geophysical Union*, 92(46), 409-410.

Filippelli, G. M., & Souch, C. (1999). Effects of climate and landscape development on the terrestrial phosphorus cycle. *Geology*, 27(2), 171-174.

Filippelli, G. M. (2008). The global phosphorus cycle: past, present, and future. *Elements*, 4(2), 89-95.

Giesen, P., & Berry, C. M. (2013). Reconstruction and growth of the early tree Calamophyton (Pseudosporochnales, Cladoxylopsida) based on exceptionally complete specimens from Lindlar, Germany (Mid-Devonian): organic connection of Calamophyton branches and Duisbergia trunks. *International Journal of Plant Sciences*, 174(4), 665-686.

Hao, S., & Xue, J. (2013). The early Devonian Posongchong flora of Yunnan: a contribution to an understanding of the evolution and early diversification of vascular plants. Science Press.

House, M. R. (2002). Strength, timing, setting and cause of mid-Palaeozoic extinctions. *Palaeogeography, Palaeoclimatology, Palaeoecology*, 181(1-3), 5-25.

House, M. R. (1985). Correlation of mid-Palaeozoic ammonoid evolutionary events with global sedimentary perturbations. *Nature*, 313(5997), 17-22.

Johnstone, G. S., & Mykura, W. (1989). Old Red Sandstone, Northern Highlands of Scotland. Retrieved from [http://earthwise.bgs.ac.uk/index.php/Old\\_Red\\_Sandstone,\\_Northern\\_Highlands\\_of\\_Scotl](http://earthwise.bgs.ac.uk/index.php/Old_Red_Sandstone,_Northern_Highlands_of_Scotl) and

Lenton, T. M., Dahl, T. W., Daines, S. J., Mills, B. J., Ozaki, K., Saltzman, M. R., & Porada, P. (2016). Earliest land plants created modern levels of atmospheric oxygen. *Proceedings of the National Academy of Sciences*, 113(35), 9704-9709.

Marshall, J. E. A., & Stephenson, B. J. (1997). Sedimentological responses to basin initiation in the Devonian of East Greenland. *Sedimentology*, 44(3), 407-419.

Marshall, J. E., Brown, J. F., & Astin, T. R. (2011). Recognising the Taghanic Crisis in the Devonian terrestrial environment and its implications for understanding land–sea interactions. *Palaeogeography, Palaeoclimatology, Palaeoecology*, 304(1-2), 165-183.

Marshall, J. E. A. (2016). Palynological calibration of Devonian events at near-polar palaeolatitudes in the Falkland Islands, South Atlantic. Geological Society, London, *Special Publications*, 423(1), 25-44.

Martin, R. (2013). *Earth's Evolving Systems: The History of Planet Earth*. Burlington, MA: Jones and Bartlett Learning.

McClay, K.R., Norton, M.G. and Coney, P. (1986) Collapse of the Caledonian orogen and the Old Red Sandstone. *Nature*, 323, 147–149.

Meyer, K. M., & Kump, L. R. (2008). Oceanic euxinia in Earth history: causes and consequences. *Annual Review of Earth and Planetary Sciences*, 36(1), 251-288.

Morris, J. L., Leake, J. R., Stein, W. E., Berry, C. M., Marshall, J. E., Wellman, C. H., ... & Beerling, D. J. (2015). Investigating Devonian trees as geo-engineers of past climates: linking palaeosols to palaeobotany and experimental geobiology. *Palaeontology*, 58(5), 787-801.

Murphy, D. C. (2005, July 9). Plants and Soils. Retrieved November 12, 2016, from <http://devoniantimes.org/opportunity/soils.html>

Percival, L. M., Davies, J. H., Schaltegger, U., De Vleeschouwer, D., Da Silva, A. C., & Föllmi, K. B. (2018). Precisely dating the Frasnian–Famennian boundary: implications for the cause of the Late Devonian mass extinction. *Scientific reports*, 8(1), 1-10.

Piombino, A. (2016). The heavy links between geological events and vascular plants evolution: a brief outline. *International Journal of Evolutionary Biology*, 2016.



Racki, G. (2005). Toward understanding Late Devonian global events: few answers, many questions. In *Developments in Palaeontology and Stratigraphy* (Vol. 20, pp. 5-36). Elsevier.

Royer, D. L., Berner, R. A., & Park, J. (2007). Climate sensitivity constrained by CO<sub>2</sub> concentrations over the past 420 million years. *Nature*, 446(7135), 530-532.

Royer, D. L., Berner, R. A., Montañez, I. P., Tabor, N. J., & Beerling, D. J. (2004). CO<sub>2</sub> as a primary driver of Phanerozoic climate. *GSA Today*, 14(3), 4-10.

Sallan, L. C., & Coates, M. I. (2010). End-Devonian extinction and a bottleneck in the early evolution of modern jawed vertebrates. *Proceedings of the National Academy of Sciences*, 107(22), 10131-10135.

Stein, W. E., Berry, C. M., Hernick, L. V., & Mannolini, F. (2012). Surprisingly complex community discovered in the mid-Devonian fossil forest at Gilboa. *Nature*, 483(7387), 78-81.

Stephenson, M. H., Leng, M. J., Michie, U., & Vane, C. H. (2006). Palaeolimnology of Palaeozoic lakes, focusing on a single lake cycle in the Middle Devonian of the Orcadian Basin, Scotland. *Earth-Science Reviews*, 75(1-4), 177-197.

Tarling, D. H. (1985). Palaeomagnetic studies of the Orcadian Basin. *Scottish Journal of Geology*, 21(3), 261-273.

Trewin, N.H. and Thirlwall, M.F. (2002) Old Red Sandstone. In: *The Geology of Scotland* (Ed. N.H. Trewin), pp. 213–249. The Geological Society, London.

Tuite Jr, M. L., & Macko, S. A. (2013). Basinward nitrogen limitation demonstrates role of terrestrial nitrogen and redox control of  $\delta^{15}\text{N}$  in a Late Devonian black shale. *Geology*, 41(10), 1079-1082.

Veizer, J., Godderis, Y., & François, L. M. (2000). Evidence for decoupling of atmospheric  $\text{CO}_2$  and global climate during the Phanerozoic eon. *Nature*, 408(6813), 698.

Vodrážková, S., Frýda, J., Suttner, T. J., Koptíková, L., & Tonarová, P. (2013). Environmental changes close to the Lower–Middle Devonian boundary; the Basal Choteč Event in the Prague Basin (Czech Republic). *Facies*, 59(2), 425-449.

Wicander, R., Clayton, G., Marshall, J. E. A., Troth, I., & Racey, A. (2011). Was the latest Devonian glaciation a multiple event? New palynological evidence from Bolivia. *Palaeogeography, Palaeoclimatology, Palaeoecology*, 305(1-4), 75-83.

CHAPTER 2. ENHANCED TERRESTRIAL NUTRIENT RELEASE DURING  
THE DEVONIAN EMERGENCE AND EXPANSION OF FORESTS:  
EVIDENCE FROM LACUSTRINE PHOSPHORUS AND GEOCHEMICAL  
RECORDS

2.1. Introduction

The Devonian was a watershed moment in Earth history, with substantial changes in biologic, ecologic, and atmospheric conditions. The expansion and radiation of land plants occurred on an unprecedented scale during this period (Algeo et al., 1995; Stein et al., 2012; Giesen and Berry, 2013; Berry and Marshall, 2015; Morris et al., 2015; Lenton et al., 2016; Stein et al., 2020; Davies et al., 2021). Coincident with this emergent terrestrial biosphere, the Devonian hosted numerous marine extinction events (Fig. 2.1), including the Late Devonian mass extinction, one of the “big five” with the loss of ~40% of marine families and 60% of genera (McGhee, 1996). Additionally, the Devonian saw a pronounced decrease in atmospheric CO<sub>2</sub> to near contemporary levels (Lenton et al., 2016). Despite these key biological innovations and planetary transitions, much is still unknown about the specific feedbacks within the Devonian ecosphere, particularly with respect to the export of plant-mobilized nutrients, such as phosphorus (P), from the terrestrial to the marine realm. Whereas it is generally accepted that the colonization of land plants and the evolution of roots would have had a marked impact on nutrient weathering, the magnitude, timing, and duration of these impacts have yet to be defined. Such insights are critical to putting together all the pieces of the Devonian puzzle, particularly as terrestrial events such as the expansion and radiation of land plants have

been implicated in the marine extinctions which occurred throughout the Period (Algeo et al., 1995; Algeo and Scheckler, 1998).

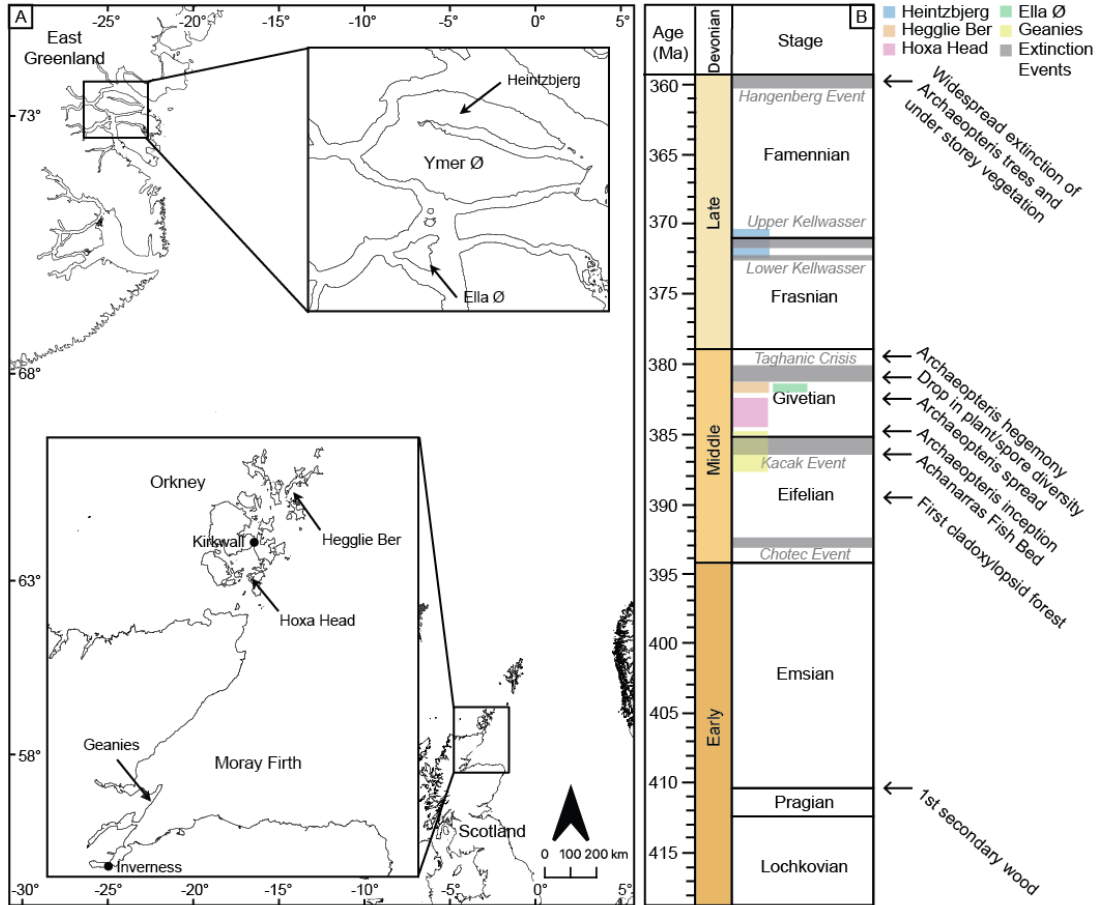


Figure 2.1. (A) Sample sites from the Orcadian Basin in East Greenland, northern Scotland and Orkney. Sample locations indicated with arrows in the insets. (B) Timeline detailing crucial events in plant development and diversity as well as key biologic crises and extinction events. Sample site coverage depicted by color code. (Becker et al., 2016; Berry and Marshall, 2015; Giesen and Berry, 2013; House, 2002; Aboussalam and Becker, 2011; Stein et al., 2007; Meyer-Berthaud et al., 2010; Stein et al., 2020; Percival et al., 2018; Marshall et al., 2007; Kaiser et al., 2016).

### 2.1.1. Importance of Phosphorus in Biogeochemical Cycling

Phosphorus is a critical biologically limiting nutrient on land (Walker and Syers, 1976; Vitousek et al., 1997; Filippelli and Souch, 1999; Vitousek et al., 2010) and in aquatic systems (Krom et al., 1991; Correll, 1999; Blomqvist et al., 2004; Planavsky et

al., 2010). Unlike other essential nutrients such as nitrogen and carbon, phosphorous has no natural stable gaseous form. Phosphorus can be transported long distances through the suspension of dust particles in the atmosphere, however this delivery method constitutes a minute fraction of the total P flux (Chadwick et al., 1999; Filippelli, 2008). Submarine groundwater discharge can potentially deliver large amounts of P, but this varies greatly depending on the sorption capacity of aquifers as well as their redox conditions and remains an extremely difficult quantity to constrain, even in modern systems (Slomp and Van Cappellen, 2004; Santos et al., 2021). P is generally removed from groundwater through sorption to iron oxides or coprecipitation with Al, Ca and Fe (Slomp and Van Cappellen, 2004), however recent studies suggest nutrient flux from submarine groundwater discharge is generally around 10% of riverine flux (Santos et al., 2021). The most significant source of P to the oceans and other bodies of water is through the weathering of continental materials and ultimate delivery by way of rivers (Holland, 1978; Filippelli and Delaney, 1994; Filippelli, 2002).

Early in landscape development, P in the mineral phase is the primary source for biologic uptake (Filippelli, 2002; Filippelli, 2008). Because plants cannot directly access mineral-bound P, they liberate P through the acidification of root pore spaces via degradation of organic matter (Filippelli, 2002; Filippelli et al., 2010) and the release of organic exudates from roots (Jurinak et al., 1986; Filippelli, 2002; Filippelli et al., 2010). Phosphorus is lost in large amounts from the mineral phase during initial landscape development, particularly in young volcanic landscapes (see McPeck et al., 2007). This refractory form of P is used quickly, and over time sources of P shift to more labile and occluded forms (Filippelli, 2002; Filippelli, 2008; Filippelli et al., 2010). In well-

developed soils, a significant amount of P is locked up in soil organic matter. In addition to shifting forms of P over time, total P within a system also decreases, with mineral-bound P being depleted and only organic and occluded fractions remaining (Fig. 2.2; Filippelli and Souch, 1999; Filippelli, 2002; Filippelli, 2008). It is thus expected that a landscape with little to no vegetation would transition through these phases stepwise, beginning with predominantly mineral sources of P and shifting to more occluded sources. Likewise, it would be expected that the overall release of P in a landscape would peak very quickly upon plant colonization and stabilize over time, as has been noted

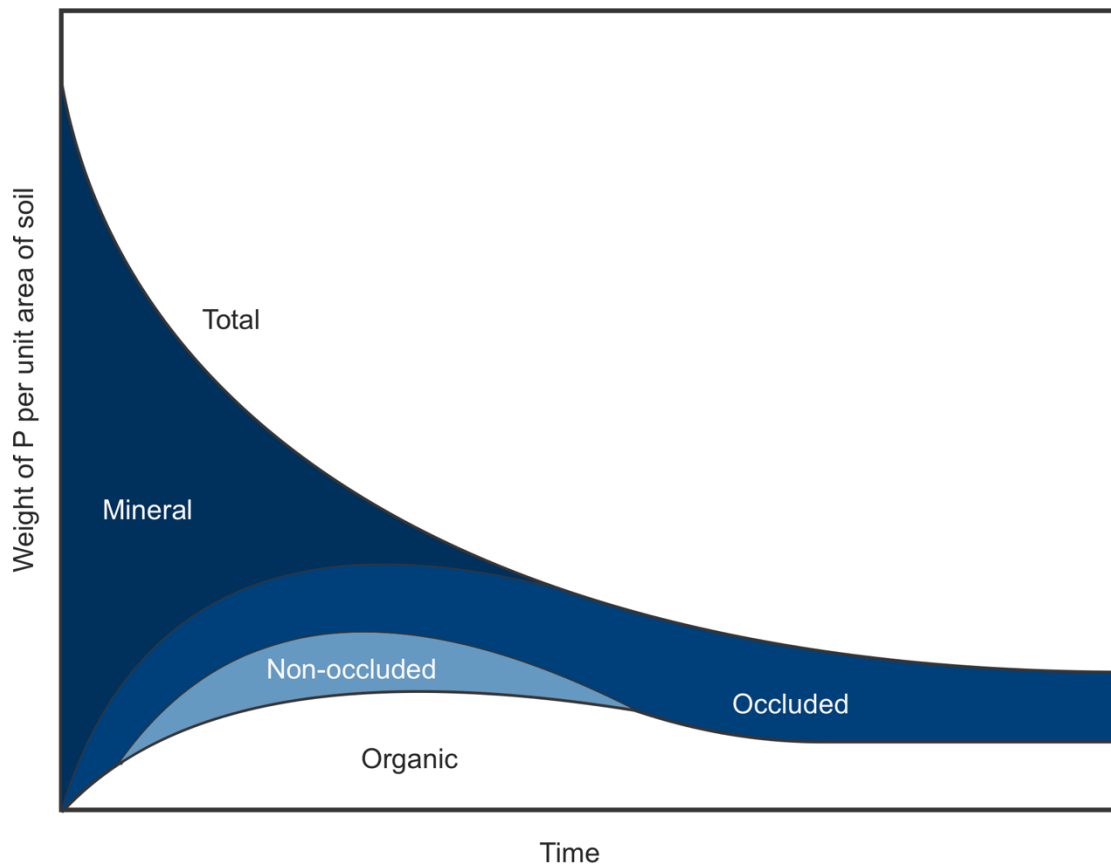


Figure 2.2. Depiction of phosphorus (P) transition with landscape evolution. As soil development proceeds, P transitions from the mineral phase to organic and occluded forms. Note the loss of P from the system with time. After Filippelli (2008).

(Filippelli and Souch, 1999; McPeck et al., 2007; Filippelli et al., 2010).

### 2.1.2. The Land Plant Revolution

Although first appearing in the Middle Ordovician (Wellman et al., 2003; but see also Strother & Foster, 2021), it was not until the Mid-Devonian that land plants (embryophytes) became widespread and occupied continental interiors. Prior to the Mid-Devonian, land plants were confined to areas immediately adjacent to bodies of water (or in wetland environments), had limited root systems and had yet to develop the necessary biological innovations that would lead to arborescence - the development of the first trees (Algeo et al., 1995; Algeo and Scheckler, 1998; Algeo et al., 2001; Stein et al., 2007; Algeo and Scheckler, 2010). Continental interiors would have been bereft of significant vegetation and well-developed (and weathered) soil profiles. From a P weathering perspective, most continental interiors would likely have been very “young,” meaning a significant amount of P was likely available in mineral form. By the Mid- to Late Devonian, land plants began to diversify and spread into continental interiors and uplands, populating the once barren landscape with vegetation (Algeo and Scheckler, 1998; Algeo et al., 2001; Piombino, 2016). The diversification and expansion of plants lead to the first appearance of trees and by the Tournaisian, the widespread propensity of plants to produce seeds (Algeo et al., 1995; Algeo and Scheckler, 1998; Algeo et al., 2001). The earliest of these trees appeared in the Eifelian and Givetian (Giesen and Berry, 2013), the most notable of which was *Archaeopteris*, a large progymnosperm that grew up to 30m in height (Algeo et al., 1995). *Archaeopteris* first appeared in the earliest Givetian, achieving hegemony by the Frasnian (Meyer-Berthaud et al., 1999; Meyer-Berthaud et al., 2010; Stein et al., 2020). While not seed-bearing, *Archaeopteris* is the

first known plant to display characteristics common in modern seed plants, possessing leaves and generating root systems that were simultaneously deep, laterally extensive and complex (Algeo et al., 2001; Stein et al., 2020). Although possibly only occupying niche biomes on inception (Stein et al., 2020), such root systems would likely have had enormous impacts on geochemical cycling in those regions.

The development of significant and complex roots systems in the Devonian is perhaps one of the single most critical events in the evolution of life in the Paleozoic and would have cascading impacts on Earth's biosphere. The earliest evidence of roots associated with vascular land plants appeared in the Early Devonian (late Pragian) and were shallow and simplistic in comparison to modern analogues (Algeo et al., 2001). Even by the Mid-Devonian, except for archaeopteridaleans, most major plant groups (aneurophytaleans, cladoxylopsids and lycopsids) had relatively simple root structures with minimal root penetration that would have had limited soil formation capabilities (Stein et al. 2012; Stein et al., 2020). More substantial root systems did not appear until the Mid- to Late Devonian and were notably associated with *Archaeopteris* (Algeo et al., 2001; Kenrick and Strullu-Derrien, 2014; Stein et al., 2020). Significant root development led to the creation of modern soil weathering processes, nutrient cycling and extensive soil development (Algeo and Scheckler, 1998; Kenrick and Strullu-Derrien, 2014; Morris et al., 2015). Unlike its contemporaries such as *Wattieza* (a cladoxylopsid whose life cycle terminated shortly after reproducing), *Archaeopteris* were likely long-lived (based on ring counts, Stein et al., 2007) and thus established significant soil profiles (Algeo and Scheckler, 1998) with a measurable impact on local biogeochemical cycling and nutrient loads into the oceans. Indeed, many studies have shown that roots



dramatically alter soil formation, and thus the soil biogeochemistry (e.g., Filippelli and Souch, 1999; Filippelli, 2008). The development of extensive root systems, stress-resistant seeds and an overall increase in size subsequently contributed to the expansion of land plants into continental interiors and uplands (Algeo and Scheckler, 1998; Algeo and Scheckler, 2010). The vast increase in land plants has been implicated in the drawdown of atmospheric CO<sub>2</sub> through photosynthesis, and elevated rates of silicate rock weathering through increased soil residence times (Algeo et al., 1995; Algeo and Scheckler, 1998; Falkowski et al., 2004; Quirk et al., 2015; Kenrick and Strullu-Derrien, 2014; Berry and Marshall, 2015; Morris et al., 2015; Lenton et al. 2016). Furthermore, this expansion likely had a marked impact on the weathering and export of P-bearing minerals to the oceans. Some have suggested that this export happened so quickly and on such a global scale that it drove immense algal blooms in the shallow Devonian seas, resulting in the creation of vast anoxic zones that ultimately drove the multiple biotic crises (Algeo et al., 1995; Algeo and Scheckler, 1998, Algeo et al., 2001; Algeo and Scheckler, 2010; Falkowski et al., 2011).

### 2.1.3. Sustainability of a Terrestrial Phosphorus Flush?

Perturbations in the P cycle have been implicated as drivers of some of the Devonian marine crises, but without direct evidence. Nearly all of the extinction events in the Devonian were characterized by widespread anoxia, with the exception of the Taghanic Crisis which had differing regional impacts and varying levels of hypoxia/anoxia (successive linked fluctuations in climate and sea level are noted as potential causal factors, though a collapse in terrestrial vegetation occurred towards the

end of the event; Marshall et al., 2011) (House, 1985; House, 2002; Racki, 2005; Aboussalam and Becker, 2011; Marshall et al., 2011; McGhee et al., 2013; Becker et al., 2016 and references therein). For these vast ocean anoxic zones to form, it is reasonable to assume an external eutrophication pulse (Meyer and Kump, 2008).

Although P is readily mobilized in young landscapes, its short residence time in the modern ocean (20-50 kyr; Ruttenger, 2003) makes it unclear whether a terrestrial nutrient pulse (or pulses) on a global or basin-wide scale is sufficient to drive significant changes in the marine system. Attempts have been made to provide such evidence utilizing nutrient signals from marine records, however this approach is problematic due to profound changes in the marine P cycle caused by ocean stratification and expansive anoxic zones in shallow seas characteristic of this period (Racki, 2005; Becker et al., 2016). Consequently, many questions remain about the mechanisms of enhanced P input to ancient oceans.

Here we present a novel approach to constraining the timing and source of nutrient pulses in the Devonian associated with terrestrialization. Through the analysis of Devonian lacustrine sequences, versus marine sediments or paleosols as has been attempted previously, we can gain proximal insights at higher temporal resolution of landscape changes and nutrient dynamics during the interval within the Devonian when plant evolution and expansion was well underway. Lacustrine sequences have long been used to study nutrient dynamics and can record vital information about weathering, nutrient flux and a host of other important parameters. Although depositional environments vary greatly, lake environments are generally low energy in nature and thus can provide a high-resolution sediment record with fine-scale laminations that can be

narrowed down to specific decadal, and even sometimes annual and seasonal variations. Constraining land plant-associated nutrient export will provide crucial evidence to link the timing and pace of land plant expansion with the marine biotic crises in the Devonian.

## 2.2. Materials and Methods

### 2.2.1. Site Selection

The target for this study was lacustrine and near-lacustrine sequences proximal to critical events and time transects within the Mid to Late Devonian (Eifelian, Givetian and Frasnian). Where possible, outcrops spanning a biotic crisis with associated marine anoxia were chosen. These include the Choteč and the Kačák Events in the Eifelian, the Taghanic Crisis in the Givetian and the Kellwasser Event in the Frasnian. All samples are archived at the University of Southampton, UK. Five distinct sites from the paleocontinent of Euramerica were chosen including three from the Orcadian Basin (Scotland and Orkney) and two from the Devonian Basin in East Greenland. Study sites include Geanies in Easter Ross, Scotland; Hoxa Head on South Ronaldsay, Orkney; Heggli Ber on Sanday, Orkney; Ella Ø (island) and Heintzbjerg in East Greenland (Fig. 1). All sites contain continuous lacustrine sequences, except for the Heintzbjerg samples, which are primarily fluvial. In most cases, samples were taken at various points throughout a given lake cycle. For the Geanies set, samples were selected from deep lake facies (the rest of the lake cycle was not sampled, however the sequence is an uninterrupted succession of lake cycles).

## 2.2.2. Geologic Setting

### 2.2.2.1. Orcadian Basin

Throughout much of the Devonian, the Orcadian Basin was the site of a series of lacustrine systems formed in extensional half graben basins with distinct depocenters (McClay et al., 1986; Marshall and Hewett, 2003). The depth and areal extent of these lakes varied based on climatic conditions but were generally shallow playa lakes with periods of deep permanent lakes (Marshall et al., 2007). During intervals of enhanced precipitation, these lakes occasionally merged to form extensive lacustrine systems, such as that which formed the distinctive Achanarras fish bed referred to as a mega-lake (Marshall et al., 2007). The Orcadian Lake (also referred to as the Achanarras Lake) is a particularly long-lived example, which at one time occupied much of the eastern Highlands of Scotland and the Moray Firth and extended as far north as the Shetland Islands and east to the margins of Norway (Trewin and Thirwall, 2002; Marshall et al., 2007). At its largest extent during the Eifelian and early Givetian, the Orcadian Lake would have been ~27,000 km<sup>2</sup> in size, or roughly the size of Belgium (Andrews and Hartley, 2015). The northern Scotland and Orkney samples (Geanies, Hoxa Head and Hegglic Ber) were all collected from Orcadian Basin lacustrine laminates and are mostly mudstone-limestones, siltstones and sandstones (Donovan et al., 1974) with fluvial sandstones and conglomerates near the margins of the Orcadian Basin along with significant features such as the Achanarras fish bed (Andrews and Hartley, 2015; Johnstone and Mykura, 1989; Trewin and Thirwall, 2002).

The paleolatitude was between approximately 20°S and 30°S, in an arid to semi-arid zone (Torsvik and Cocks, 2004). Although the area experienced many phases of transgression and regression (most likely due to climatic forcing), in general the depositional environment is characterized as low energy, with fine-grained facies providing the potential for high resolution data collection and analyses (Andrews and Hartley, 2015). The Geanies samples represent a series of cyclic lacustrine deposits near Tain, Scotland in Easter Ross, of which 12 distinct lake cycles were sampled. The oldest samples in the Geanies sequence lie in the Balintore Formation (the first nine lake cycles), continue into Jessie Port (a fish bed equivalent to the distinctive Achanarras fish beds in Caithness correlative with the onset of the Kačák Event and spanning two lake cycles), and terminate in the latest Eifelian in the Geanies Formation (the final lake cycle of the sequence) (Marshall et al., 2007; Marshall et al., 2011) (Fig. 2.3). The Hoxa Head samples represent a similar cyclic lacustrine sequence with 21 lake cycles collected from an outcrop on northwestern South Ronaldsay, Orkney. They are sourced from the Rousay Flagstone Formation (the uppermost section of the Upper Stromness Flagstone Formation; Fig. 2.3) and are early Givetian (Speed, 1999; Trewin and Thirlwall, 2002) occurring above the Kačák Event (Fig. 2.1). The Hegglic Ber sequence originates from southwestern Sanday, Orkney (Fig. 2.1). This continuous but thin sequence also contains cyclic lacustrine deposits with at least three distinct lake cycles. It was collected from the Eday Flagstone Formation (Fig. 2.3) and is mid-Givetian in age (Marshall, 1996; Marshall et al. 2011).

		Biotic Crisis	Orkney	Caithness	Easter Ross	East Greenland	
Mid Devonian	Givetian	Late	Upper Eday Sandstone Formation	Dunnet Head Sandstone	Tarbat Ness Formation	Sofia Sund Formation	
		Mid	Taghanic	Eday Marl Formation	Ashy Geo	Rockfield Formation	Ankerbjergsølv Formation
				M.Eday Sst Lower Eday Sandstone Formation	John O'Groats Sandstone Group		
	Early		Upper Stromness Flagstone Formation	Upper Caithness Flagstone Group	Geanies Formation	Viddal Group	
		Kačák	Sandwick Fish Bed	Achanarras Limestone			Jessie Port
	Eifelian		Lower Stromness Flagstone Formation	Lower Caithness Flagstone Group	Balintore Formation	Solstrand Formation	
		Choteč*		Sandside Bay Formation			Bighouse Formation

Figure 2.3. Middle Devonian stratigraphy from Orkney, Caithness, Easter Ross and East Greenland. Note the Choteč Event location is listed for temporal reference only as evidence for this extinction event has yet to be found in the Orcadian Basin (House, 2002). Sections highlighted in gray indicate sample coverage in this study. The location of the Eifelian/Givetian boundary in East Greenland is estimated based on current literature. After Marshall et al. (2011) with East Greenland stratigraphy from Blom et al. (2007).

#### 2.2.2.2. Devonian Basin of East Greenland

The lacustrine sequences in Ella Ø formed under similar conditions as lakes that were comparable in size in the Orcadian Basin (McClay et al., 1986; Marshall and Stephenson, 1997; Trewin and Thirlwall, 2002). Devonian deposits comprise the entire southeast corner of the ~145 km<sup>2</sup> island and represent the fringes of lakes preserved amongst the topography on an unconformity surface (Marshall and Stephenson, 1997 and

references contained therein). Samples are from the Solstrand Formation and collected from a primarily eastward-draining braid-plain systems with a lacustrine bed present at three separate localities (Marshall and Stephenson, 1997; Larsen et al., 2008). The sample set presented here represents a single, but complete lake cycle (Marshall and Stephenson, 1997) of Givetian age, occurring between the end of the Kačák Event and the beginning of the Taghanic Crisis (Fig. 2.1). During monsoon periods, it is possible that the outflow from this lake linked to that from the Orcadian Lake and may be correlative with the 3rd lake cycle within the Eday Group (Marshall and Hemsley, 2003).

The Heintzbjerg samples represent a continuous 1100 m sequence on nearby Ymer Ø from the Sofia Sund, Midnatspas, Zoologdalen and Andersson Land Formations consisting of fluvial deposits and abandoned channel lakes. They range in age from the Frasnian to early Famennian and encompass a portion of the Lower Kellwasser Event (LKW) as well as the entirety of the Upper Kellwasser Event (UKW) (Larsen et al., 2008) (Fig. 2.1). This Devonian basin stage is marked by a shift in drainage direction to the south and is comprised of mostly fluvial systems with rare aeolian intercalations (Larsen et al., 2008).

### 2.2.3. Age Constraints

Age constraints for these samples were obtained via precise palynological calibrations and in some cases in combination with fossil fish assemblages (see Marshall and Stephenson, 1997; Marshall and Hemsley, 2003). Precision dating of the Kellwasser Events by Percival et al. (2018) enabled the employment of age control points for the Heintzbjerg samples, specifically bounding the end of the LKW, the beginning of the

UKW, and the Frasnian/Famennian boundary and thus establishing a 525,000-year span between the oldest and youngest of these events. This allowed the determination of both sedimentation rates and P accumulation rates for the Heintzbjerg sequence using bulk density data (with an average value of 2.33 g/cm<sup>3</sup>) estimated from published U.S. Geological Survey data (Manager, 1963) for similar Devonian sequences. For the remaining sample sets, relative age control points were estimated by counting lake cycles present in the sequence, with one lake cycle defined as beginning at the base of one organic matter rich layer and ending before the appearance of the next organic matter rich layer. Lake cycles in the Orcadian Basin and the east Greenland Devonian Basin recur with Milankovitch cyclicity, specifically with the eccentricity parameter approximately every 100,000 years (Astin, 1990; Kelly, 1992; Olsen et al., 1994; Marshall 1996; Andrews and Trewin, 2010; Andrews et al., 2016). This allowed calculation of individual sedimentation rates and P accumulation rates for each lake cycle in each sample set.

#### 2.2.4. Sample Preparation and Analysis

Samples were collected from whole rocks at the archives of the University of Southampton. Between 5-10 g of sample was removed with care taken to avoid collecting weathered surfaces, washed with Milli-Q water, dried and then powdered by hand using a porcelain mortar and pestle.

##### 2.2.4.1. Aluminum, Calcium, Iron, Phosphorus and Titanium

Approximately 100 mg of each homogenized sample was acidified with 6N HCl and then digested in a microwave system for 30 minutes using a variation of EPA method



3052. Samples were then spun in a centrifuge at 10,000 RPM for 10 minutes and the supernatant extracted. In preparation for inductively coupled plasma-optical emission spectrometry (ICP-OES) analysis, samples were diluted in accordance with expected concentrations of the analyte. In general, a dilution ratio of 1:10 was used for P and Ti, and 1:50 for Al, Ca and Fe. ICP-OES analysis was performed on a Perkin Elmer Optima 7000DV using three replicates per sample, with analytical precision within 5%.

Total digestion was chosen over a sequential extraction for three reasons. The first was the uncertainty about the diagenetic impacts on the various P fractions in nearly 400-million-year-old rocks. Second, while some of the smaller lakes analyzed may have had intervals where they were likely oligotrophic and oxic (based on the presence of fossilized fish scales; Marshall and Stephenson, 1997), lakes within the Orcadian Basin had a varied redox history with evidence of intervals of anoxia (Trewin and Thirlwall, 2002; Andrews and Hartley, 2015). This is important as redox cycling in anoxic environments could provide misleading P geochemical results (as addressed in detail below). Third, total element ratios enable the comparison of total P to detrital elements such as Al, Ca and Ti as well as redox cycling via total Fe. Comparing total P to detrital inputs provides an estimate of P enrichment (either from authigenic accumulation of P or from elevated levels of P within the detrital signal as would be expected during soil development in a young landscape) while eliminating the bias introduced by sediment focusing, turbidity currents, in situ carbonate and aluminum hydroxide production, etc. Titanium serves as a reliable proxy for terrigenous input, with elevated P/Ti values suggesting an increase in P content of the detrital fraction. Elevated P/Ti on its own however, is not definitive due to complex geochemical cycling within the water column

as well as potential organic acid facilitated Ti mobility in immature sediment (see Pe-Piper et al., 2011). The P signal must be decoupled from authigenic P, thus comparing P to Al, Ca and Fe is necessary. Ca is used as an indicator of in situ carbonate production and Al an indicator of both terrigenous input and potential photochemical production of Al hydroxides. Using a suite of elements provides a more accurate portrayal of detrital inputs as Al is prone to some alteration during settling primarily due to biogenic scavenging, but this is most common in deep marine settings (Murray and Leinen, 1996; Pattan and Shane, 1999). Comparing total P to total Fe is useful in addressing concerns stemming from the redox condition during deposition. Under oxic conditions, orthophosphates within the water column are adsorbed onto Fe-oxyhydroxides which become stored within the sediment and may go on to form authigenic phosphate minerals (Filippelli, 2002). Under anoxic conditions, P bound to Fe-oxyhydroxides readily dissolves, releasing P into the water column to actively participate in the continued biologic cycling of P (Filippelli, 2002). The fate of both P and Fe are intertwined; thus, the P/Fe ratio is useful in separating the P signal from reductive dissolution of the Fe-oxyhydroxides. An elevated P/Fe ratio indicates an increase in terrestrial delivery of P, independent of redox cycling. While useful, as with any geochemical proxy, P/Fe on its own cannot be used to accurately determine redox conditions (this is addressed in 2.2.4.3). To complement the analyses and assist with interpretations, correlations between P and various other analytes were performed and statistical significance calculated using GraphPad Prism (only significant results are presented in section 4, but all statistical analyses are included in Appendix A). Additionally, as both Al and Ti are prone to some alteration, correlations between Al and Ti were calculated for each site. Although no

geochemical proxy can be universally reliable, significant correlation between Al and Ti serves as an indicator of their utility as terrestrial input proxies in this study (Appendix A).

#### 2.2.4.2. Total Organic Carbon

Total C and total inorganic C (TIC) was measured using an ELTRA CS-580 Carbon/Sulfur Analyzer with attached TIC module. The amount of total organic carbon (TOC, also referred to as  $C_{org}$ ) was calculated as the difference between total C and TIC. The  $C_{org}$  values were used in combination with  $P_{tot}$  determinations to determine the  $C_{org}:P_{tot}$  ratio, one of multiple paleoredox proxies used. Analytical precision was within 5% based on replicate analyses of standard reference materials.

#### 2.2.4.3. Aluminum, Copper, Chromium, Lead, Molybdenum, Nickel, Rubidium, Silicon, Strontium, Titanium, Uranium and Zirconium

Powdered samples were analyzed for Al, Cu, Cr, Mo, Ni, Pb, Rb, Si, Sr, Ti, U and Zr using an Olympus X-ray fluorescence (XRF) instrument. These elemental abundances were used to calculate ratios of Rb/Sr, Sr/Cu, Si/Al, Ti/Al and Zr/Al and metal enrichment factors (EF) for  $Cu_{EF}$ ,  $Cr_{EF}$ ,  $Mo_{EF}$ ,  $Ni_{EF}$ ,  $Pb_{EF}$  and  $U_{EF}$ .

In lake sediments, the Rb/Sr ratio has been used as both a chemical weathering indicator as well as a proxy for mass accumulation rate from terrestrial input (see Xu et al., 2010). Elevated values of Rb relative to Sr is indicative of material that has been weathered with respect to its source rocks and is interpreted here as elevated terrestrial input. Si/Al ratios are similarly used as a weathering proxy, but unlike Rb/Sr are generally indicative of

physical weathering intensity. As quartz is resistant to chemical weathering and is coarser than clay minerals, higher values of Si/Al will reflect a greater degree of physical weathering (Calvert and Pedersen, 2007). Similarly, Ti/Al and Zr/Al ratios have been used as proxies for grain size, specifically silt to clay ratio as both are transported in the silt/fine sand portion (see Calvert and Pederson, 2007; Wei and Algeo, 2020). Sr/Cu ratios have been used in both paleolacustrine and paleomarine settings as paleoclimate indicators (e.g., Moradi et al., 2016; Tang et al., 2019; Li et al., 2020; Pan et al., 2020). Strontium is readily released from source rocks via chemical weathering and under hot and arid conditions, will tend to concentrate in lake waters (Liang et al., 2014). Copper will precipitate as  $\text{Cu}_2\text{S}$  in organic rich environments and is generally found in larger quantities in biologically productive aquatic environments associated with warm and humid environments (Liang et al., 2014). Thus, low ratios of Sr/Cu are suggestive of warm and humid conditions (values between 1-10 are generally indicative of these conditions, although some authors have suggested values of 1-5) and higher Sr/Cu values indicate hot and arid conditions (generally for Sr/Cu values  $>10$ , again some authors argue that values of  $>5$  should be used) (Liang et al., 2014; Cao et al., 2015; Jinhua et al., 2018; Li et al., 2020). Sr/Cu tends to vary inversely with Rb/Sr such that a high Sr/Cu ratio accompanied by a low Rb/Sr ratio indicates hot and arid conditions with low weathering, and vice versa (Cao et al., 2015; Shen et al., 2020).

Given that geochemical proxies can be highly variable between and within formations (Algeo and Liu, 2020), a suite of seven proxies were selected in combination with P/Fe to provide a robust approach to characterizing paleoredox. Multiple proxies allow for comparison among lakes in the various sequences from distinct geographic

regions and potentially different elemental inventories. Many of these proxies were designed for marine environments and their utility for paleolacustrine environments is unclear. Also, because TOC for the different sample sites varied (and sometimes significantly within a given sequence), it was necessary to have proxies effective in both anoxic (organic-rich) and oxic-suboxic (organic-poor) environments as both could be encountered in the Devonian sequences.

Most samples (but not all) were expected to be relatively organic-poor, thus  $Pb_{EF}$  was chosen as these values generally display a negative covariation with TOC (see Algeo and Liu, 2020).  $C_{org}:P_{tot}$ ,  $Cu_{EF}$ ,  $Cr_{EF}$ ,  $Mo_{EF}$ ,  $Ni_{EF}$  and  $U_{EF}$  were chosen due to their varying effectiveness under oxic and anoxic conditions (i.e., Cr and U are mobilized by oxic weathering and sequestered into sediments in anoxic environments, Mo enrichments are highest under euxinic conditions, etc.). We chose  $C_{org}:P_{tot}$  (total P, versus reactive P) for ease of comparison with other paleomarine and paleolacustrine studies. This serves as a proxy for  $C_{organic}:P_{reactive}$  and is generally effective in areas where the detrital P fraction is minor (Algeo and Ingall, 2007), though we acknowledge that the detrital fraction may be significantly larger in some of our sequences. The remainder of the proxies used ( $Cu_{EF}$ ,  $Cr_{EF}$ ,  $Mo_{EF}$ ,  $Ni_{EF}$ ,  $Pb_{EF}$  and  $U_{EF}$ ) represent enrichment factors for the various elements. Similar to Liu and Algeo (2020), the detrital fraction of each element was estimated. The enrichment factor (relative to the detrital fraction) was calculated using the following formula:

$$X_{EF} = X_{Total} - Al (X/Al)_{Detrital} \quad (1)$$

Where X is the element and  $(X/Al)_{Detrital}$  are the average concentrations of the element and Al of upper continental crust as reported by McLennan (2001). Average upper

continental crust values used are 8.04 wt. % for Al, 25 ppm for Cu, 83 ppm for Cr, 1.5 ppm for Mo, 44 ppm for Ni, 17 ppm for Pb and 2.8 ppm for U (McLennan, 2001). All seven paleoredox proxies were employed for each separate sequence and reported here. For the purposes of determining the effectiveness of each proxy at each locality, correlations among each of the seven proxies to each other and TOC were calculated and only those whose correlations were statistically significant were considered viable for redox determinations.

### 2.3. Results

Results are presented here by section from oldest to youngest. Each section contains a figure comparing the P input relative to metal ions (P/Al, P/Ca, P/Fe and P/Ti; henceforth abbreviated as P/Me), P accumulation rate, the weathering proxy Rb/Sr, the paleoclimate proxy Sr/Cu, elemental enrichment factors,  $C_{org}$  and  $C_{org}:P_{tot}$ .

#### 2.3.1. Geanies

Results for the Eifelian samples at the Geanies locality are shown in Fig. 2.4. At the base of the section, P/Ti is elevated in lakes 9 and 10 and gradually decreases to less than 1 within lakes 12-15 (Fig. 2.4a). A gradual increase in P/Ti begins again during lake 15, reaching values around 2 by the end of lake 16. P/Fe generally tracks P/Ti for lakes 9 and 10 but remains at background values like the other P/Me ratios. Significant perturbations are observed in P/Al in lakes 14, 17 and 20, aligning with maxima in Rb/Sr (Fig. 2.4c). Phosphorus accumulation rate is relatively low at the base of the sequence and increases to greater than  $300 \mu\text{mol P cm}^{-2} \text{ kyr}^{-1}$  for lakes 11-14, peaks during lake 15

and peaks again at the end of lake 16 into lake 17. Lakes 10, 12, 16 and 19 have the highest concentrations of  $C_{org}$  ( $> 3$  wt. %; Fig. 2.4e). The Rb/Sr values remain relatively low for most of the sequence, but notably increase at the end of lake 14, decrease to minimum values during lake 16 and return to relatively higher values in lakes 17, 18 and 20. The Sr/Cu values are generally antithetic to the Rb/Sr values, with significant maxima during lakes 9, 14, 16 and 19 (Fig. 2.4c). Paleoredox proxies exhibit high enrichment factors in lakes 9, 10, 12, 16 and 19 (Fig. 2.4d). Notably,  $Cu_{EF}$  does not trend like the other EFs in lakes 9 and 10 but is in relative agreement with the other enrichment factors in the remainder of the sequence. Additionally,  $Cr_{EF}$  does not appear to show elevated values during lakes 12 and 19. Peaks in  $C_{org}:P_{tot}$  are observed during lakes 10, 16 and 19.

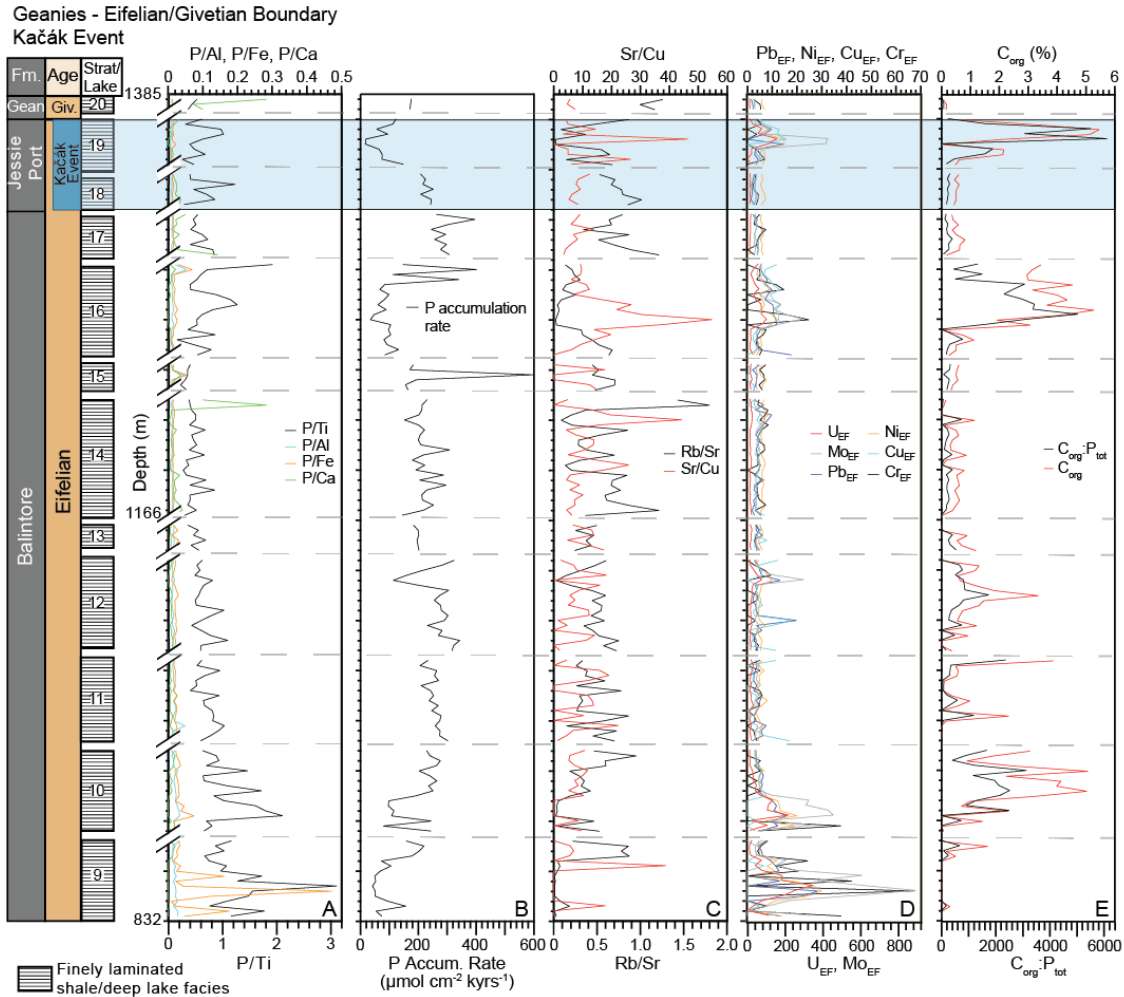


Figure 2.4. Geochemical data from the Geanies locality, Easter Ross, Scotland. The figure is divided by lake cycle, with each lake cycle representing only the deep lake facies. Lakes 9-17 are from the Balintore Formation., lakes 18-19 from Jessie Port (Easter Ross Achanarras equivalent and coincident with the onset of the Kačák Event, also highlighted in blue) and lake 20 is from the Geanies Formation. All are of Eifelian in age. The y-axis represents depth (m) with breaks between each lake cycle which were not sampled. Within each lake cycle, samples were taken every 10 cm, therefore inflated scales are shown for clarity between laminations. A: Phosphorus to metal ion ratios. B: Phosphorus accumulation rate ( $\mu\text{mol P cm}^{-2} \text{kyr}^{-1}$ ). C: Paleoclimate proxy strontium/copper and paleoweathering proxy rubidium/strontium ratios. D: Paleoredox proxies comprising enrichment factors for chromium, copper, molybdenum, nickel, lead and uranium. E: Organic carbon (wt. %) and paleoredox proxy total organic carbon/total phosphorus ratio (molar ratio).



### 2.3.2. Hoxa Head

Results from the Givetian sequence at Hoxa Head, South Ronaldsay, Orkney are shown in Fig. 2.5. P/Me ratios show some variation, but magnitudes are low, except for P/Ti which varies between 0.4 and 1.8 (Fig. 2.5a) throughout the record. P accumulation rates range from 13 to near 100  $\mu\text{mol P cm}^{-2} \text{ kyr}^{-1}$  (Fig. 2.5b). Maxima in P/Ca align with Rb/Sr maxima at 16, 53, 65, 96, 102 m and between 120-140 m. Concurrent maxima are observed in all P/Me ratios at 14, 63, 132 and 145 m.  $C_{\text{org}}$  ranges between 0-7 wt. %, with values above 5 wt. % recorded in five samples (Fig. 2.5e). The maxima and minima in  $C_{\text{org}}$  coincide with those in Sr/Cu (which are opposite in magnitude to variations in Rb/Sr; (Fig. 2.5c)—trends which continue throughout the sequence. Trace element enrichments are observed at 14, 60, 68, 116, 130, 146 and 176 m (Fig. 5d).  $C_{\text{org}}:P_{\text{tot}}$  is in general agreement with maxima observed in EF's, with highest values at 14, 22, 36, 60, 68, 85, 112-134 and 146 m (Fig 2.5e).

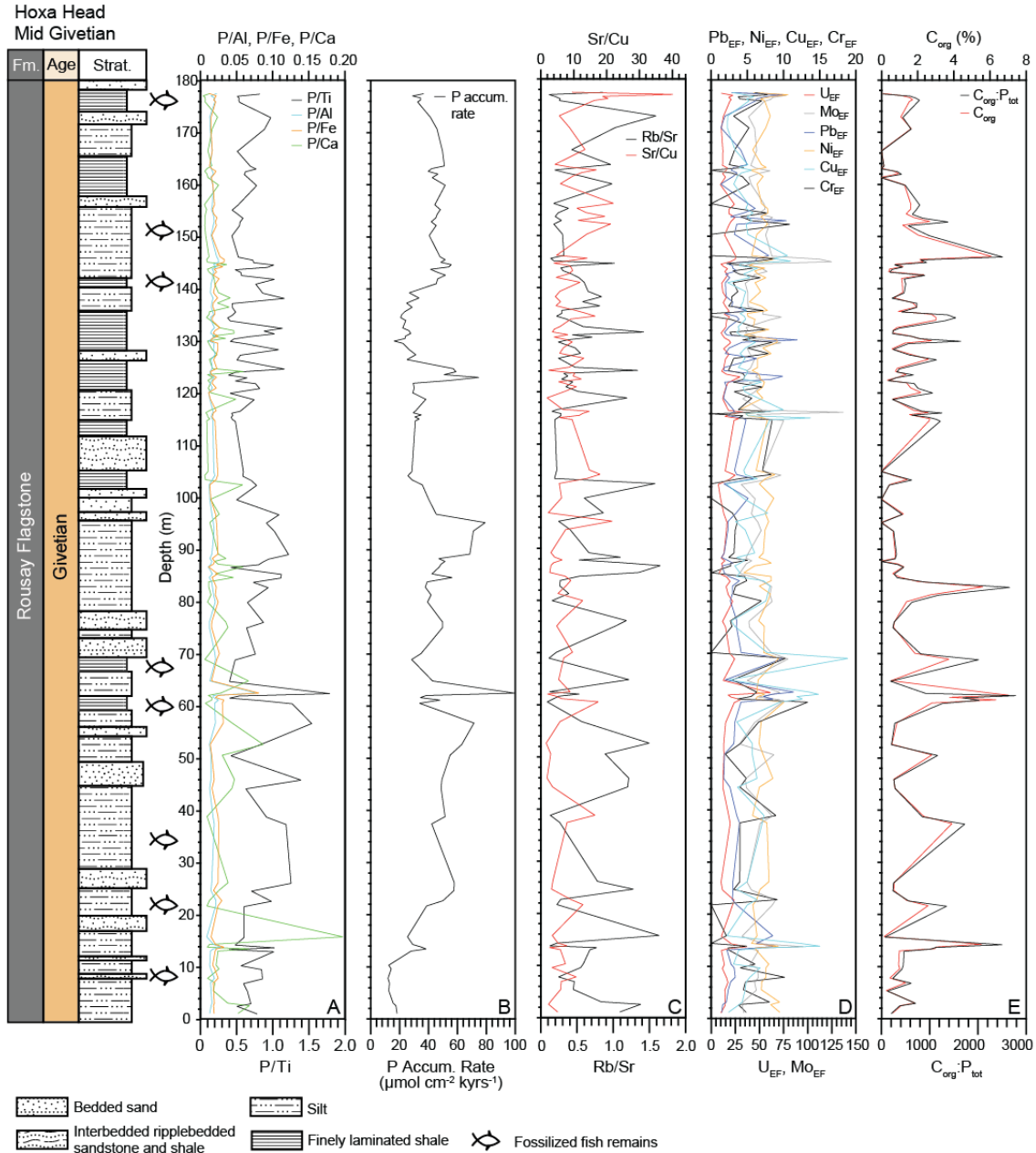


Figure 2.5. Geochemical data from Hoxa Head, South Ronaldsay, Orkney plotted vs depth (m). Samples are from the Rousay Flagstone Formation (top of the Upper Stromness Flagstone Formation) and are of early Givetian in age. The y-axis also shows formation, age and stratigraphy. Fossilized fish remains found during collection are also noted on the y-axis. A: Phosphorus to metal ion ratios. B: Phosphorus accumulation rate ( $\mu\text{mol P cm}^{-2} \text{ kyr}^{-1}$ ). C: Paleoclimate proxy strontium/copper and paleoweathering proxy rubidium/strontium ratios. D: Paleoredox proxies comprising enrichment factors for chromium, copper, molybdenum, nickel, lead and uranium. E: Organic carbon (wt. %) and paleoredox proxy total organic carbon/total phosphorus ratio (molar ratio).

### 2.3.3. Ella Ø

Results from the Givetian sequence at Ella Ø, Greenland are shown in Fig. 2.6.

P/Ti values are relatively high at the bottom of the sequence and at 0.85 m and 1.1 m (Fig. 2.6a). Phosphorus accumulation rates (Fig. 2.6b) and the remaining P/Me ratios have similar patterns as P/Ti. The exception being P/Al at 0.7 m and 1 m which appears to trend out of phase with the other P/Me ratios in those samples. Notably, fossilized plant remains were discovered at various points in this sequence, including in proximity to the two latter P perturbations .85 and 1.05 m.  $C_{org}$  varies from below 1 wt. % to around 2 wt. %, with a pattern that is roughly similar that of  $C_{org}:P_{tot}$ , the exception being between 0.85-1.0 m (Fig. 2.6e). Sr/Cu values are low at the bottom of the sequence and trend towards higher values at the top of the sequence, which is opposite to the patterns

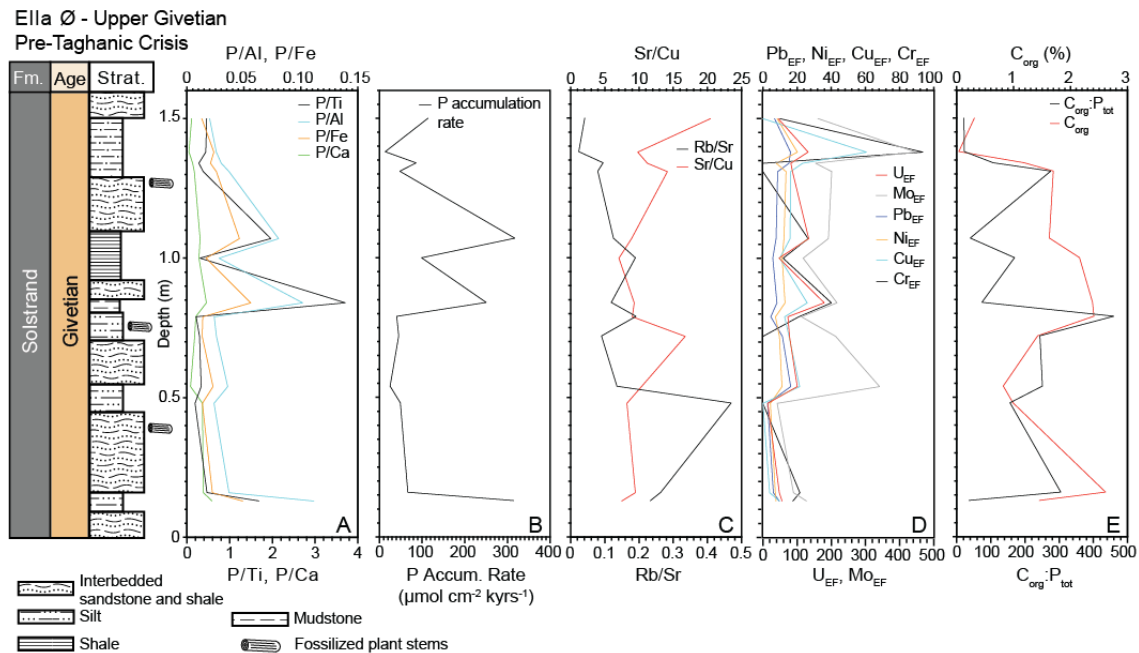


Figure 2.6. Geochemical data from Ella Ø, Greenland plotted vs depth (m). Samples are from the Solstrand Formation and are of Givetian age. The y-axis also shows formation, age and stratigraphy. Fossilized plant stems found during collection are also noted on the y-axis. A: Phosphorus to metal ion ratios. B: Phosphorus accumulation rate ( $\mu\text{mol P cm}^{-2} \text{ kyr}^{-1}$ ). C: Paleoclimate proxy strontium/copper and paleoweathering proxy rubidium/strontium ratios. D: Paleoredox proxies comprising enrichment factors for chromium, copper, molybdenum, nickel, lead and uranium. E: Organic carbon (wt. %) and paleoredox proxy total organic carbon/total phosphorus ratio (molar ratio).

observed in Rb/Sr (Fig. 2.6c). The paleoredox proxies exhibit maxima at 0.85 m and 1.35 m for most EFs (Fig. 2.6d).  $Mo_{EF}$  records a peak at 0.85 m that is not substantially expressed in the other EFs (particularly not  $Cu_{EF}$ ). The  $C_{org}:P_{tot}$  ratios are generally opposite patterns exhibited in the EFs (Fig. 2.6e). The peak in the  $C_{org}:P_{tot}$  values occurs at 1.6 m, notably prior to the P/Ti peak and is not in agreement with other paleoredox proxies.

#### 2.3.4. Heggli Ber

Results from the Givetian sequence at Heggli Ber, Sanday, Orkney are shown in Fig. 2.7. One sample at 10 m has relatively high P/Me ratios (Fig. 2.7a), P accumulation rates (Fig. 2.7b) and  $C_{org}$  concentrations (Fig. 2.7e). Notably, the P/Ti peak value is the largest measured in all the Devonian sequences presented here. The Rb/Sr ratio and Sr/Cu are again broadly opposite one another (Fig. 2.7c). With the exception of  $Cr_{EF}$ , paleoredox EFs exhibit maxima at 10 m (Fig. 2.7d). The general trend for  $C_{org}:P_{tot}$  aligns with the EFs with a maximum value of 700 at 10 m (Fig 2.7e).

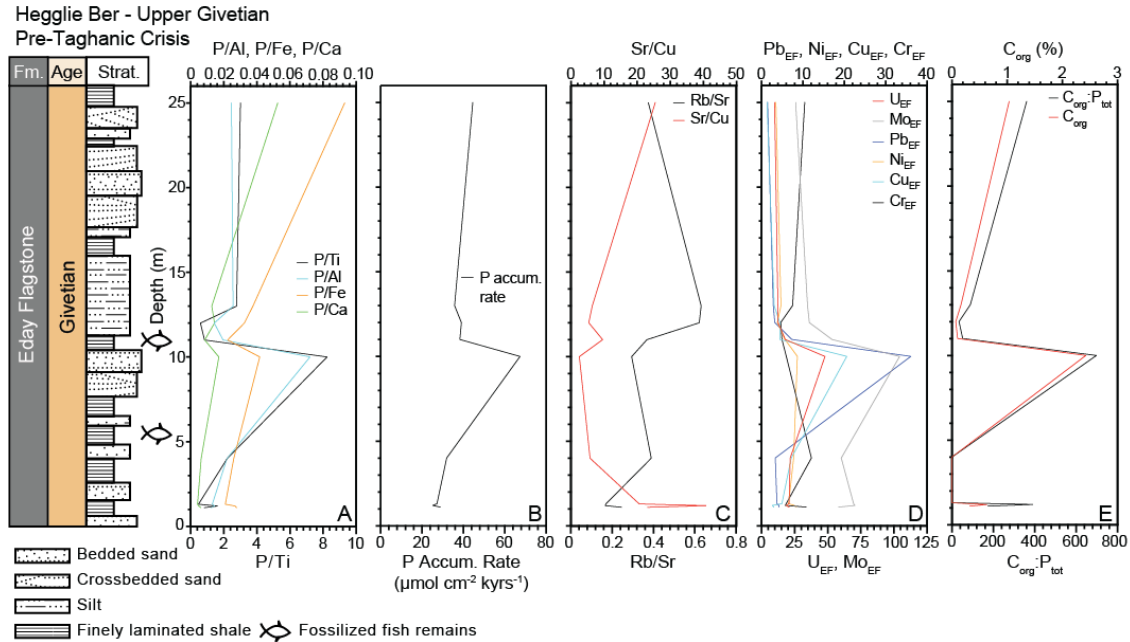


Figure 2.7. Geochemical data from Hegglic Ber, Sanday, Orkney plotted vs depth (m). Samples are from Eday Flagstone Formation and are of Givetian in age. The y-axis also shows formation, age and stratigraphy. Fossilized fish remains found during collection are also noted on the y-axis. A: Phosphorus to metal ion ratios. B: Phosphorus accumulation rate ( $\mu\text{mol P cm}^{-2} \text{ kyr}^{-1}$ ). C: Paleoclimate proxy strontium/copper and paleoweathering proxy rubidium/strontium ratios. D: Paleoredox proxies comprising enrichment factors for chromium, copper, molybdenum, nickel, lead and uranium. E: Organic carbon (wt. %) and paleoredox proxy total organic carbon/total phosphorus ratio (molar ratio).

### 2.3.5. Heintzbjerg

Results from the Frasnian/Famennian sequence at Heintzbjerg, Greenland are shown in Fig. 2.8. At the base of the record during the LKW (lower blue shaded region), pronounced increases in P/Fe, P/Ca, P/Al (Fig. 2.8a) and Rb/Sr (Fig. 2.8c) ratios are observed at 15 and 51 m. P/Ti values are elevated when compared to values between the end of the LKW and beginning of the UKW (Fig. 2.8a). Sr/Cu drops rapidly from maxima near 15 at the bottom of the sequence to less than 5 by the end of the LKW and then fluctuates between 2 and up to 8 for the remainder of the LKW and the intermission between the LKW and UKW, (Fig. 2.8c). Although generally low ( $<0.65$  wt. %),  $C_{\text{org}}$  (Fig. 2.8e) maxima within the LKW coincides with those in the P/Me ratios. All P/Me

ratios decrease to background levels between the end of the LKW and the beginning of the UKW. The Rb/Sr ratio (Fig. 2.8c) is elevated prior to the beginning of the UKW, notably leading increases in P accumulation (Fig. 2.8b) and  $C_{org}$ . The most significant P/Ti perturbation occurs during the latter half of the UKW beginning around 600 m and is reflected across all P/Me ratios and P accumulation, after which all values (with the exception of a pronounced increase in P/Ca at the F/F boundary) return to background levels in the transition from the latest Frasnian into the Famennian. Of note, P accumulation markedly increases at the onset of the UKW and peaks near  $8000 \mu\text{mol P cm}^{-2} \text{ kyr}^{-1}$  at 680 m, which is the highest rate observed across all sequences presented here. Sustained values above  $1500 \mu\text{mol P cm}^{-2} \text{ kyr}^{-1}$  are observed for the entire portion of the UKW in which P accumulation rates were calculated (P accumulation rates were not calculated for the LKW, the latest Frasnian and the Famennian due to the lack of age control points for those portions of the sequence).  $C_{org}$  remains low and variable for the rest of the sequence after peaking near 1 wt. % at the beginning of the UKW. Rb/Sr values fluctuate throughout most of the UKW, the largest values within the UKW aligning with the beginning of positive trend in P/Me and P accumulation just below 600 m before dropping in the latest Frasnian and rising sharply in the Famennian around 1000 m. Sr/Cu similarly fluctuates during the UKW, with minima also coincident with maxima in both P/Me and P accumulation and maxima of 12.6 at the bottom of the Zoologdalen Fm. The paleoredox proxies show significant maxima in EFs (Fig. 2.8d) during the LKW (10 meters) and again during the UKW (720 m). Prominent enrichments are observed in  $\text{Pb}_{EF}$  at 240 m and 620 m. The peak at 240 m corresponds with modest increases in the other EFs whereas the peak at 620 m does not correlate with other EFs. The  $C_{org} \cdot \text{P}_{tot}$  data (Fig.

2.8e) is highly variable, but peaks are present during the LKW, the beginning of the UKW at 350 m and the end of the UKW beginning at 700 m and extending past 800 m into the Famennian.

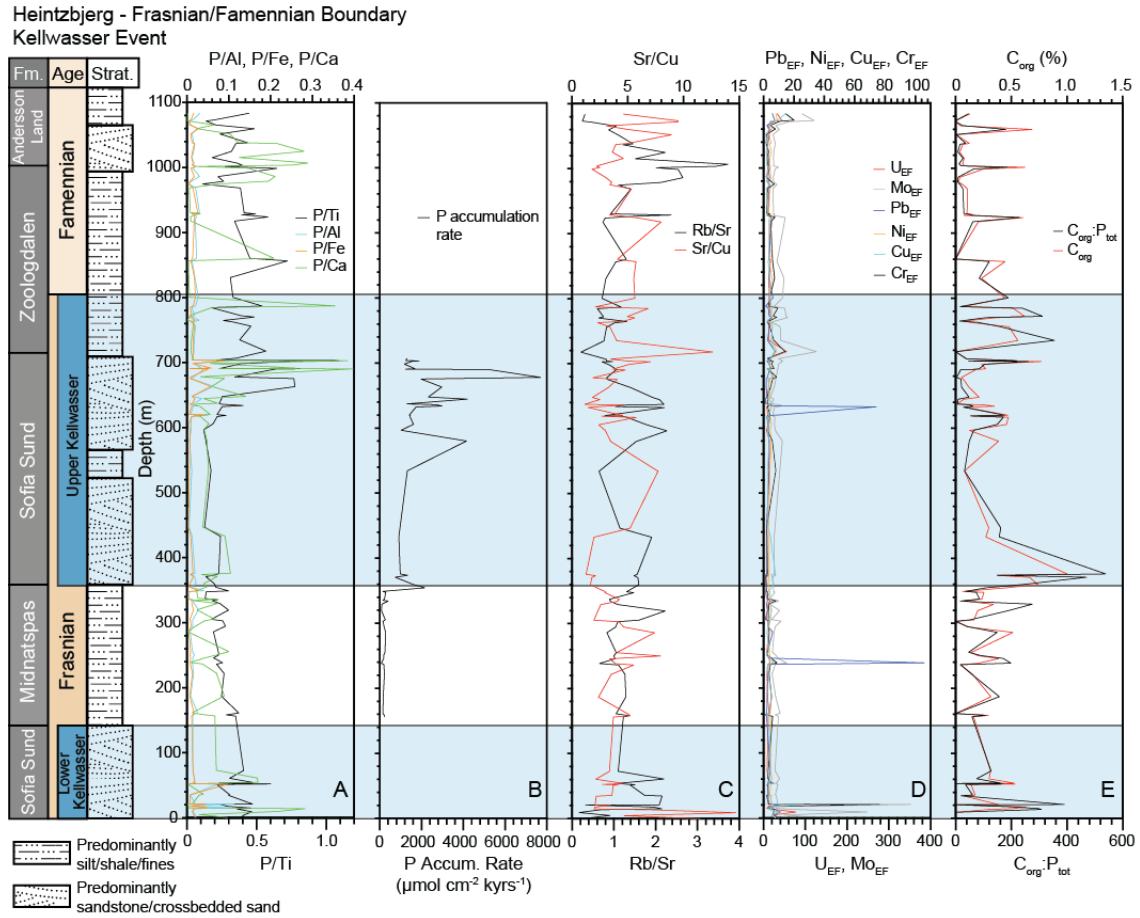


Figure 2.8. Geochemical data from Heintzbjerg, Ymer Ø, Greenland. The y-axis also shows formation, age and simplified stratigraphy. The blue shaded regions represent the upper and lower Kellwasser Events. A: Phosphorus to metal ion ratios. B: Phosphorus accumulation rate ( $\mu\text{mol P cm}^{-2} \text{ kyr}^{-1}$ ). C: Paleoclimate proxy strontium/copper and paleoweathering proxy rubidium/strontium ratios. D: Paleoredox proxies comprising enrichment factors for chromium, copper, molybdenum, nickel, lead and uranium. E: Organic carbon (wt. %) and paleoredox proxy total organic carbon/total phosphorus ratio (molar ratio).

## 2.4. Discussion

### 2.4.1. Broad Observations

Overall, the data from these sequences provide insight into geochemical cycling in Devonian lacustrine environments. In general, increases in P concentrations, particularly if there is a consistent P/Me increase, in a lacustrine stratigraphic sequence indicates an increase in net P input to the system (e.g., Filippelli, 2002). Sediment concentrations of a given element can also reflect dilution or enrichment in a mixed input system, such as one where terrigenous allochthonous input and autochthonous in-situ production both impact net sedimentation. This is typically constrained by normalizing to different elements—in the case of this study, normalizing to Ti (and Al) to constrain terrigenous input and Ca to constrain in-situ carbonate production. Uniformly, our records show a mostly stable background P signal with brief intervals of higher P concentrations, and higher P/Me ratios. Combining P/Me ratios with redox data adds additional detail regarding the genesis of P enrichment within the lakes. Paleoredox determinations remain one of the largest challenges in studies of ancient marine and particularly ancient lacustrine systems. Local lithological variations combined with changes in sedimentation rates as well as diagenetic impacts may render certain proxies ineffective (e.g., Algeo and Liu, 2020), however the general agreement of the majority of proxies employed here provides a reasonable argument that their interpretation is the most likely scenario. Overall, the striking agreement between the six EFs utilized and, to a lesser extent with  $C_{org}:P_{tot}$ , at the different sample sites is persuasive evidence that they are sentinels of actual redox conditions in these Devonian lacustrine systems. Combining



redox determinations with paleoclimate and weathering proxies was particularly effective for most sequences, providing additional context for interpretation of both redox conditions and nutrient input into the lakes.

#### 2.4.2. Climate and Weathering Interpretations

The weathering proxy Rb/Sr and paleoclimate proxy Sr/Cu generally display an antithetic relationship in each of the study sites presented here. This is important in establishing a relational link between weathering and climate in both the Orcadian Basin and the Devonian Basin in East Greenland. During wetter periods (low Sr/Cu values), higher amounts of precipitation and runoff would result in enhanced weathering (elevated Rb/Sr values). The reverse would be expected during more arid periods (elevated Sr/Cu values) with reduced precipitation and runoff resulting in a reduction in weathering rates (low Rb/Sr values). While there is sample to sample variation within the data, the inverse relationship between Rb/Sr and Sr/Cu is maintained almost universally at each of the five sites.

In the higher resolution records such as Geanies (Fig. 2.4), Hoxa Head (Fig. 2.5) and Heintzbjerg (Fig. 2.8), cyclic trends can be observed where wetter periods lead into arid periods before returning to wetter periods. These trends are consistent with what is known about regional climate in both the Orcadian Basin and the Devonian Basin in East Greenland. As discussed earlier, lake cycles within East Greenland and the Orcadian Basin are linked to Milankovitch cyclicality, with Milankovitch orbital parameters the genesis for climate variation driving the cyclicality (Astin, 1990; Kelly, 1992; Olsen, 1994; Marshall 1996; Andrews and Trewin, 2010; Andrews et al., 2016). Deep and semi-

permanent lakes formed during wetter periods followed by progressive shallowing into playa lake environments as aridity returns (Marshall and Stephenson, 1997). This approximately 100 kyr cycle is most easily identifiable in the Geanies sequence (with 12 distinct lake cycles) and particularly so in the upper half of the sequence. While the lake cycles at the Hoxa Head sequence are more difficult to separate, the samples presented here represent 21 separate lake cycles and most can be identified by the alternation of Sr/Cu from wetter to arid. Even among the smaller data sets such as Ella Ø (Fig. 2.6) and Heggli Ber (Fig. 2.7), this cyclicity can be observed. Ella Ø represents one lake cycle (thus approximately 100 kyr) and a clear trend of increasing aridity can be observed with Sr/Cu values near 5 at the base of the record, rising to 20 in the upper portion of the record. Heggli Ber represents three distinct lake cycles (~ 300 kyr) and while it is difficult to identify three lake cycles solely based on Sr/Cu ratios, there is a clear change from arid at the base of the record, to wet by 10 m, and back to arid by 25 m. Thus, the general agreement between Sr/Cu data reported here and known regional climate cyclicity combined with the expected antithetic behavior of Sr/Cu and Rb/Sr suggest that these data are generally reflective of climate and weathering conditions present at each site.

#### 2.4.3. Redox Conditions

The general agreement between the six distinct enrichment factors with both  $C_{org}$  and  $C_{org} \cdot P_{tot}$  lend confidence that these proxies are effectively capturing redox conditions within the lakes at each of these sites. In the five records presented here, all exhibit distinct periods of anoxia, with the one exception being the Heintzbjerg record. In the

Geanies sequence, significant periods of anoxia occur during lakes 9, 10, 16 and 19 (Fig. 2.4d, e). At Hoxa Head, five distinct periods of anoxia can be identified which are nearly in line with the largest increases in  $C_{org}$  at 12, 62, 68, 82 and 146 m (Fig. 2.5d, e). At Ella Ø, the presence of amorphous organic matter, and thus anoxia, throughout the sequence noted by Marshall and Stephenson (1997) is supported at various intervals by the EFs, specifically at 0.55, 0.8, 1.05 and 1.4 m (Fig. 2.6d, e). In this case,  $C_{org}:P_{tot}$  values seem out of phase with the EFs complicating redox determinations, however elevated values of  $C_{org}$  near or above 2 wt. % are present in much of the sequence which suggest that this lake was likely anoxic/suboxic from about 0.55 m to 1.5 m. At Heggli Ber, there is a clearly defined anoxic period at around 10 m, with the rest of the sequence reflecting likely oxic conditions (Fig. 2.7d, e). At Heintzbjerg, the organic matter content of this sequence was low, with  $C_{org}$  mostly below 1 wt. % (Fig. 2.8e). This is not surprising for a fluvial sequence predominantly composed of sandstone, but higher values of  $C_{org}$  are observed during both the LKW and UKW. Interestingly, elevated values of  $C_{org}:P_{tot}$  are observed during the LKW, at the onset of the UKW and at the end of the UKW. Aside from  $C_{org}:P_{tot}$ , redox proxies generally do not support the existence of anoxia in the channel lakes of this fluvial system, save for the bottommost portion of the sequence as well as at 720 m during the UKW. What is most significant across all the sites presented here is that there are distinct periods when each site hosted both oxic and anoxic systems. In some cases, such as the anoxia observed in lakes 16 and 19 at Geanies, climate fluctuations likely played a significant role in the development of anoxia as increased aridity may have led to water column stagnation, stratification and anoxia. Other cases,

such as lake 10 at Geanies, are more complex and will be discussed in detail in the following sections.

#### 2.4.4. Evidence of Enhanced Terrestrial Phosphorus Flux

In each sequence presented, there is evidence for varying levels of P enrichment throughout a given record. While the magnitude of P enrichment varies between the different sites, the relative agreement between P/Ti and other P/Me ratios in most cases suggests that P perturbations were indeed occurring. The Geanies sequence is our earliest evidence of elevated terrestrial P input. Enrichments in P/Ti and P/Fe in lake 9, and to a lesser extent lake 10, lead the sequence, both of which gradually decrease until reaching minima at the end of lake 14 (Fig. 2.4a). Concurrently, the P accumulation rate is lowest at the bottom of the sequence, building rapidly through lake 10, steadily through lake 12 and then remaining stable through lake 14 (Fig. 2.4b). The antithetic trends observed between P/Ti and P accumulation rate align with expectations if a large and relatively rapid nutrient flux perturbed this lacustrine system. Similar trends are observed in the upper portion of lake 16, lower portion of lake 18 and in lake 19 (lakes 18 and 19 concurrent with the Kačák Event) accompanying climatic shifts to wetter conditions with increases in P/Me ratios and accompanying increases in P accumulation. Beyond the Geanies sequence, these patterns are again observed at Ella Ø at 0.15, 0.85 and 1.10 m (Fig. 2.6); Heggli Ber at 10 m and, to a lesser extent, at 25 m (Fig. 2.27); and at Heintzbjerg in the first 60 m of the LKW and between 600-700 m in the UKW (Fig. 2.8). The magnitudes of the P/Ti maxima at Geanies (~ 3.1), Ella Ø (~3.7), Heggli Ber (~8.2) and Heintzbjerg (~1.1) are all significantly above background for each sequence and in

most cases sustained across multiple samples (the magnitude at Heintzbjerg is relatively small in comparison, but this is likely due to the fluvial nature of this sequence with the lithology being primarily sandstone with fine-grained material interspersed). In many of the above cases, anoxia or suboxia is concurrent with P/Ti maxima, introducing the possibility of reductive dissolution of Fe-bound P minerals driving increases in P/Ti values. However, in each instance there is either an accompanying increase in P/Fe or an increase in P accumulation rate, either of which would be indicative of an external P source. Additionally, strong correlations of P vs Ti, P vs Al, and Ti vs Al during nearly all of these elevated P/Ti intervals indicate terrestrial origin is likely (Appendix A).

Unlike the other four sites, Hoxa Head is significantly different and shows no evidence of significant nor sustained P/Ti maxima. The magnitude of the P/Ti and P accumulation rate maxima are significantly lower than most other sites and there are no observable trends in the data. The lack of an observable trend in P/Me ratios (correlations run between P and Me returned no significant values for almost the entire sequence; Appendix A) combined with the low rates of P accumulation suggest there is no significant P flux occurring throughout the entirety of this 2.1 Myr record. While this record lacks a definable P flux, it is important to consider the temporal location of this sequence (Fig. 2.1). Located in the early Givetian, Hoxa Head is well removed from the Kačák Event (latest Eifelian) and the Taghanic Crisis (late Givetian). This critical point is considered in detail in section 2.4.6.

#### 2.4.5. Model for Lake Response to Climate and Nutrient Perturbations

When designing this study, it was suspected that analyses of Devonian lacustrine and near lacustrine sequences would reveal much about both terrestrial nutrient flux and geochemical cycling within these systems. What was not necessarily expected was how similar these Devonian lakes were to extant systems regarding their internal geochemical response to external nutrient flux and climate perturbations. Our record of P input into lakes and fluvial systems ranges from the Eifelian to the early Famennian. In each case presented here, P input and climate perturbations (or both) are catalysts for a geochemical response within the lake. This is perhaps best demonstrated in the Geanies sequence given that it hosts pronounced climate fluctuations as suggested by the Sr/Cu data. At the beginning of lake 16, low Sr/Cu values are concurrent with low values of C<sub>org</sub> and no indications of anoxia. A shift from low values of Sr/Cu to high values signifies a shift to more arid conditions. Coincident with Sr/Cu maxima are indications of anoxia and a rapid rise in C<sub>org</sub> to around 4 wt. %. With the development of anoxia, P is mobilized from Fe-bound minerals and P accumulation rate drops (only slightly in this case) and P/Ti increases, reflecting an overall increase as P is liberated from the anoxic portion of the lake. This scenario is observed also in the middle of lake 19; at 56-60 m and 174-178 m at Hoxa Head; and between 1.0-1.5 m at Ella Ø. This geochemical response to arid conditions is similar to what would be expected in a modern lake.

As conditions shift from arid to wet, a similar model for lake response can be constructed. Continuing with the example of lake 16, as aridity transitions to wetter conditions, more oxic conditions would prevail within the lake as runoff increases and water column stagnation decreases. However, as conditions become wetter, redox

conditions alternate between reducing and oxidized (evidenced by the brief drop in EFs as well as  $C_{org}:P_{tot}$ ) until P input and P accumulation both rise significantly, leading to the continuation of anoxic conditions. This likely occurred for one of two reasons. The first is that wetter conditions contributed to a larger and deeper lake, briefly increasing mixing, but ultimately promoting development of stratification at depth and anoxia. The second possibility is that elevated terrestrial nutrient influx, as suggested by the P/Ti values, promoted eutrophication in the water column, sustaining anoxic conditions and increasing  $C_{org}$  preservation. The latter is the more likely for several reasons. First, elevated values of P relative to detrital input (P/Ti and P/Al) and redox cycling (P/Fe) in the upper portion of lake 16 are coincident with anoxia, suggesting an external P source. Additionally, P accumulation increases significantly in the upper portion of lake 16. Finally, sustained high values of  $C_{org}$  (around 3-5 wt. %) persist through the end of lake 16, supporting an increase in net primary production (NPP). This model of terrestrial nutrient driven eutrophication during wetter periods is observed during lakes 9, 10 and at the beginning of lake 19 (prior to the onset of arid conditions). It is also observed at Hoxa Head at 12, 62 and 145 m; at Ella Ø between 0.8-1.1 m; and at Heggli Ber between 4-11 m. At the fluvial sequence at Heintzbjerg, a nearly identical response is observed between 20-80 m during the LKW and again between 600-700 m during the UKW. Although Heintzbjerg lacks a similar redox response, the turbulence of fluvial systems tends to promote exchange with the atmosphere and more oxic conditions. Nevertheless, like the lake systems presented here, a climatically driven change to wetter conditions was accompanied by an increase in terrestrial P flux and a significant increase in P accumulation rates.

The geochemical responses to changing climatic conditions and terrestrial nutrient flux allow the construction of a basic geochemical model for Devonian freshwater systems in the Orcadian Basin and the Devonian Basin in East Greenland (Fig. 2.9). Intensely arid periods in this region are characterized generally by low rates of weathering, stable/background values of terrestrial nutrient input, and frequently, stratification-driven anoxia. During wetter periods, elevated terrestrial nutrient flux appears to drive eutrophication, sustaining high rates of  $C_{org}$  deposition and anoxia. The robustness of this model extends across each sequence presented here, beginning in the late Eifelian and extending into the early Famennian, a period spanning roughly 15 Myrs. This begs the question, what is causing the increase in terrestrial nutrient flux during some wet periods and not others?

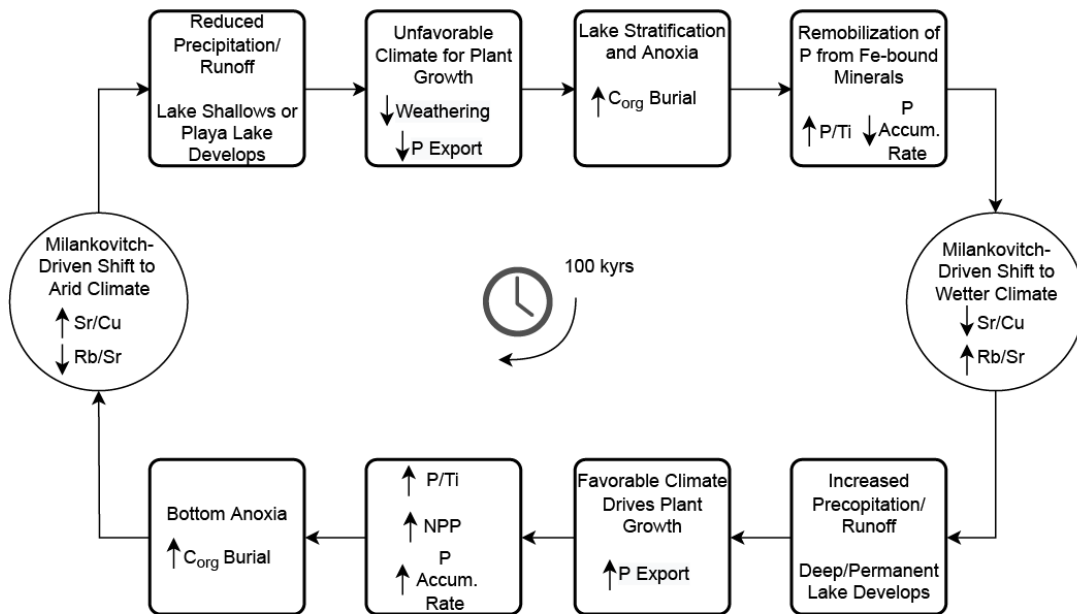


Figure 2.9. Model for internal geochemical lake response to Milankovitch-driven climatic fluctuations and terrestrial nutrient flux.



#### 2.4.6. The Land Plant Connection

A common thread connecting the most significant P/Ti perturbations in each sequence is their occurrence during the wettest conditions. This is most evident at lakes 9 and 10 at Geanies (Fig. 2.4); 0.15 m and 0.85 m at Ella Ø (Fig. 2.6); 10 m at Heggli Ber (Fig. 2.7); and between 600-700 m at Heintzbjerg (Fig. 2.8). At face value, this might suggest increased runoff resulted in increased net export. Paradoxically, some P/Ti maxima occur during periods of reduced weathering such as in lakes 9, 10, 16 and 19 at Geanies; 62 m at Hoxa Head; 1.10 m at Ella Ø; and during the first 20 m at Heintzbjerg. Thus, the explanation that increased terrestrial nutrient delivery is simply a result of increased runoff cannot fully explain the data. However, wetter conditions would produce a more favorable environment for plant growth, which could drive elevated nutrient export from the land. The significant P/Ti and P/Fe maxima observed at Geanies in lake 9 followed by the overall decrease in P input (inferred by the gradual decrease in P/Ti) from lakes 9 to 15 is consistent with what would be expected as plants colonize a young landscape, using up the readily available mineral phosphate (Fig. 2.1; Filippelli, 2008). This possibility is further evidenced by the gradual increase in P accumulation through lake 15. Similar trends between P/Me and P accumulation rates can be observed in the Heintzbjerg sequence during the UKW, with notable differences at Heintzbjerg being lower P/Ti maxima and much greater P accumulation rates. The former was addressed in section 2.4.4, but the latter could be a result of several different factors which will be explored below.

The most significant P/Ti perturbations at Heintzbjerg occur during the UKW, where P accumulation rates increase from a background value of between 100-200  $\mu\text{mol}$

P cm<sup>-2</sup> kyr<sup>-1</sup> to peak values between 4,000-8,000 μmol P cm<sup>-2</sup> kyr<sup>-1</sup> (Fig. 2.8b). These values compare strikingly well, both in magnitude and behavior, to studies of post-glacial Holocene lakes (e.g., Filippelli and Souch, 1999) and relatively well to P accumulation rates on continental margins with ranges of 80-1,200 μmol P cm<sup>-2</sup> kyr<sup>-1</sup> for the margin of Baja California and 1,100- 8,000 μmol P cm<sup>-2</sup> kyr<sup>-1</sup> for the St. Lawrence Seaway (see Filippelli, 1997 and references therein). By this stage in the Devonian, the progymnosperm *Archaeopteris* had achieved hegemony in Euramerica. During both the LKW and UKW, a warm and wet climate driven by high atmospheric CO<sub>2</sub> concentrations (a likely result of the eruption of large igneous provinces (LIPs); Racki, 2020) would have resulted in a favorable environment for plant growth. The favorable environmental conditions would have encouraged further expansion of *Archaeopteris* in Euramerica, with its substantial root systems serving to accelerate soil development in areas that had previously only been colonized by much more primitive plants. The increased plant growth and soil formation would have served to mobilize large amounts of P from relatively under-weathered or un-weathered areas. The products of this mobilization would have been effectively transported to lakes and oceans via the enhanced runoff experienced due to the wetter climate. Thus, the prevalence of deeply rooting plants combined with climatic and tectonic drivers could explain the marked difference in P accumulation rates between Geanies and Heintzbjerg while simultaneously addressing the similarity between Late Devonian and Holocene values.

Despite the favorable comparison with Holocene and modern P accumulation rate values, the comparison breaks down somewhat when considering the landscape stabilization timeframe. Where the Pleistocene-Holocene transition analog stabilized over

a period of 5-10 kyr (Filippelli and Souch, 1999), the Late Devonian landscape at Heintzbjerg reflects a stabilization time frame closer to 34 kyr. The Mid-Devonian landscape at Geanies reflects an even greater stabilization time frame on the order of 600 kyr. There are several reasons why this could be the case. First, the lakes studied by Filippelli and Souch (1999) were all small and from upland areas in headwater catchments. Thus, given their limited catchments, it is possible that landscape stabilization occurred relatively rapidly. Second, landscape colonization by plants may have been staggered throughout the catchments and not all areas were colonized at the same time. Given Milankovitch driven climatic variations in the region, it is possible that the arid/wet sequences which produced the well-defined lake cycles in the Orcadian Basin and the Devonian Basin in East Greenland, also contributed to the episodic expansion of land plants throughout the respective drainage basins, resulting in extended periods of P accumulation. Wetter periods would serve to promote growth and expansion, slowing during the subsequent arid periods, and repeating during the next climate cycle. Within each cycle, the available mineral phosphate would weather quickly, and the landscape would stabilize, with less and less total P in the system each cycle. This would result in diminished P export over a period of approximately 600 kyr as seen at Geanies. Additionally, the ubiquity and biodiversity of vascular land plants in the Holocene compared to that of the Devonian may have facilitated a much more rapid stabilization timeframe in the Holocene. A variation of this point can also be utilized to partially explain the difference in stabilization rates between Geanies and Heintzbjerg. The shallow and primitive root systems of Mid-Devonian land plants coupled with their

limited reach into continental interiors would likely have resulted in significantly slower weathering rates.

The above discussion can also serve as a partial explanation for the more short-lived P perturbations which occur in the upper half of the Geanies record (to include during the Kačák Event) as well as at Ella Ø and Heggli Ber. As land plants continued to evolve and expand into continental interiors and weather deeper soil profiles, P would be mobilized from previously un-weathered or under-weathered areas. It is possible that Milankovitch driven arid/wet cycles may have been one of the key factors driving this expansion. For example, During the Kačák Event (Geanies lakes 18 and 19), Milankovitch-driven climate cycles resulted in an insolation maximum, driving enhanced warming in the southern low latitudes (up to 6° C warmer than elsewhere on Earth; Suttner et al. 2021). This seasonal insolation maximum would have served to reinforce the continental high-pressure cell, subsequently drawing in more moisture-laden air which would then cool and precipitate out through orographic lifting over the nearby Caledonian Mountains (Marshall et al., 2007). The increased rainfall, or monsoon, would primarily manifest in the mountains, but runoff would eventually make its way through the drainage basin, feeding the lakes in the Orcadian Basin. The increased runoff resulted in the growth and interconnection of many lakes within the Orcadian Basin, forming a mega-lake, with some portions of the basin sustaining lakes which persisted through the accompanying arid periods, likely up to three lake cycles or roughly 300 kyr (Marshall et al., 2007). Our data may support this interpretation as elevated P/Ti values during lake 18 coincide with minima in Sr/Cu and elevated Rb/Sr (Fig. 2.4). Enhanced terrestrial nutrient export would be a likely result of seasonal monsoons. It is possible that the

increased rainfall in the distant mountains fueled plant growth in that region, with the nutrient pulse eventually making its way to the lakes at Geanies. While the magnitude of the P/Ti pulses seen near the Kačák Event are modest compared with others at Geanies or our other study sites, they would have likely been influenced by the geographic separation between the Caledonian Mountains and the Geanies region. A similar scenario can be applied to other lakes in the upper portion of the Geanies sequence (i.e., lake 16) and indeed to both Ella Ø and Heggli Ber. The lakes at Ella Ø and Heggli Ber however, mark a notable step forward in time to a period when both macrofossil and microfossil evidence of *Archaeopteris* existed within the region (i.e., Marshall, 1996; Marshall and Stephenson, 1997). At Ella Ø, fossilized stems of *Archaeopteris* were found at several locations throughout the sequence (Fig. 2.6), having likely floated from shore and sank in deeper water (Marshall and Stephenson, 1997). While Heggli Ber lacks similar macrofossil evidence of *Archaeopteris*, there is abundant spore evidence for its widespread presence within the Eday Flags (Marshall, 1996) along with macrofossil evidence of cladoxylopsida, another major Mid-Devonian vascular land plant group (Berry and Hilton, 2006). Both Ella Ø and Heggli Ber contain significant P/Ti perturbations (the two largest maxima observed in all five sequences) which occur during the wettest period of each record (Fig. 2.6 and Fig. 2.7, respectively). Like the upper lakes at Geanies, climate appears to be driving land plant expansion. At Ella Ø and Heggli Ber however, more advanced vascular land plants elicit a more dramatic nutrient release. Together, this evidence would seem to support the hypothesis that P weathering was episodic in nature and linked to both climate and land plant evolution.

The final piece of crucial evidence supporting the hypothesis of episodic plant expansion is the record from Hoxa Head. Unlike the other four sequences, Hoxa Head contains no substantial evidence of a terrestrial P pulse (Fig. 2.5). Indeed, the variability and lack of significant trends or maxima in P/Ti suggest a relatively stable terrestrial P flux. Given its location under an arid climate between two biologic crises, the lack of significant P perturbations within this record is perhaps its most compelling aspect. While large amounts of fossilized fish were present throughout the sequence, no fossilized plant remains were noted. If the evolution and radiation of land plants played a role in the extinction events of the Devonian, then we would not necessarily expect to find significant nutrient pulses so far outside of any known biotic crisis. Additionally, the lack of macro/microfossil evidence for the presence of *Archaeopteris* during this period in Orkney (Marshall, 1996) suggests deeply rooting plants had not yet begun to colonize this region. There is abundant spore evidence that suggests colonization by aneurophytalean progymnosperms, among other vascular plants (Marshall, 1996). However, as discussed above, the less complex root systems possessed by early Devonian vascular land plants may not have been sufficient to mobilize large amounts of P from the landscape, or the initial nutrient export may have occurred earlier in this region leaving no evidence later in the record (keeping in mind this sequence occurs well after the Kačák Event). In effect, Hoxa Head may be reflective of a landscape that had long since stabilized with respect to terrestrial P export and is likely to have remained in equilibrium until a significant event, such as the appearance of more deeply rooting plants, perturbed the system. If nothing else, Hoxa Head serves as evidence that despite the occurrence of

numerous events in the Devonian which significantly impacted biogeochemical cycling, there were periods of regional equilibrium which likely lasted millions of years.

#### 2.4.7. Global Implications

The observed peaks in P at multiple locations throughout the Mid- to Late Devonian indicate substantial global changes in the terrestrial P cycle. While these peaks may not necessarily coincide in time or in magnitude, land plant colonization was certainly not a single punctuated event, but likely staggered geographically, peaking at different times in different parts of Euramerica, and other parts of the Devonian Earth. Additionally, the evolution of root systems throughout the Devonian occurred gradually, leaving open the possibility that more deeply rooting plants could impact terrestrial nutrient export even in areas previously colonized by more primitive vascular land plants. Thus, temporal alignment of nutrient export events is not necessarily crucial. Additionally, these results point to the conclusion that large nutrient export episodes into the ocean were transitory events, lasting for brief periods at each site as colonization took hold and the initial pool of mineral-bound P was depleted. This is analogous to what is seen in post-glacial records and consistent with soil weathering trends (see Filippelli and Souch, 1999).

As plants evolved and proliferated, large scale changes to terrestrial P inventories, weathering regimes and soil development were all but inevitable. As P is mobilized and used within a system (or catchment), the total amount of reactive P will decrease over time (Fig. 2.1; Filippelli; 2008). Thus, in a large, but also geographically constrained region such as the Orcadian Basin and the Devonian Basin in East Greenland, the amount

of P in the region would be expected to decline over the roughly 15 Myrs represented by these study sites. A trendline fit across all five data sets displays a shallow, but significant negative trend in P/Ti ratios from the Eifelian to the early Famennian (Fig. 2.10a), indicating the predicted decrease in P over time. Similarly, as plants proliferate and colonize progressively more of the landscape, a transition would occur from a predominantly physical weathering regime to a primarily chemical weathering regime. Rb/Sr is most frequently used as a chemical weathering proxy, while Si/Al is a proxy for physical weathering (see section 2.2.4.3). The striking antithetic relationship between Rb/Sr and Si/Al seen in the composite records (Figs. 2.10c, d) is confirmation that this transition is taking place in the region encompassing the study sites over the course of 15 Myrs. Finally, as land plants colonize a landscape, significant changes in the ratio of silt to clay would be expected. More mature landscapes would be expected to have a higher clay content. Ti/Al and Zr/Al have been utilized as a proxy for clay content (lower values of both ratios being indicative of higher clay content). While linear fits to both Ti/Al and Zr/Al plots reveal no global trends in the data (Figs. 2.10e, f), locally weighted scatterplot smoothing (LOWESS) reveals significant smaller scale trends. There is a marked decrease in the silt/clay ratio concurrent with landscape stabilization noted in the lower half of the Geanies record, with fluctuations in the latter half of the record perhaps reflecting the noted climate instability. Through the Hoxa Head sequence, the silt/clay ratio remains low for most of the sequence, indicative of a more mature and stable landscape as suggested by interpretations of the P/Me data. While interpretations for the remainder of the record are mixed, Ti/Al ratios reflect increasing clay content exiting the LKW while Zr/Al ratios reflect increasing clay content exiting the UKW, potentially



indicating an increase in soil maturity during each event. Based on this evidence, it is clear that the colonization of land plants had a significant long-term impact on P inventory, weathering and soil development in this region.

Most studies which have attempted to address the impact of land plants on the Devonian biosphere have done so utilizing marine records, and have been crucial to our understanding of events. The redox proxy  $C_{org}:P_{tot}$  utilized in this study has been extensively reported in Devonian marine records and is often used as a proxy for benthic nutrient fluxes. In a study performed by Algeo and Ingall (2007), median  $C_{org}:P_{tot}$  ratios were compiled from 91 Phanerozoic studies, including numerous in the Devonian. Algeo and Ingall (2007) identified a significant negative trend in  $C_{org}:P_{tot}$  ratios from the Mid Devonian to the Late Devonian where median values decreased from as high as ~1625:1 to as low as 200:1. A similar negative trend is observed from Geanies to Heintzbjerg with median values dropping from 314:1 to 63:1 (Fig. 2.10b). While lacustrine and marine records would not necessarily be expected to agree, it is significant that a substantial decrease in  $C_{org}:P$  ratios observed in marine records is reflected across our terrestrial records as well. The decrease observed in marine records is likely directly related to the increase in atmospheric  $O_2$  concentrations and reflects a transition from Mid to Late Devonian of increasing ocean ventilation (Algeo and Ingall, 2007). Using this model, if Devonian seas were poorly ventilated, then it is likely that lakes shared a

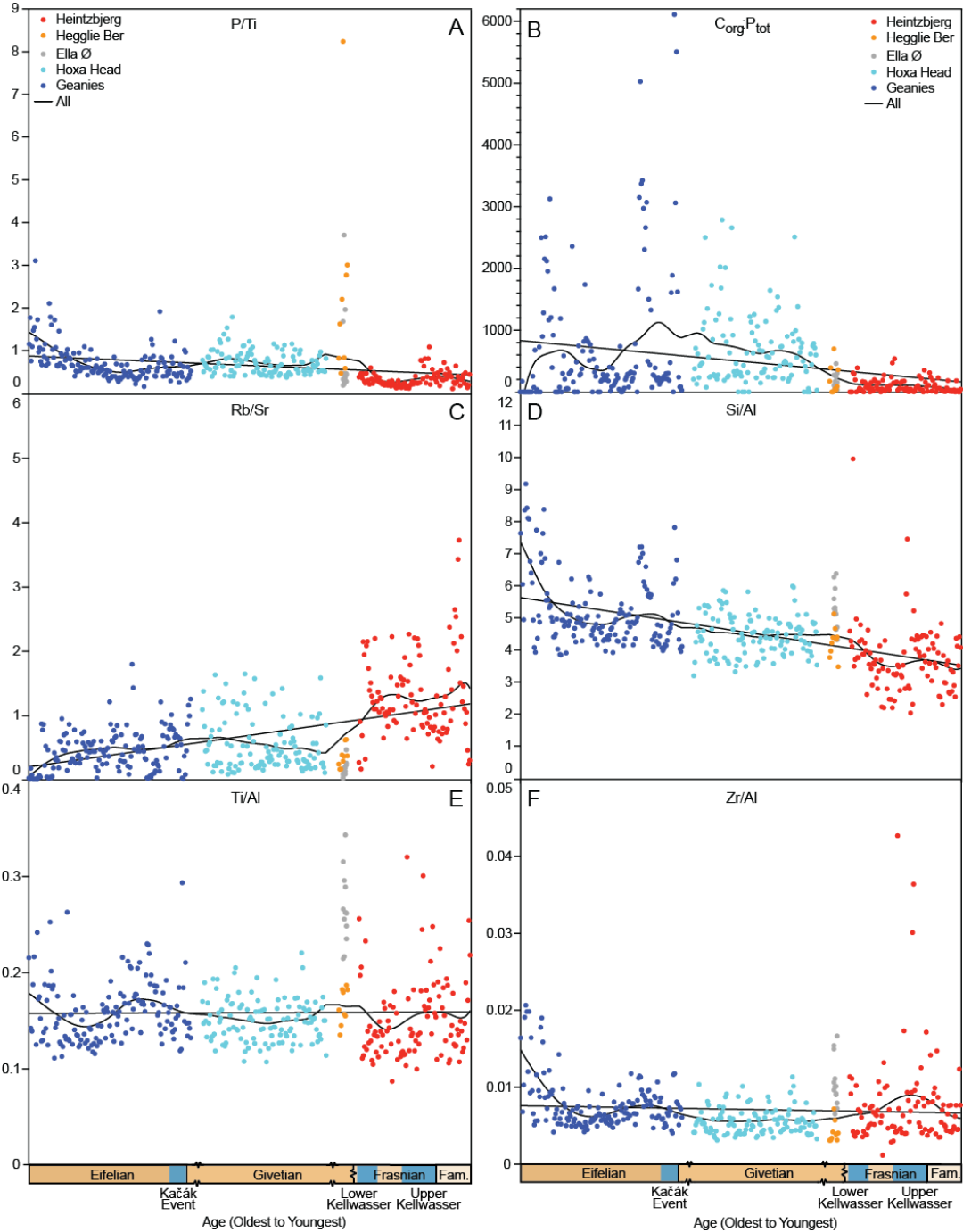


Figure 2.10. Combined data from all five sites for six distinct geochemical proxies plotted vs relative geologic age. Note the individual geologic time intervals are not plotted to scale, but are condensed to allow easier comparison amongst the individual sample sites. Trendlines in each tile are fit across the entire data set. Straight lines represent a simple linear fit, while curved lines were generated utilizing locally weighted scatterplot smoothing. The locations of the two biologic crises which can be directly associated with the sample intervals are noted with blue shading. The Taghanic Crisis in the late Givetian has been omitted to avoid the impression that the samples overlap this interval (both Ella Ø and Heggli Ber are temporally proximal, but both sequences terminate prior to the onset of the Taghanic Crisis). A: Terrestrial nutrient flux proxy phosphorus to titanium ratios. B: Total organic carbon/total phosphorus ratio (molar ratio). C: Chemical weathering proxy rubidium/strontium ratios. D: Physical

similar fate based on  $C_{\text{org}}:P_{\text{tot}}$  ratios reported here. A poorly ventilated sea would more easily be pushed into anoxia, as would a poorly ventilated lake.

Earth's oceans have been described as “on the edge of anoxia” (Watson, 2016) such that even small changes in marine NPP driven by any significant increase in P delivery to oceans have the potential to drive the formation of anoxic zones (Watson et al., 2017). This is particularly relevant in the Devonian given the prevalence of shallow, restricted and poorly ventilated seas. The particulate load of rivers would presumably have had a higher proportion of P held in primary apatite minerals, which are essentially unreactive in the marine system (Ruttenberg and Berner, 1993; Filippelli and Delaney, 1996). Some of the particulates may be in the form of early soil forming materials which could have contained P trapped in iron oxides and oxyhydroxides. Under anoxic conditions, these minerals readily dissolve, releasing P back into the water column where it can be utilized once again, driving an increase in NPP (Filippelli, 2002; Murphy et al., 2000). If plant colonization took place in the staggered manner suggested, the presence of significant P pulses staggered temporally and geographically (but in proximity to one another with respect to geologic time), whether transient or sustained, have the potential to cause a positive feedback loop in an anoxic environment and create self-sustaining eutrophication long after termination of the P pulse.

This presents an interesting possibility regarding sustained eutrophication in Devonian oceans. Given the residence times for P in modern oceans of 15-30 kyr (Ruttenberg, 1993; Filippelli and Delaney, 1997) and assuming a similar value for Devonian oceans, it is possible that that the geographically distinct weathering events may be a driving factor in sustained marine eutrophication. As elevated nutrient input

declines in one region, eutrophication would be self-sustaining for multiple residence times, which may be long enough for colonization to occur in a separate geographic region and thus drive another distinct eutrophication pulse. Additionally, with widespread eutrophication-driven anoxia, this residence time might be longer given an active P-Fe shuttle remobilizing deep P. This would, in effect, provide the catalyst to drive sustained eutrophication events present in Devonian oceans. Ultimately, new P supply to marine environments is controlled by the weathering of continental rocks, which is significantly increased by biota (Lovelock and Watson, 1982; Watson et al., 2017). As demonstrated by Lenton et al. (2012), the presence of a biological agent such as moss increases P weathering by as much as a factor of 60. Thus, even if plant colonization increased by just a few percent of the land surface, this would effectively double the flux of P into the Devonian oceans (Lenton et al., 2012).

Our record of P input into lakes and fluvial systems ranges from the Eifelian to the early Famennian. In each case presented here, P input is a catalyst for a geochemical response within the lake (Fig. 2.9). Devonian lakes appear to respond similarly to modern lakes, which brings up another series of interesting possibilities. If Devonian lakes responded no differently than modern lakes, were land plants and forest development truly that important with respect to geochemical cycling in lakes? Or (perhaps an entirely different scenario, given the similarity with modern lakes) could it be that significant plant-enhanced P weathering began before the Mid Devonian, and ecosystems had stabilized to a pseudo modern state? Did vascular land plants impact global biogeochemical cycling far earlier than we suspect, causing Devonian lakes to look so much like modern lakes? After all, it was during the Devonian that atmospheric CO<sub>2</sub> and

O<sub>2</sub> reached levels comparable to the Holocene. Given that land plants have been around since at least the Silurian, this scenario seems more than plausible. Were it not for the record at Heintzbjerg, this argument is supported. Given the similarity in P response during the UKW to those of Holocene analogues, there is little doubt that we are seeing initial landscape stabilization in this region. The fact that this nutrient export is concurrent with a major Paleozoic extinction event provides a compelling argument that elevated nutrient export driven by land plant expansion certainly played a role in exacerbating at least one biotic crisis in the Devonian. If this were still occurring in the Frasnian, it could have occurred earlier in the Devonian in other regions and suggests that landscape stabilization had not occurred everywhere even by the Late Devonian. The timing of regional colonization by deeply rooting plants such as *Archaeopteris* would have likely played a major factor in determining how and when such pulses would have impacted the Devonian biosphere. With the recent discovery of mid-Givetian forests containing *Archaeopteris* (as well as significant root systems; Stein et al., 2020), this is certainly plausible. Given the success in deciphering geochemical cycling in Devonian lacustrine environments in this study, these methods can and should be applied to other Devonian lacustrine sequences in geographically distinct locations to support or refute the implication of land plants in the biotic crises of the Period. Additionally, it would be prudent to investigate early Devonian and even Late Silurian lacustrine sequences.

## 2.5. Conclusions

Large-scale changes in the terrestrial P cycle occurred at critical evolutionary intervals in the Devonian in at least one portion of Euramerica. Significant mobilization

of P occurred in close temporal proximity to global biotic crises. These transient pulses sustained a long-term eutrophication feedback. Similar behavior to modern lacustrine systems was observed in all five study locations with respect to internal geochemical responses to external nutrient input and climate variability. Sites in proximity to a biotic crisis displayed evidence of enhanced nutrient input, except for the Hoxa Head sequence which is not temporally proximal to a biotic crisis. The Hoxa Head sequence provides a >2-million-year record of steady state lacustrine cycling free from significant external nutrient pulses, thus providing a basis with which to compare the other four sequences.

Land plant expansion on different continents was likely staggered, but if evidence on multiple continents occurring within a few million years of each other is shown for major transient P pulses such as those reported here for East Greenland, Easter Ross and Orkney, we can more confidently develop a temporally relevant model of nutrient inputs. The terrestrial evolution of the soil pool and marine extinction events typically last multiple millions of years, making timing differences of a few millions of years among different continents largely irrelevant. Much work remains to be done to constrain the global picture, particularly with the addition of data for lacustrine and near-lacustrine sequences from Gondwana and other parts of Euramerica and paleo-China, but putting together these pieces of the paleogeographic puzzle, section by section, should lead to answers to the long-standing questions of the role of plant evolution in the extraordinary biotic events of the Devonian.

## 2.6. References

Aboussalam, Z.S., and Becker, R.T., 2011, The global Taghanic Biocrisis (Givetian) in the eastern Anti-Atlas, Morocco: *Palaeogeography, palaeoclimatology, palaeoecology*, v. 304, p. 136–164.

Algeo, T.J., and Ingall, E., 2007, Sedimentary Corg:P ratios, paleocean ventilation, and Phanerozoic atmospheric pO<sub>2</sub>: *Palaeogeography, palaeoclimatology, palaeoecology*, v. 256, p. 130–155.

Algeo, T.J., and Liu, J., 2020, A re-assessment of elemental proxies for paleoredox analysis: *Chemical geology*, v. 540, p. 119549.

Algeo, T.J., and Scheckler, S.E., 2010, Land plant evolution and weathering rate changes in the Devonian: *Journal of earth science*, v. 21, p. 75–78.

Algeo, T.J., and Scheckler, S.E., 1998, Terrestrial-marine teleconnections in the Devonian: links between the evolution of land plants, weathering processes, and marine anoxic events: *Philosophical transactions of the Royal Society of London. Series B, Biological sciences*, v. 353, p. 113–130.

Algeo, T.J., Scheckler, S.E., and Maynard, J.B., 2001, 12. Effects of the middle to late Devonian spread of vascular land plants on weathering regimes, marine biotas, and global

climate, in Gensel, P.G. and Edwards, D. eds., *Plants Invade the Land*, New York Chichester, West Sussex, Columbia University Press, p. 213–236.

Algeo, T. J., Berner, R. A., Maynard, J. B., & Scheckler, S. E., 1995, Late Devonian oceanic anoxic events and biotic crises: “rooted” in the evolution of vascular land plants: *GSA today*, v. 5, p. 45–66.

Andrews, S.D., Cornwell, D.G., Trewin, N.H., Hartley, A.J., and Archer, S.G., 2016, A 2.3 million year lacustrine record of orbital forcing from the Devonian of northern Scotland: *Journal of the Geological Society*, v. 173, p. 474–488.

Andrews, S.D., and Hartley, A.J., 2015, The response of lake margin sedimentary systems to climatically driven lake level fluctuations: Middle Devonian, Orcadian Basin, Scotland: *Sedimentology*, v. 62, p. 1693–1716.

Andrews, S.D., and Trewin, N.H., 2010, Periodicity determination of lacustrine cycles from the Devonian of Northern Scotland: *Scottish journal of geology*, v. 46, p. 143–155.

Astin, T.R., 1990, The Devonian lacustrine sediments of Orkney, Scotland; implications for climate cyclicity, basin structure and maturation history: *Journal of the Geological Society*, v. 147, p. 141–151.



Becker, R.T., Königshof, P., and Brett, C.E., 2016, Devonian climate, sea level and evolutionary events: an introduction: Geological Society Special Publication, v. 423, p. 1–10.

Berry, C.M., and Hilton, J., 2006, Givetian (Middle Devonian) cladoxylopid ‘ferns’ from Orkney, northern Scotland: Transactions of the Royal Society of Edinburgh Earth Sciences, v. 97, p. 65–73.

Berry, C.M., and Marshall, J.E.A., 2015, Lycopoid forests in the early Late Devonian paleoequatorial zone of Svalbard: Geology, v. 43, p. 1043–1046.

Blom, H., Clack, J. A., Ahlberg, P. E., & Friedman, M., 2007, Devonian vertebrates from East Greenland: a review of faunal composition and distribution: Geodiversitas, v. 29, p. 119–141.

Blomqvist, S., Gunnars, A., and Elmgren, R., 2004, Why the limiting nutrient differs between temperate coastal seas and freshwater lakes: A matter of salt: Limnology and oceanography, v. 49, p. 2236–2241.

Cao, H., Guo, W., Shan, X., Ma, L., and Sun, P., 2015, Paleolimnological environments and organic accumulation of the Nenjiang Formation in the southeastern Songliao Basin, China: Oil Shale, v. 32, p. 5.

Chadwick, O.A., Derry, L.A., Vitousek, P.M., Huebert, B.J., and Hedin, L.O., 1999, Changing sources of nutrients during four million years of ecosystem development: *Nature*, v. 397, p. 491–497.

Clay, M., Norton, M.G., Coney, P., and Davis, G.H., 1986, Collapse of the Caledonian orogen and the Old Red Sandstone: *Nature*, v. 323, p. 147–149.

Correll, D.L., 1999, Phosphorus: a rate limiting nutrient in surface waters: *Poultry Science*, v. 78, p. 674–682.

Davies, N. S., Berry, C. M., Marshall, J. E., Wellman, C. H., & Lindemann, F. J., 2021, The Devonian Landscape Factory: plant-sediment interactions in the Old Red Sandstone of Svalbard and the rise of vegetation as a biogeomorphic agent: *Journal of the Geological Society*, v. 178, p. 202–225.

De Boer P. L. & Smith D. G., O.H., 1994, Orbital forcing on continental depositional systems—lacustrine and fluvial cyclicity in the Devonian of East Greenland: *Alluvial Sedimentation*, v. 19, p. 429–438.

Donovan, R.N., Foster, R.J., and Westoll, T.S., 1974, 8.—A stratigraphical revision of the Old Red Sandstone of north-eastern Caithness: *Transactions of the Royal Society of Edinburgh*, v. 69, p. 167–201.

Falkowski, P.G. et al., 2011, Ocean deoxygenation: Past, present, and future: *Eos*, v. 92, p. 409–410.

Filippelli, G.M., 1997, Controls on phosphorus concentration and accumulation in oceanic sediments: *Marine Geology*, v. 139, p. 231–240.

Filippelli, G.M., 2002, The Global Phosphorus Cycle: Reviews in Mineralogy and Geochemistry, v. 48, p. 391–425.

Filippelli, G.M., 2008, The global phosphorus cycle: Past, present, and future: *Elements (Quebec)*, v. 4, p. 89–95.

Filippelli, G.M., and Delaney, M.L., 1996, Phosphorus geochemistry of equatorial Pacific sediments: *Geochimica et Cosmochimica Acta*, v. 60, p. 1479–1495.

Filippelli, G.M., and Delaney, M.L., 1994, The oceanic phosphorus cycle and continental weathering during the Neogene: *Paleoceanography*, v. 9, p. 643–652.

Filippelli, G.M., and Souch, C., 1999, Effects of climate and landscape development on the terrestrial phosphorus cycle: *Geology*, v. 27, p. 171.

Filippelli, G.M., Souch, C., Horn, S.P., and Newkirk, D., 2010, The pre-Colombian footprint on terrestrial nutrient cycling in Costa Rica: insights from phosphorus in a lake sediment record: *Journal of Paleolimnology*, v. 43, p. 843–856.

Fu, J., Li, S., Xu, L., and Niu, X., 2018, Paleo-sedimentary environmental restoration and its significance of Chang 7 Member of Triassic Yanchang Formation in Ordos Basin, NW China: *Petroleum Exploration and Development*, v. 45, p. 998–1008.

Giesen, P., and Berry, C.M., 2013, Reconstruction and growth of the early tree calamophyton (pseudosporochnales, cladoxylopsida) based on exceptionally complete specimens from Lindlar, Germany (mid-Devonian): Organic connection of calamophyton branches and duisbergia trunks: *International Journal of Plant Sciences*, v. 174, p. 665–686.

House, M.R., 1985, Correlation of mid-Palaeozoic ammonoid evolutionary events with global sedimentary perturbations: *Nature*, v. 313, p. 17–22.

House, M.R., 2002, Strength, timing, setting and cause of mid-Palaeozoic extinctions: *Palaeogeography, Palaeoclimatology, Palaeoecology*, v. 181, p. 5–25.

Jurinak, J.J., Dudley, L.M., Allen, M.F., and Knight, W.G., 1986, The role of calcium oxalate in the availability of phosphorus in soils of semiarid regions: A thermodynamic study: *Soil Science*, v. 142, p. 255–261.

Kaiser, S.I., Aretz, M., and Becker, R.T., 2016, The global Hangenberg Crisis (Devonian–Carboniferous transition): review of a first-order mass extinction: Geological Society Special Publication, v. 423, p. 387–437.

Kelly, S.B., 1992, Milankovitch cyclicity recorded from Devonian non-marine sediments: Terra Nova, v. 4, p. 578–584.

Kenrick, P., and Strullu-Derrien, C., 2014, The origin and early evolution of roots: Plant Physiology, v. 166, p. 570–580.

Krom, M.D., Kress, N., Brenner, S., and Gordon, L.I., 1991, Phosphorus limitation of primary productivity in the eastern Mediterranean Sea: Limnology and Oceanography, v. 36, p. 424–432.

Larsen, P.-H., Olsen, H., and Clack, J.A., 2008, The Devonian basin in East Greenland—Review of basin evolution and vertebrate assemblages, in Memoir 202: The Greenland Caledonides: Evolution of the Northeast Margin of Laurentia, Geological Society of America, p. 273–292.

Lenton, T.M., Crouch, M., Johnson, M., Pires, N., and Dolan, L., 2012, First plants cooled the Ordovician: Nature Geoscience, v. 5, p. 86–89.

Lenton, T.M., Dahl, T.W., Daines, S.J., Mills, B.J.W., Ozaki, K., Saltzman, M.R., and Porada, P., 2016, Earliest land plants created modern levels of atmospheric oxygen: *Proceedings of the National Academy of Sciences of the United States of America*, v. 113, p. 9704–9709.

Li, Q., Wu, S., Xia, D., You, X., Zhang, H., and Lu, H., 2020, Major and trace element geochemistry of the lacustrine organic-rich shales from the Upper Triassic Chang 7 Member in the southwestern Ordos Basin, China: Implications for paleoenvironment and organic matter accumulation: *Marine and petroleum geology*, v. 111, p. 852–867.

Liang, J., Tang, D., Xu, H., Tao, S., Li, C., and Gou, M., 2014, Formation conditions of Jimusaer oil shale at the northern foot of Bogda Mountain, China: *Oil Shale*, v. 31, p. 19.

Liu, J., and Algeo, T.J., 2020, Beyond redox: Control of trace-metal enrichment in anoxic marine facies by watermass chemistry and sedimentation rate: *Geochimica et cosmochimica acta*, v. 287, p. 296–317.

Lovelock, J.E., and Watson, A.J., 1982, The regulation of carbon dioxide and climate: Gaia or geochemistry: *Planetary and Space Science*, v. 30, p. 795–802.

Manger, G.E., 1963, Porosity and bulk density of sedimentary rocks: Washington D.C., United States Government Printing Office.

Marshall, J.E.A., 1996, *Rhabdosporites langii*, *Geminospora lemurata* and *Contagisporites optivus*: an origin for heterospory within the progymnosperms: *Review of Palaeobotany and Palynology*, v. 93, p. 159–189.

Marshall, J.E.A., Astin, T.R., Brown, J.F., Mark-Kurik, E., and Lazauskiene, J., 2007, Recognizing the Kačák Event in the Devonian terrestrial environment and its implications for understanding land–sea interactions: *Geological Society Special Publication*, v. 278, p. 133–155.

Marshall, J.E.A., Brown, J.F., and Astin, T.R., 2011, Recognising the Taghanic Crisis in the Devonian terrestrial environment and its implications for understanding land–sea interactions: *Palaeogeography, Palaeoclimatology, Palaeoecology*, v. 304, p. 165–183.

Marshall, J.E.A., and Hemsley, A.R., 2003, A Mid Devonian seed-megaspore from East Greenland and the origin of the seed plants: *Palaeontology*, v. 46, p. 647–670.

Marshall, J E A & Hewett, T, 2003, Devonian, in Evans, D., Graham, C., Armour, A. & Bathurst, P. ed., *The Millennium Atlas*, London, Geological Society.

Marshall, J.E.A., and Stephenson, B.J., 1997, Sedimentological responses to basin initiation in the Devonian of East Greenland: *Sedimentology*, v. 44, p. 407–419.

McGhee, G., 1996, *The Late Devonian mass extinction: The Frasnian/Famennian crisis*: New York, NY, Columbia University Press.

McLennan, S.M., 2001, Relationships between the trace element composition of sedimentary rocks and upper continental crust: trace element composition and upper continental crust: *Geochemistry, Geophysics, Geosystems*: G(3), v. 2, doi:10.1029/2000gc000109.

McPeck, T., Wang, X., Brown, K., & Filippelli, G., 2007, Rates of carbon ingrowth and nutrient release from young Icelandic basalts: *Jökull*, v. 57, p. 37–44.

Meyer, K.M., and Kump, L.R., 2008, Oceanic Euxinia in Earth history: Causes and consequences: *Annual Review of Earth and Planetary Sciences*, v. 36, p. 251–288.

Meyer-Berthaud, B., Scheckler, S.E., and Wendt, J., 1999, *Archaeopteris* is the earliest known modern tree: *Nature*, v. 398, p. 700–701.

Meyer-Berthaud, B., Soria, A., and Decombeix, A.-L., 2010, The land plant cover in the Devonian: a reassessment of the evolution of the tree habit: *Geological Society Special Publication*, v. 339, p. 59–70.



Morris, J.L. et al., 2015, Investigating Devonian trees as geo-engineers of past climates: linking palaeosols to palaeobotany and experimental geobiology: *Palaeontology*, v. 58, p. 787–801.

Murphy, A.E., Sageman, B.B., Hollander, D.J., Lyons, T.W., and Brett, C.E., 2000, Black shale deposition and faunal overturn in the Devonian Appalachian Basin: Clastic starvation, seasonal water-column mixing, and efficient biolimiting nutrient recycling: *Paleoceanography*, v. 15, p. 280–291.

Murray, R.W., and Leinen, M., 1996, Scavenged excess aluminum and its relationship to bulk titanium in biogenic sediment from the central equatorial Pacific Ocean: *Geochimica et Cosmochimica Acta*, v. 60, p. 3869–3878.

Old red sandstone, northern highlands of Scotland Bgs.ac.uk,  
[http://earthwise.bgs.ac.uk/index.php/Old\\_Red\\_Sandstone,\\_Northern\\_Highlands\\_of\\_Scotl](http://earthwise.bgs.ac.uk/index.php/Old_Red_Sandstone,_Northern_Highlands_of_Scotl)  
and (accessed November 2021).

Olsen, H., & Larsen, P. H., 1993, Structural and climatic controls on fluvial depositional systems: Devonian, North-East Greenland: *Alluvial Sedimentation*, v. 17, p. 401–423.

Pan, Y., Huang, Z., Li, T., Guo, X., Xu, X., and Chen, X., 2020, Environmental response to volcanic activity and its effect on organic matter enrichment in the Permian Lucaogou

Formation of the Malang Sag, Santanghu Basin, Northwest China: *Palaeogeography, Palaeoclimatology, Palaeoecology*, v. 560, p. 110024.

Pattan, J.N., and Shane, P., 1999, Excess aluminum in deep sea sediments of the Central Indian Basin: *Marine Geology*, v. 161, p. 247–255.

Pe-Piper, G., Karim, A. and Piper, D.J., 2011, Authigenesis of titania minerals and the mobility of Ti: new evidence from pro-deltaic sandstones, Cretaceous Scotian Basin, Canada: *Journal of Sedimentary Research*, v. 81, p. 762-773.

Percival, L.M.E., Davies, J.H.F.L., Schaltegger, U., De Vleeschouwer, D., Da Silva, A.-C., and Föllmi, K.B., 2018, Precisely dating the Frasnian–Famennian boundary: implications for the cause of the Late Devonian mass extinction: *Scientific Reports*, v. 8, doi:10.1038/s41598-018-27847-7.

Piombino, A., 2016, The heavy links between geological events and vascular plants evolution: A brief outline: *International Journal of Evolutionary Biology*, v. 2016, p. 9264357.

Planavsky, N.J., Rouxel, O.J., Bekker, A., Lalonde, S.V., Konhauser, K.O., Reinhard, C.T., and Lyons, T.W., 2010, The evolution of the marine phosphate reservoir: *Nature*, v. 467, p. 1088–1090.

Quirk, J., Leake, J.R., Johnson, D.A., Taylor, L.L., Saccone, L., and Beerling, D.J., 2015, Constraining the role of early land plants in Palaeozoic weathering and global cooling: *Proceedings. Biological Sciences*, v. 282, p. 20151115.

Racki, G., 2005, Toward understanding Late Devonian global events: few answers, many questions: *Developments in Palaeontology and Stratigraphy*, v. 20, p. 5–36.

Racki, G., 2020, A volcanic scenario for the Frasnian-Famennian major biotic crisis and other Late Devonian global changes: more answers than questions?: *Global and Planetary Change*, v. 189, p. 103174.

Ruttenberg, K.C., 1993, Reassessment of the oceanic residence time of phosphorus: *Chemical Geology*, v. 107, p. 405–409.

Ruttenberg, K.C., 2003, The Global Phosphorus Cycle, in *Treatise on Geochemistry*, Elsevier, p. 585–643.

Ruttenberg, K.C., and Berner, R.A., 1993, Authigenic apatite formation and burial in sediments from non-upwelling, continental margin environments: *Geochimica et Cosmochimica Acta*, v. 57, p. 991–1007.

Santos, I.R., Chen X., Lecher, A.L., Sawyer, A.H., Moosdorf, N., Rodellas, V., Tamborski, J., Cho, H.M., Dimova, N., Sugimoto, R. and Bonaglia, S., 2021, Submarine

groundwater discharge impacts on coastal nutrient biogeochemistry: *Nature Reviews Earth and Environment*, v. 2, p. 307-323.

Shen, L., Wang, J., Shen, H., Fu, X., Wan, Y., Song, C., Zeng, S., Dai, J., and Wang, D., 2020, Geochemistry of the Eocene clastic sediments (Suonahu Formation) in the North Qiangtang Basin, Tibet: implications for paleoclimate conditions, provenance and tectonic setting: *Canadian Journal of Earth Sciences*, v. 57, p. 40–55.

Slomp, C.P., and Van Cappellen, P., 2004, Nutrient inputs to the coastal ocean through submarine groundwater discharge: controls and potential impact: *Journal of Hydrology*, v. 295, p. 64-86.

Speed, R.G., 1999, Kerogen variation in a Devonian half graben system: University of Southampton. Thesis or Dissertation citation here

Stein, W.E. et al., 2020, Mid-Devonian *Archaeopteris* roots signal revolutionary change in earliest fossil forests: *Current Biology: CB*, v. 30, p. 421- 431.e2.

Stein, W.E., Berry, C.M., Hernick, L.V., and Mannolini, F., 2012, Surprisingly complex community discovered in the mid-Devonian fossil forest at Gilboa: *Nature*, v. 483, p. 78–81.

Stein, W.E., Mannolini, F., Hernick, L.V., Landing, E., and Berry, C.M., 2007, Giant cladoxylopsid trees resolve the enigma of the Earth's earliest forest stumps at Gilboa: *Nature*, v. 446, p. 904–907.

Strother, P.K., and Foster, C., 2021, A fossil record of land plant origins from charophyte algae: *Science (New York, N.Y.)*, v. 373, p. 792–796.

Suttner, T.J., Kido, E., Joachimski, M.M., Vodrážková, S., Pondrelli, M., Corradini, C., Corrigan, M.G., Simonetto, L., and Kubajko, M., 2021, Paleotemperature record of the Middle Devonian Kačák Episode: *Scientific Reports*, v. 11, p. 1-10.

Tang, L., Song, Y., Pang, X., Jiang, Z., Guo, Y., Zhang, H., Pan, Z., and Jiang, H., 2020, Effects of paleo sedimentary environment in saline lacustrine basin on organic matter accumulation and preservation: A case study from the Dongpu Depression, Bohai Bay Basin, China: *Journal of Petroleum Science & Engineering*, v. 185, p. 106669.

Torsvik, T.H., and Cocks, L.R.M., 2004, Earth geography from 400 to 250 Ma: a palaeomagnetic, faunal and facies review: *Journal of the Geological Society*, v. 161, p. 555–572.

Trewin, N.H., and Thirlwall, M.F., 2002, The old red sandstone, in Trewin, N.H. ed., *The Geology of Scotland*, The Geological Society of London, p. 213–249.

Vitousek, P. M., and Farrington, H., 1997, Nutrient limitation and soil development: Experimental test of a biogeochemical theory: *Biogeochemistry*, v. 37, p. 63–75.

Vitousek, P.M., Porder, S., Houlton, B.Z., and Chadwick, O.A., 2010, Terrestrial phosphorus limitation: mechanisms, implications, and nitrogen-phosphorus interactions: *Ecological applications: a publication of the Ecological Society of America*, v. 20, p. 5–15.

Vosoughi Moradi, A., Sarı, A., and Akkaya, P., 2016, Geochemistry of the Miocene oil shale (Hançili Formation) in the Çankırı-Çorum Basin, Central Turkey: Implications for Paleoclimate conditions, source–area weathering, provenance and tectonic setting: *Sedimentary geology*, v. 341, p. 289–303.

Walker, T.W., and Syers, J.K., 1976, The fate of phosphorus during pedogenesis: *Geoderma*, v. 15, p. 1–19.

Watson, A.J., 2016, Oceans on the edge of anoxia: *Science (New York, N.Y.)*, v. 354, p. 1529–1530.

Watson, A.J., Lenton, T.M., and Mills, B.J.W., 2017, Ocean deoxygenation, the global phosphorus cycle and the possibility of human-caused large-scale ocean anoxia: *Philosophical transactions. Series A, Mathematical, physical, and engineering sciences*, v. 375, p. 20160318.

Wei, W., and Algeo, T.J., 2020, Secular variation in the elemental composition of marine shales since 840 Ma: Tectonic and seawater influences. *Geochimica et Cosmochimica Acta*, 287, pp.367-390.

Wellman, C.H., Osterloff, P.L., and Mohiuddin, U., 2003, Fragments of the earliest land plants: *Nature*, v. 425, p. 282–285.

Winchester, J.W., 1978, *The Ocean-Atmosphere System: The Chemistry of the Atmosphere and Oceans*. Heinrich D. Holland. Wiley-Interscience, New York, 1978. xvi, 352 pp., illus.: *Science* (New York, N.Y.), v. 202, p. 1179–1180.

Xu, H., Liu, B., and Wu, F., 2010, Spatial and temporal variations of Rb/Sr ratios of the bulk surface sediments in Lake Qinghai: *Geochemical Transactions*, v. 11, p. 3.

## CHAPTER 3. LAND PLANT EVOLUTION AND VOLCANISM LED TO THE LATE DEVONIAN MASS EXTINCTION

### 3.1. Introduction

The Late Devonian mass extinction (also called the Frasnian-Famennian extinction and alternatively the Kellwasser Event) is one of the “Big Five” Phanerozoic mass extinctions (Raup and Sepkoski, 1982; McGhee et al., 2013). It is characterized by two distinct episodes of widespread marine anoxia (Bond et al., 2004; Carmichael et al., 2019) expressed in the sedimentary record by the deposition of distinct black shale horizons (Bond et al., 2004; Carmichael et al., 2019; Joachimski and Buggisch, 1993). It is largely thought to have occurred in two distinct pulses, the earlier being the Lower Kellwasser (LKW) and the latter the Upper Kellwasser (UKW). Both pulses are associated with significant global carbon cycle perturbations, with positive carbon-isotope excursions ( $\delta^{13}\text{C}$ ) ranging up to 4‰ (Carmichael et al., 2019; Joachimski and Buggisch, 1993; Joachimski and Buggisch, 2002; Chen et al., 2005). The development of sustained marine anoxia is linked to the demise of bottom-dwelling marine species (Bond et al., 2004; House, 1985; Buggisch, 1991), and it is also thought that water column oxygen depletion played a direct role in the catastrophic collapse of Devonian reef ecosystems (McGhee et al., 2013; Bond et al., 2013). Proposed mechanisms for the Late Devonian extinction include climate perturbations (both warming and cooling (Thompson and Newton, 1988; Joachimski et al., 2002; Xu et al., 2012; Huang et al., 2018; Wang et al., 2018), astronomical forcing (Da Silva et al., 2020; Lu et al., 2021), bolide impacts (Claeys et al., 1992; McGhee, 2001), large igneous province (LIP)



eruptions (Racki et al., 2018; Racki, 2020), enhanced terrestrial weathering associated with mountain building (Averbuch et al., 2005; Percival et al., 2019) and the evolution and expansion of land plants (Algeo et al., 1995; Algeo and Scheckler, 1998; Smart et al., 2022). Despite the lack of agreement on a single initiating event, many studies cite nutrient influx either from elevated terrestrial input or marine upwelling as a contributing factor (Carmichael et al., 2019; Smart et al., 2022; Percival et al., 2020).

Global biogeochemical perturbations associated with the Late Devonian extinction have been widely reported (i.e., global positive  $\delta^{13}\text{C}$  excursions). Numerous investigations into the geologic record across the KW events revealed additional global trends which exist independent of extinction ascription, such as the precipitous decline in atmospheric  $\text{CO}_2$  (Royer et al., 2007; Franks et al., 2014; Royer, 2014; Lenton et al., 2018), the rise in atmospheric  $\text{O}_2$  to near modern levels (Lenton et al., 2018; Algeo and Ingall, 2007; Berner, 2009; Zhang et al., 2020) and the overall increase in global average temperature (Scotese et al., 2021). Given the wealth of information in the geologic record, the question arises as to whether global biogeochemical cycling supports any of these theories regarding the causal factor (or factors) driving the Late Devonian extinction. This question is particularly relevant as it relates to two diverging theories regarding extinction initiation, large scale volcanism and enhanced terrestrial nutrient export related to land plant evolution and expansion. Three significant LIP eruptions occurred temporally proximal to the KW events (Fig. 3.1b), suggesting large scale volcanism had some impact on biogeochemical cycling, and may have played a significant role in contemporaneous mass extinction. At the same time, land plant evolution reached a zenith in the Late Devonian as the earliest trees with significant root

systems achieved hegemony by the late Famennian (Meyer-Berthaud et al., 1999; Meyer-Berthaud et al., 2010; Stein et al., 2020). These magmatic and biotic events potentially influenced global geochemical cycles in the Devonian, each leaving their own forensic footprint in the geologic record. Here we investigate the global geochemical impact of each of these events by utilizing new proximal continental lacustrine records of phosphorus accumulation rate changes and employing an Earth system box model to simulate the carbon, nitrogen, phosphorus, oxygen and sulfur biogeochemical cycles. We explore both pulses of the Late Devonian extinction to determine which of these two processes, magmatic or biologic, could most plausibly have resulted in the observed geochemical changes recorded in the rock record.

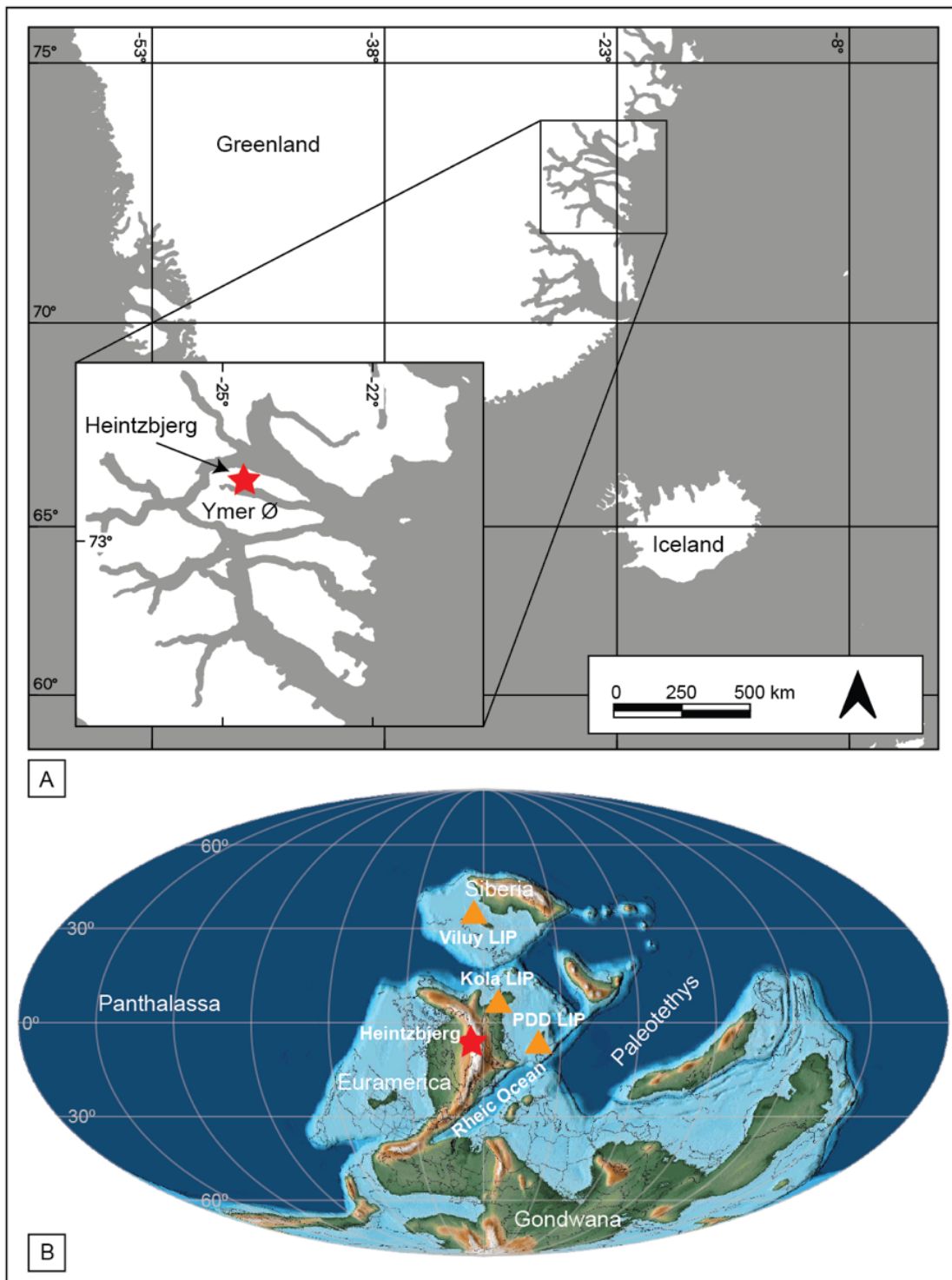


Figure 3.1. A. Location of the study site from which model data is derived (indicated by a star). B. Late Devonian (~370 Ma) paleogeographic reconstruction with the study location indicated by a star as well as the relative locations of significant Late Devonian large igneous provinces (LIPs) indicated by triangles. Significant LIPs include the Viluy LIP in Siberia, the Kola LIP in the Kola Peninsula and the Pripjat-Dnieper-Donets (PDD) LIP in East Europe. The base map was created using GPlates with reconstructions from Scotese (2016). Locations of LIPs as described by Racki (2020).

### 3.2. Enhanced Phosphorus Export During the Late Devonian Mass Extinction

The role of land plants in Devonian biotic crises has long been a subject of debate. First suggested by Algeo et al. (1995), the theory proposes that the expansion of land plants into continental interiors along with the development of significant root systems and arborescence led to an unprecedented flux of terrestrial nutrients into Devonian seas. The relatively large and rapid nutrient load would have stimulated primary productivity leading to eutrophication, elevated organic matter deposition and subsequent bottom water anoxia. Occurring on a large enough scale, this could drive marine mass extinctions, which were relatively common throughout the Devonian (Algeo et al., 1995). Until recently however, no studies have focused on quantifying a potential terrestrial nutrient pulse from land plant expansion by interrogating weathering-proximal terrestrial lacustrine records. Smart et al. (2022) reported two such pulses in a fluvial sequence in the Devonian Basin of East Greenland associated with the LKW and UKW (Fig. 3.2). These pulses are directly associated with land plant expansion and were both significant in magnitude and sustained in duration (Smart et al., 2022), enabling their use in geochemical models. The increases in phosphorus accumulation rates (Smart et al., 2022) compare favorably to revegetation following glacial retreat in Holocene analogues, lending confidence in the utility of their data (Appendix B). Furthermore, the paleogeographic location of the Heintzbjerg study site was on the flanks of the Caledonian mountains and within a drainage basin that fed the Rheic Ocean (Fig. 3.1). Thus, elevated nutrient export from this location likely had a marked impact on the relatively restricted Rheic Ocean, making this site an ideal candidate from which to estimate global phosphorus flux.

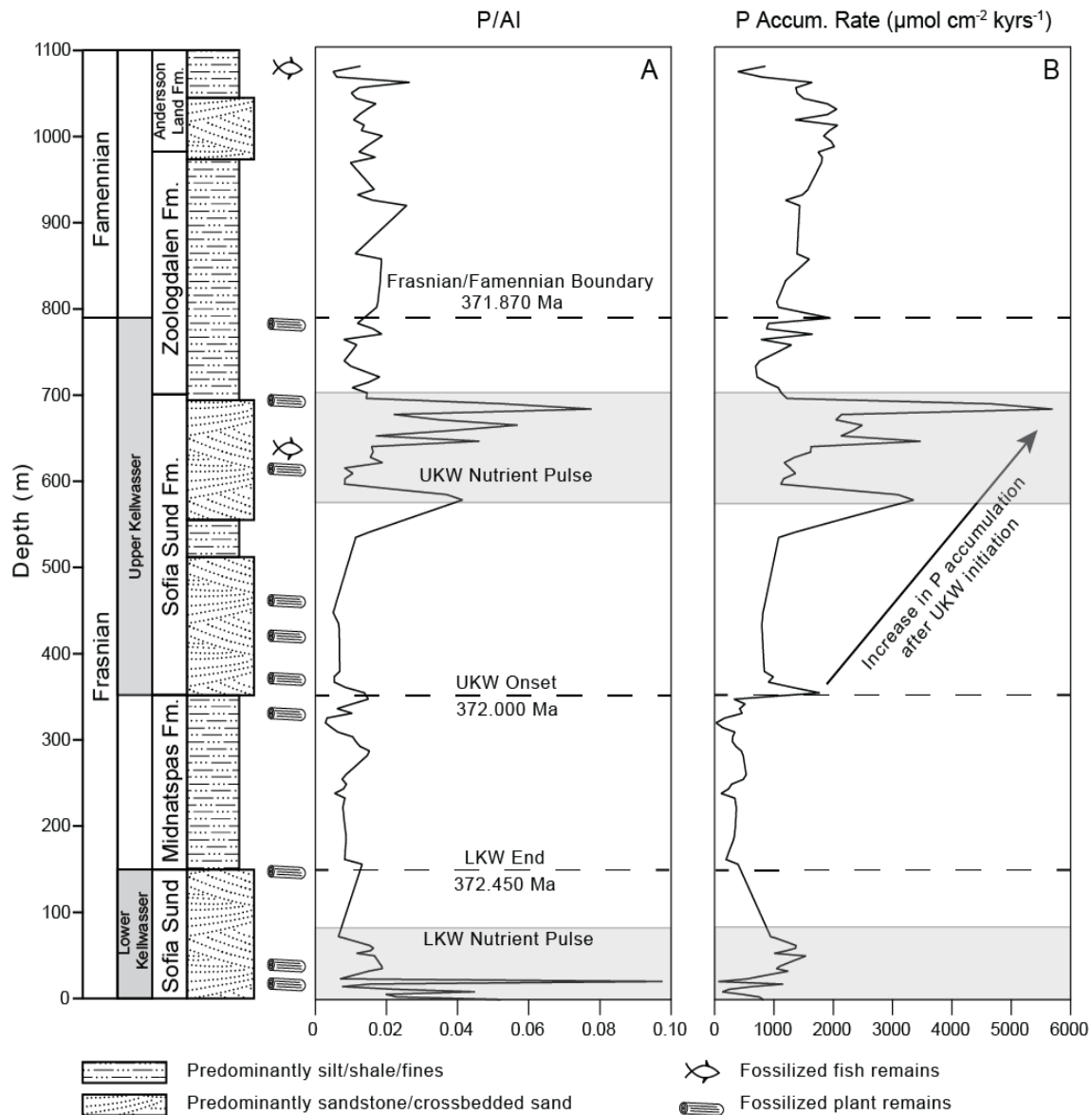


Figure 3.2. Geochemical source data from the study location (Smart et al., 2022). The Heintzbjerg sequence contains 1100 m of continuous fluvial record capturing a portion of the Lower Kellwasser (LKW) as well as the entirety of the Upper Kellwasser (UKW) events comprising the Frasnian-Famennian extinction. Stratigraphy has been simplified due to the size of the sequence. Black dashed lines represent the age control points used to calculate sedimentation rates based on recent age estimates (Da Silva et al., 2020; Percival et al., 2020). Shaded regions represent nutrient pulses during the LKW and UKW based on P/Al data (Smart et al., 2022). A. Phosphorus/aluminum ratios used to estimate riverine phosphorus flux. Based on this data, two distinct nutrient pulses can be identified. B. Phosphorus accumulation rate data calculated using estimated sedimentation rates based on cyclostratigraphy and used to simulate terrestrial phosphorus input in a separate simulation. These data show a greatly reduced nutrient pulse during the

### 3.3. Materials and Methods

#### 3.3.1. P/Al and Phosphorus Accumulation Data

P/Al data was taken directly from Smart et al. (2022) (Fig. 3.2) and scaled as described below. Due to limitations in the sample repository at the University of Southampton from which the Heintzbjerg samples were sourced, the initiation of the LKW was not covered in the Heintzbjerg sample set and thus, Smart et al. (2022) were unable to establish an age control point at the base of the LKW (nor were they able to establish an age control point for the significant number of samples in the Famennian). Age control points were available for the end of the LKW, base of the UKW and the Frasnian-Famennian boundary and were used to calculate average sedimentation rates and phosphorus (P) accumulation rates between each of those sections (Smart et al., 2022). Although the P/Al data is informative of terrestrial phosphorus export, P accumulation rate is a more robust parameter from which to gauge phosphorus weathering by land plants and subsequent landscape stabilization (see Smart et al., 2022; Filippelli and Souch, 1999; Filippelli, 2002). In order to use P accumulation data as an input into our model however, it was critical that sedimentation rates, and thus P accumulation rates, be calculated for the entire sequence to capture not only the LKW, but also the post-UKW geochemical response.

Recent refinements in the age of the Frasnian-Famennian boundary from similar sequences (Da Silva et al., 2020; Percival et al., 2020) make it possible to use relative dating techniques to established estimated ages for the entire sequence based on this anchor point, thus allowing calculation of sedimentation rates and P accumulation rates

for the entire Heintzbjerg sequence. The field of astrochronology has long used Milankovitch cycles to gauge the passage of time in sedimentary sequences. Climatic oscillations recorded in the sedimentary record can be tied to changes in the Earth's orbital parameters. Specifically, the ellipticity of Earth's orbit (referred to as eccentricity, with periods of 405 kyr, 123 kyr and 95 kyr), tilt (referred to as obliquity, with a modern period of 41 kyr and varying periods in deep time (Berger et al., 1992)) and precession (with a modern period of 20 kyr and also varying in deep time (Berger et al., 1992)). Meyers (2015) (further refined in Meyers (2019)) utilized a statistical optimization method called TimeOpt in the *Astrochron* package in the R platform (Core Team, 2022) in order to correlate climatic changes in the stratigraphic record with Milankovitch cycles to establish relative age of a sedimentary sequence. We employ a similar approach here, but utilize the timeOptTemplate function which was designed for more complex sedimentation models (Meyers, 2019) which we expected to encounter given the wet/arid climatic shifts noted in the Heintzbjerg sedimentary sequence. The timeOptTemplate function allows the use of proxy or lithology-specific templates which greatly enhance the spectral alignment and overall fit for complex sedimentary sequences. We evaluated the utility of multiple climate-related proxies using this method along with geochemical data from 26 ultimately selecting Rb/Sr and Log Ti as proxies which produced the best spectral alignment and overall fit (e.g., Da Silva et al., 2020). Eccentricity periods of 94.9, 98.9, 123.8, 130.7 and 405 kyr (Laskar et al., 2011) along with precession periodicities for the Devonian of 16.85 and 19.95 kyr (Berger et al., 1992) were utilized. The sedimentation rates estimated using timeOptTemplate were compared with sections calculated by Smart et al. (2022) and found to be of similar magnitude (Midnatspas

average sedimentation rate =  $43 \text{ cm kyr}^{-1}$  (see Smart et al., 2022) compared with  $71.9 \text{ cm kyr}^{-1}$  (timeOptTemplate); UKW average sedimentation rate =  $272 \text{ cm kyr}^{-1}$  (see Smart et al., 2022) compared with  $228.6 \text{ cm kyr}^{-1}$  (timeOptTemplate). Age estimates were then determined based on the Frasnian-Famennian boundary (371.870 Ma (Da Silva et al., 2020)) as an anchor point and compared with age estimates for similar published sequences (Da Silva et al., 2020; Percival et al., 2020). Using timeOptTemplate estimations, we calculated the base of the UKW of our sequence at 372.06 Ma (compared with 372.00 – 372.02 Ma based on Da Silva et al. (2020) and Percival et al. (2020)) and the end of the LKW at 372.49 Ma (compared with 372.45 Ma based on Da Silva et al. (2020)), a mere 40 kyr difference for each and lending confidence in the validity of the timeOptTemplate results.

Based on the relative confirmation of the timeOptTemplate results, new P accumulation rates were calculated for the entire Heintzbjerg sequence. Once again, these results were compared with those sections calculated in Smart et al. (2022) and found to be strikingly similar in overall trends, but notably with somewhat differing magnitudes (Fig. 3.3). The differences in magnitude, however, do not change the overall interpretation by Smart et al. (2020). Thus, these new P accumulation rates were used as input into our model as described below.



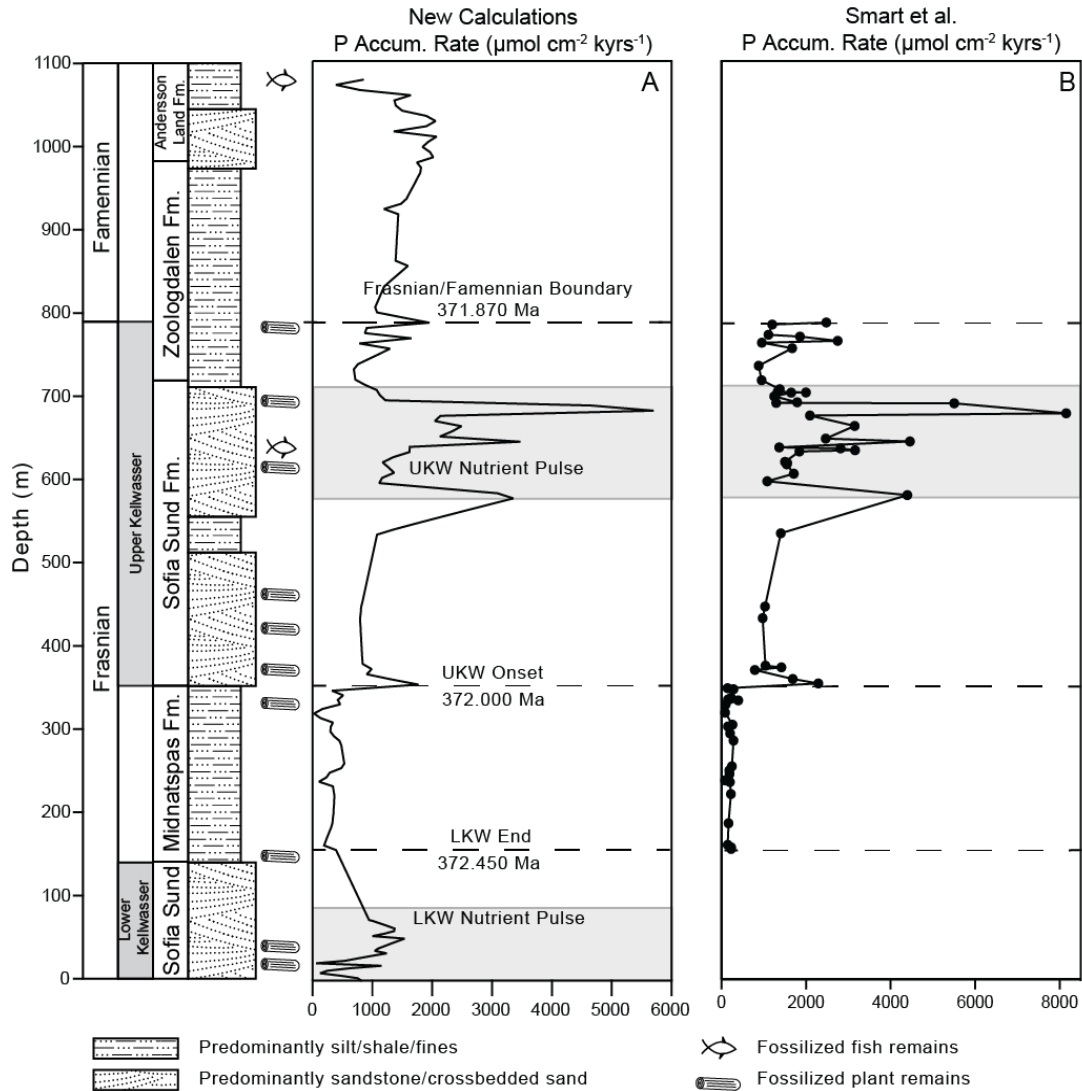


Figure 3.3. Comparison of phosphorus accumulation rates calculated using sedimentation rates derived from astrochronological calibrations (A) to those using only available age control points from Smart et al. (2020) (B). The location of age control points is indicated with dashed lines using ages derived from Da Silva et al. (2020) and Percival et al. (2020).

### 3.3.2. Earth System Box Model

In this study, we employ an Earth system box model of the coupled C-N-P- O<sub>2</sub>-S biogeochemical cycles developed by Ozaki and Reinhard (2021). The model includes a series of biogeochemical processes operating on the planetary surface but is abstracted enough to allow the simulations on geologic time scales. The basic model design was based on the Carbon Oxygen Phosphorus Sulfur Evolution (COPSE) model (Bergman et

al., 2004; Lenton et al., 2016), which has been extensively tested and validated against geologic records during the Phanerozoic. We incorporate refinements to this model from Ozaki and Reinhard (2021) and extend the biogeochemical framework for the global methane (CH<sub>4</sub>) cycle without altering the basic behavior of the model. While Ozaki and Reinhard (2021) include the mass exchange between the surface system (atmosphere-ocean-crust) and the mantle, we ignore this in this study. We conduct several different runs in which we explore biological and tectonic factors individually. First, we explore the possible impacts of enhanced phosphorus weathering by land plant colonization using both P/Al and phosphorus accumulation rate data from Heintzbjerg, Greenland. In the sensitivity experiments, discrete episodes of phosphorus weathering are assumed with different timing and amplitude. Sharp increases followed by decreases of phosphorus weathering are meant to represent possible phases of selective phosphorus weathering associated with land plant colonization and a subsequent drop due to the establishment of phosphorus recycling in soil systems (Lenton et al., 2016). We also explore the impacts of variations in degassing rates from LIPs that were active during the upper Devonian (Fig. 3.1b). In this scenario, we simulate two episodes of large-scale volcanism, a smaller event at the onset of the LKW and a larger event at the onset of the UKW. We initialized the model at 600 Ma and ran the model forward in time until the end Famennian. Specific model parameters for each experiment are outlined in the following two sections.

### 3.3.3. Enhanced Terrestrial Nutrient Export Model

To test the enhanced P export hypothesis, we introduced a forcing factor,  $f_{pP}$ , which represents the amplification factor for the terrestrial phosphorus weathering flux:

$$J_P^w = f_{pP} \left( \frac{2}{12} \frac{J_{sil}^w}{J_{sil}^{w*}} + \frac{5}{12} \frac{J_{carb}^w}{J_{carb}^{w*}} + \frac{5}{12} \frac{J_{orgC}^w}{J_{orgC}^{w*}} \right) J_P^{w,*} \quad (1)$$

where  $J_P^w$ ,  $J_{sil}^w$ ,  $J_{carb}^w$ , and  $J_{orgC}^w$  denote the rates of phosphorus weathering, silicate weathering, carbonate weathering, and the oxidative weathering of organic matter on land, respectively, and \* represents the reference value (pre-industrial flux; see Ozaki and Reinhard, 2021 and Bergman et al., 2004). To assess the uncertainty in the timing and amplitude of pulses in phosphorus weathering, we explored the following different scenarios: (i) In an attempt to reproduce the 2-3‰ positive excursions in  $\delta^{13}C$ , the following forcing factors were assumed; (LKW)  $f_{pP} = 1 \rightarrow 2 \rightarrow 1$  over 372.72-372.54-372.36 Ma. (UKW)  $f_{pP} = 1 \rightarrow 2 \rightarrow 1$  over 372.1-371.91-371.73 Ma. (ii) As i but decreasing the forcing factor to 1.5 for both the LKW and UKW. (iii) As i but decreasing the forcing factor to 1.5 for the LKW only. (iv)  $f_{pP}$  based on the P/Al data from Heintzbjerg, Greenland (Fig. 3.4, left panel), with a scaling factor of 0.5 (see below). (v)  $f_{pP}$  based on P accumulation data from Heintzbjerg (Fig. 3.4, right panel) and applying a scaling factor of 0.15 to account for the hypothesized episodic expansion of land plants as predicted by Smart et al. (2022) and Retallack and Huang (2011), assuming a maximum value of  $f_{pP} = 3.35$ .

To convert the sedimentary data of P (P/Al or P accumulation rate) into the forcing factor of  $f_{pP}$  in (iv) and (v), we first calculate the typical ‘non-event’ value by

averaging data between LKW and UKW (Midnatspas Fm.),  $X_{avg}$ . Then,  $f_{pP}$  is calculated, as follows:

$$f_{pP} = 1 + \frac{X - X_{avg}}{X_{avg}} a, \quad (2)$$

where X denotes the sedimentary data of P (P/Al or P accumulation rate) and a represents the scaling factor. When  $a = 1$ ,  $f_{pP}$  (and global P loading flux) simply reflects the variation of P flux observed at Heintzbjerg. But, in this case, our model predicts an extremely large positive excursion of  $\delta^{13}C$  (10%), inconsistent with geologic records. The scaling factor is therefore introduced to represent the relationship between the Heintzbjerg P records to global P export flux. The value of a was tuned so that the model produces a reasonable positive excursion of  $\delta^{13}C$  of 2-3%.

#### 3.3.4. Enhanced Volcanic Activity Model

To understand the biogeochemical consequences of the enhanced volcanic activity, we introduced a forcing factor,  $f_{LIP}$ , which is multiplied by the degassing rate of  $CO_2$  via carbonate and organic carbon metamorphism:

$$J_{carb}^m = f_{LIP} f_G f_C \left( \frac{C}{C^*} \right) J_{carb}^{m,*}, \quad (3)$$

$$J_{org}^m = f_{LIP} f_G \left( \frac{G}{G^*} \right) J_{org}^{m,*}, \quad (4)$$

where  $J_{carb}^m$  and  $J_{org}^m$  denote carbon dioxide ( $CO_2$ ) degassing flux via metamorphism of sedimentary carbonate (C) and organic carbon (G), respectively (\* represent reference values found in 41).  $f_G$  and  $f_C$  represent the forcing factors of degassing flux and pelagic carbonate deposition which are used in the original model. By varying the value of  $f_{LIP}$ , we explore the possible impacts of  $CO_2$  degassing rate on global biogeochemistry (Fig.

3.5):  $f_{LIP} = 1 \rightarrow 2 \rightarrow 1$  over 372.72-372.54-372.36 Ma. (UKW)  $f_{LIP} = 1 \rightarrow 5 \rightarrow 1$  over 372.1-371.91-371.73 Ma.

### 3.4. Results and Discussion

Results for the enhanced terrestrial nutrient export scenario are shown in Fig. 3.4. Our model demonstrates the increases in riverine phosphorus flux to the ocean promotes oceanic eutrophication and deoxygenation (as shown as increases in DOA, or degree of anoxia). For the LKW, the enhanced burial of organic matter in the ocean leads to a drop

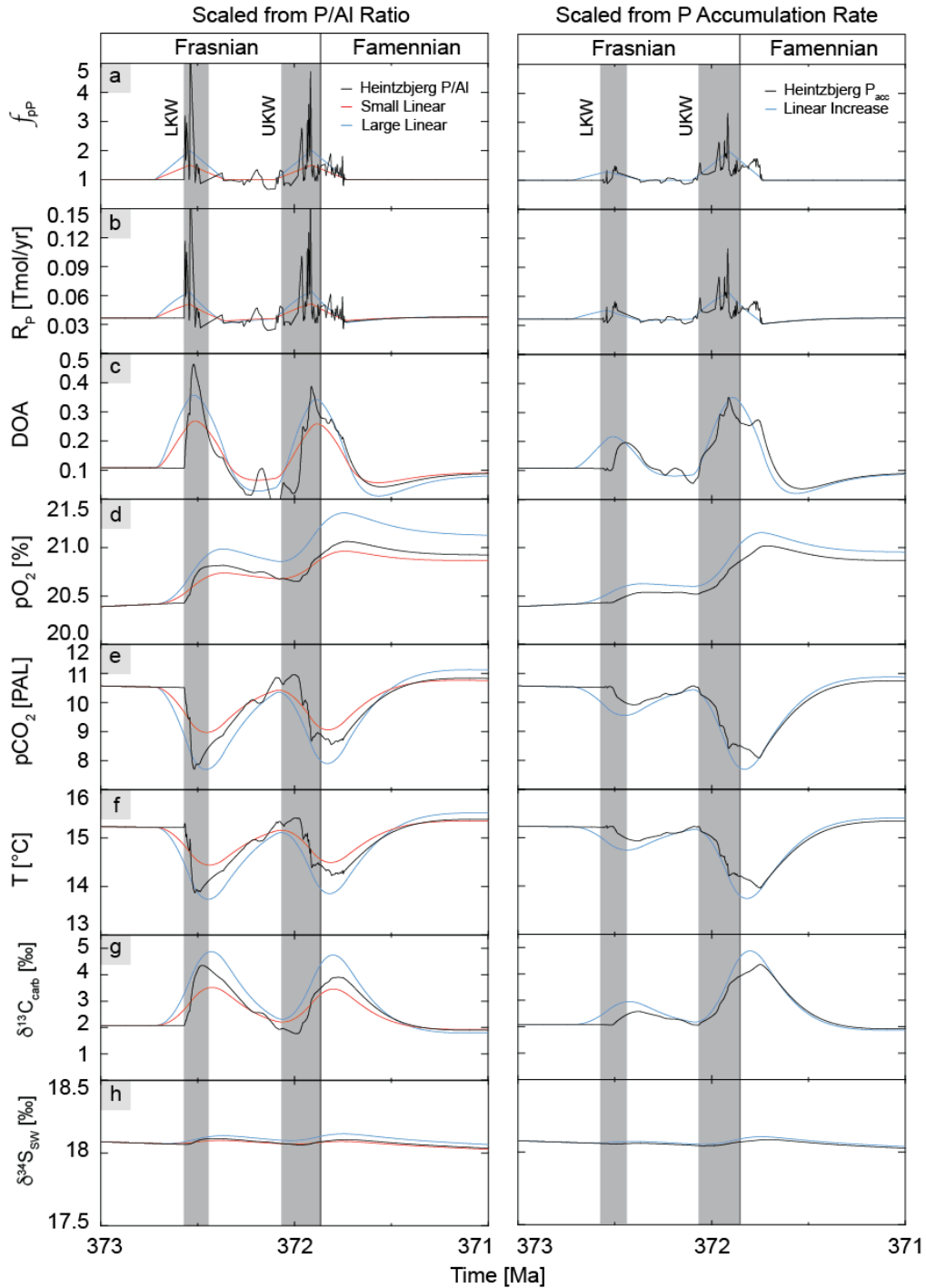


Figure 3.4. Biogeochemical dynamics induced by elevated episodes of P weathering on land. Gray shaded regions represent the two pulses of the Kellwasser extinction. (a) Phosphorus weathering forcing factor,  $f_{PP}$ . Several different scenarios are explored: red and blue lines assume episodes with linear increase and decrease around the LKW and UKW, and black line is obtained by scaling the P/Al (left panel) and phosphorus accumulation rate (right panel) records from Heintzbjerg, Greenland. (b) Riverine P flux to the ocean. (c) Degree of oceanic anoxia. (d) Atmospheric  $O_2$  level. (e) Atmospheric  $CO_2$  level. PAL = present atmospheric level. (f) Global average surface temperature. (g) Carbon isotopic value of burying carbonates. (h) Seawater sulfate sulfur isotope.

in atmospheric CO<sub>2</sub> levels (from ~10.5 present atmospheric level (PAL) to ~7.5-9 PAL) and associated climate cooling of 0.5-1.5°C. This is accompanied with a positive excursion in δ<sup>13</sup>C of 1.5 to 3.0‰. These trends are observed in both the red/blue simulations as well as the scaled P/Al data from Heintzberg (black line in Fig. 3.4). Also observed is that greater phosphorus weathering results in larger environmental changes. In the large linear simulation (blue line in Fig. 3.4), atmospheric O<sub>2</sub> levels exhibit a stepwise increase to the modern level of 21%. On the other hand, the sulfur isotopic value of seawater sulfate is largely insensitive to the variations of phosphorus weathering. Results based on the phosphorus accumulation rate data are similar, with a notable difference being the much smaller perturbations associated with the LKW.

Results for the enhanced volcanic degassing scenarios are shown in Fig. 3.5. A two-fold increase in degassing rate produces a positive excursion in δ<sup>13</sup>C (1‰) for the LKW, and a five-fold increase is required to produce the 2‰ excursion for the UKW. Such an enhanced volcanic flux during the UKW results in atmospheric CO<sub>2</sub> levels of >20 PAL and associated >4°C increase in global temperatures. Under such conditions, an enhanced greenhouse accelerates terrestrial phosphorus weathering, promoting oceanic eutrophication and deoxygenation. This, in turn, leads to the enhanced burial of organic matter in marine sediments and a stepwise increase in atmospheric oxygen (O<sub>2</sub>).

The terrestrial nutrient export scenarios and volcanic activity scenarios both demonstrate enhanced riverine phosphorus input flux, resulting in similar behaviors with respect to oceanic biogeochemical dynamics (eutrophication, deoxygenation, and enhanced burial of organic matter) and the secular evolution of atmospheric O<sub>2</sub> levels. In contrast, these scenarios demonstrate different climatic variations. Specifically, the

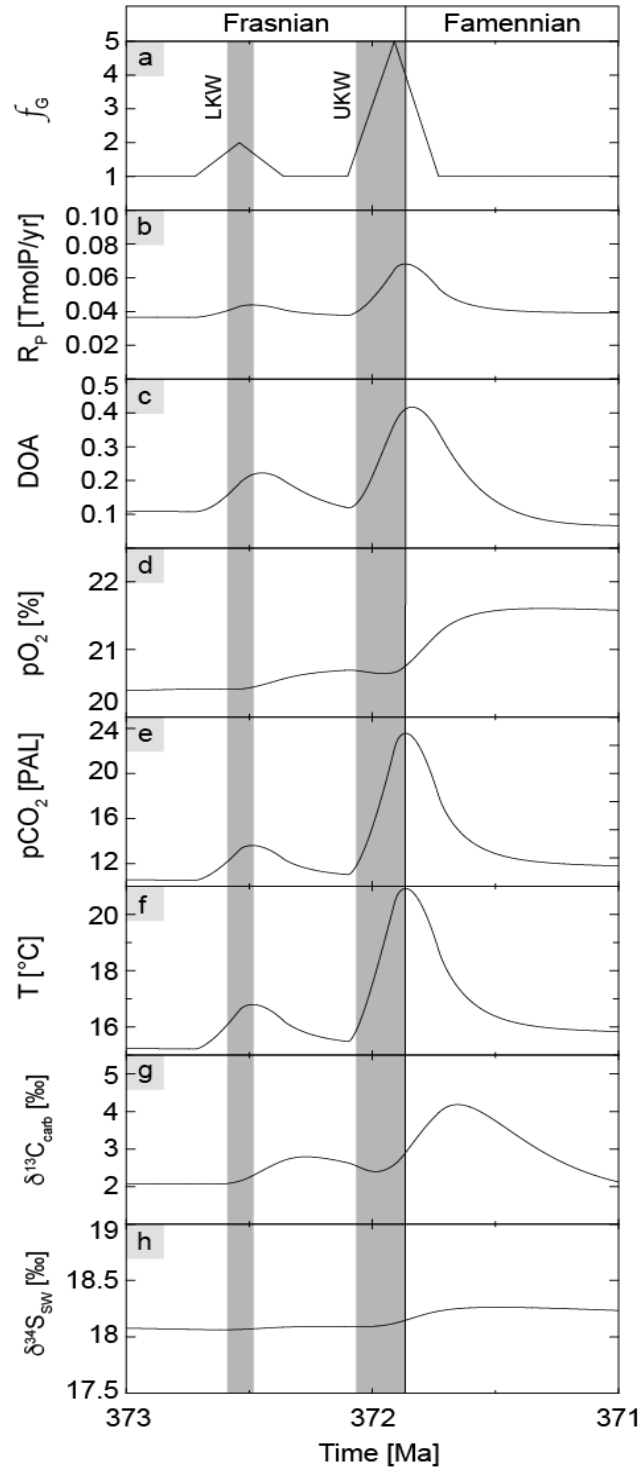


Figure 3.5. Biogeochemical dynamics induced by enhanced volcanic activity. Black line represents two distinct volcanic events, one during the LKW and a second during the UKW based on the presence of two distinct weathering events in the Heintzbjerg, Greenland data. Gray shaded region represents the two pulses of the Kellwasser extinction. (a) Degassing factor,  $f_g$ . (b) Riverine P flux to the ocean. (c) Degree of anoxia. (d) Atmospheric  $O_2$  level. (e) Atmospheric  $CO_2$  level. PAL = present atmospheric level. (f) Global average surface temperature. (g) Carbon isotopic value of burying carbonates. (h) Seawater sulfate sulfur isotope.



enhanced terrestrial nutrient export scenarios suggest a marked decrease in atmospheric CO<sub>2</sub> and global cooling of >1°C whereas the enhanced volcanic activity results in the two-fold increase in atmospheric CO<sub>2</sub> levels and global warming of >4°C. Additionally, while both scenarios achieve the positive δ<sup>13</sup>C excursion recorded in the geologic record, the longevity of the excursions in the enhanced volcanic activity scenario tends to be longer than those of the terrestrial nutrient export scenarios because of the increased residence time of inorganic carbon in the ocean-atmosphere system. Additionally, maxima in climate cooling in the enhanced terrestrial nutrient export scenario correspond to the largest positive excursion in δ<sup>13</sup>C, whereas in the enhanced volcanic activity scenario, the δ<sup>13</sup>C excursion is delayed and occurs after the temperature maxima.

Both scenarios are somewhat at odds with the geologic record in differing respects. While an overall warming trend is observed through the end-Devonian, conodont oxygen isotope records from numerous studies suggest cooling leading into both the LKW and UKW (Joachimski and Buggisch, 2002; Huang et al., 2018; Balter et al., 2008; Joachimski et al., 2009). If large scale volcanism (either from LIP or multiple arc volcanic events; Racki et al., 2018) was an initiating event, the enhanced volcanic activity scenario requires warming on a global scale (Fig. 3.5f) which is not universally supported by conodont oxygen isotope records. Additionally, atmospheric CO<sub>2</sub> decreased substantially throughout the Devonian. Our model predicts large scale volcanism sufficient to drive anoxia would have increased atmospheric CO<sub>2</sub> to levels which are likewise not supported in the geologic record. A compilation published by Franks et al. (2014) compares Paleozoic CO<sub>2</sub> estimates from paleosol carbonates, fossil records and

model estimates using GEOCARBSULF and reports a likely atmospheric CO<sub>2</sub> range of between 500-3000 ppm for the Late Devonian, substantially below >20 PAL required by our model (see also Royer, 2014; Lenton et al., 2018). However, many of these records lack the temporal resolution to detect short-time scale perturbations, so although current evidence does not support rapid and dramatic increases in atmospheric CO<sub>2</sub> due to large scale volcanism it cannot be completely ruled out.

Our model results are most consistent with enhanced terrestrial nutrient export as an important causal factor in at least the UKW extinction pulse as the predicted cooling, decrease in atmospheric CO<sub>2</sub>, and increase in atmospheric O<sub>2</sub> are all supported by the geologic record. The P/Al based model predicts larger geochemical perturbations during the LKW, which is inconsistent with most records that suggest the UKW was the more significant. This contrasts with phosphorus accumulation rate-based data which accurately predicts the UKW as the more significant event. Additionally, the similarities in geochemical response between the Heintzbjerg sequence and the linear simulations further reinforce the supposition that the terrestrial nutrient export model is the more likely of the two scenarios. However, the timing of the terrestrial nutrient pulses<sup>26</sup> seems to preclude plant expansion as an initiating event. Although there is evidence of elevated nutrient export during the LKW and at the start of the UKW, the most significant and sustained nutrient export event occurs in the second half of the UKW, closer to the Frasnian-Famennian boundary (Fig. 3.2). While land plants may not have directly initiated the UKW, the concurrent extinction of both benthic species and the collapse of Devonian Reefs systems suggest the possibility of multiple extinction mechanisms.

Rather than singular triggers, we suggest multiple elements of current theories contributed to biotic crises in the marine biosphere.

### 3.5. A Multifaceted Extinction Mechanism

The Heintzbjerg sequence is a terrestrial equivalent to marine expressions of the KW events and is characterized by the deposition of two intervals of thick sandstones representing intense fluvial activity followed by stacks of paleosols representing intense and prolonged intervals of aridity (see Fig. 3.2) (Larsen et al., 2008). These sedimentary markers suggest that the deposition of the UKW horizon at Heintzbjerg marks a defined shift in climate regimes from arid to warm and wet (Smart et al., 2022; Larsen et al., 2008). Concurrent with this shift in climatic regimes is evidence of elevated terrestrial phosphorus export (Fig. 3.2). Such a climate shift would bring about conditions generally more favorable for plant growth, potentially explaining enhanced terrestrial phosphorus export at the start of the UKW. Additionally, at least one pulse of both the Viluy and Pripyat-Dnieper-Donets (PDD) LIPs (the largest Devonian LIPs and the two most closely associated temporally with the KW events) occurred during the UKW (Racki, 2020; Ernst et al., 2020). While our model predictions appear to rule out cataclysmic volcanism as a sole extinction mechanism, they do not discount it completely.

At the onset of the UKW, our model predicts substantial geochemical changes with increased terrestrial nutrient delivery driving positive  $\delta^{13}\text{C}$  excursions, corresponding increases in  $\text{O}_2$  and DOA and significant decreases in  $\text{CO}_2$  and temperature. One possibility suggested by the model data is that a significant volcanic event increased atmospheric  $\text{CO}_2$  prior to the UKW, but was insufficient in magnitude to

drive extinction on its own. A high CO<sub>2</sub> environment catalyzed by large scale volcanism combined with a climatic shift to wetter conditions at the UKW onset would drive increased rates of silicate rock weathering, increase carbon sequestration and eventually draw down atmospheric CO<sub>2</sub>. Additionally, high atmospheric CO<sub>2</sub> would create a favorable environment for plant growth (i.e., the CO<sub>2</sub> fertilization effect; Ueyama et al.,

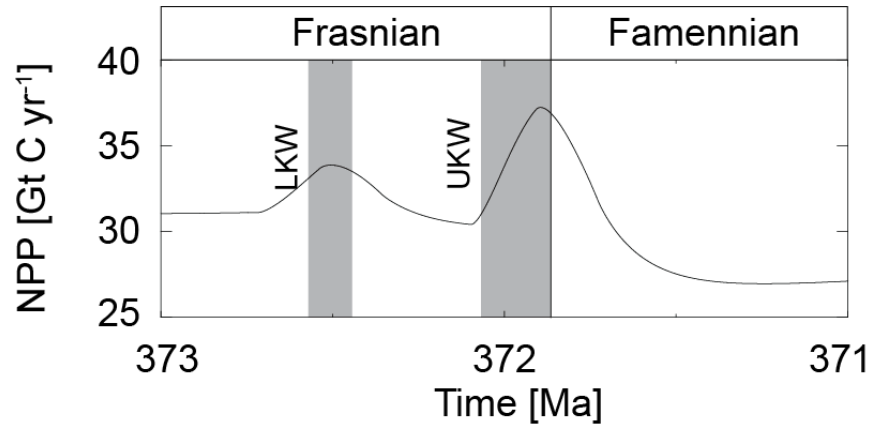


Figure 3.6. Changes in net primary production (NPP) on land as predicted by the enhanced volcanic activity model in Gt C yr<sup>-1</sup>. Shaded regions represent the LKW and UKW extinction pulses. Note the maxima in NPP observed during the UKW occurs roughly coincident with maxima in terrestrial P flux in both P/Al and phosphorus accumulation rate data from Heintzbjerg.

2020). Indeed, our model predicts an increase in net primary production (NPP) on land for the enhanced volcanic degassing scenario accompanying both the LKW and UKW extinction pulses on the order of 2.5 and 6.2 Gt C yr<sup>-1</sup> for each, respectively (Fig. 3.6). Combined with a warm and wet climate, a large but transitory increase in atmospheric CO<sub>2</sub> may have been sufficient to sustain a rapid expansion of land plants in the late Frasnian, resulting in the observed massive terrestrial export of phosphorus<sup>26</sup>. This phosphorus would have made its way to the Rheic Ocean, driving anoxia not only in the deeper portions of the basin, but also eutrophication of the shallower margins, partially explaining the decimation of Devonian reef systems observed at the Frasnian-Famennian boundary. Plant expansion tied to transitory increases in atmospheric CO<sub>2</sub> concentrations and climatic shifts has previously been proposed as an explanation for the staggered

expansion of land plants in Mid-Devonian New York, USA (Retallack and Huang, 2011) and appears possible in the Devonian Basin in East Greenland as well (Smart et al., 2022). Our model, supported by geochemical data, suggests that climatic changes possibly in concert with large scale volcanism encouraged plant expansion in East Greenland. The geochemical instability initiated by large scale volcanism combined with the rapid geochemical feedbacks produced by the collective effects of increased rates of silicate rock weathering and land plant expansion would have been sufficient to drive widespread ocean anoxia culminating in mass extinction.

Extinction events are complex systemic responses, and with rare exceptions have seldom been attributed to a single cataclysm. The various theories regarding the initiation of the KW events may each be correct in that they likely contributed to the ecological crisis, although their true timing and sequence clearly need refinement. Our results suggest that neither large scale volcanism nor land plant evolution can be implicated as the sole initiating factor in the KW event. Instead, the KW event was the timely combination of multiple events ultimately resulting in the decimation of Devonian seas. Evidence presented here challenges a single extinction mechanism and demonstrates the need for further work integrating multiple theories to bring together the exact timing and sequence of events which culminated in one of the Phanerozoic's most significant mass extinctions.

### 3.6. References

Algeo, T. J., Berner, R. A., Maynard, J. B., & Scheckler, S. E. (1995). Late Devonian oceanic anoxic events and biotic crises: “rooted” in the evolution of vascular land plants. *GSA Today*, 5(3), 45-66.

Algeo, T. J., & Scheckler, S. E. (1998). Terrestrial-marine teleconnections in the Devonian: links between the evolution of land plants, weathering processes, and marine anoxic events. *Philosophical Transactions of the Royal Society of London. Series B: Biological Sciences*, 353(1365), 113-130.

Algeo, T. J., & Ingall, E. (2007). Sedimentary Corg: P ratios, paleocean ventilation, and Phanerozoic atmospheric pO<sub>2</sub>. *Palaeogeography, Palaeoclimatology, Palaeoecology*, 256(3-4), 130-155.

Averbuch, O., Tribouillard, N., Devleeschouwer, X., Riquier, L., Mistiaen, B., & Van Vliet-Lanoe, B. (2005). Mountain building-enhanced continental weathering and organic carbon burial as major causes for climatic cooling at the Frasnian–Famennian boundary (c. 376 Ma)? *Terra Nova*, 17(1), 25-34.

Balter, V., Renaud, S., Girard, C., & Joachimski, M. M. (2008). Record of climate-driven morphological changes in 376 Ma Devonian fossils. *Geology*, 36(11), 907-910.

Berger, A., Loutre, M. F., & Laskar, J. (1992). Stability of the astronomical frequencies over the Earth's history for paleoclimate studies. *Science*, 255(5044), 560-566.

Bergman, N.M., Lenton, T.M., Watson, A.J., 2004. COPSE: A new model of biogeochemical cycling over Phanerozoic time. *American Journal of Science* 304, 397-437.

Berner, R. A. (2009). Phanerozoic atmospheric oxygen: New results using the GEOCARBSULF model. *American Journal of Science*, 309(7), 603-606.

Bond, D., Wignall, P. B., & Racki, G. (2004). Extent and duration of marine anoxia during the Frasnian–Famennian (Late Devonian) mass extinction in Poland, Germany, Austria and France. *Geological Magazine*, 141(2), 173-193.

Bond, D. P., Zatoń, M., Wignall, P. B., & Marynowski, L. (2013). Evidence for shallow-water ‘Upper Kellwasser’ anoxia in the Frasnian–Famennian reefs of Alberta, Canada. *Lethaia*, 46(3), 355-368.

Buggisch, W. (1991). The global Frasnian-Famennian» Kellwasser Event «. *Geologische Rundschau*, 80(1), 49-72.

Carmichael, S. K., Waters, J. A., Koenigshof, P., Suttner, T. J., & Kido, E. (2019). Paleogeography and paleoenvironments of the Late Devonian Kellwasser event: A

review of its sedimentological and geochemical expression. *Global and Planetary Change*, 183, 102984.

Chen, D., Qing, H., & Li, R. (2005). The Late Devonian Frasnian–Famennian (F/F) biotic crisis: insights from  $\delta^{13}\text{C}_{\text{carb}}$ ,  $\delta^{13}\text{C}_{\text{org}}$  and  $87\text{Sr}/86\text{Sr}$  isotopic systematics. *Earth and Planetary Science Letters*, 235(1-2), 151-166.

Claeys, P., Casier, J. G., & Margolis, S. V. (1992). Microtektites and mass extinctions: evidence for a Late Devonian asteroid impact. *Science*, 257(5073), 1102-1104.

Core Team, R. R: *A language and environment for computing* (2022).

Da Silva, A. C., Sinnesael, M., Claeys, P., Davies, J. H., de Winter, N. J., Percival, L. M. E., ... & De Vleeschouwer, D. (2020). Anchoring the Late Devonian mass extinction in absolute time by integrating climatic controls and radio-isotopic dating. *Scientific Reports*, 10(1), 1-12.

Ernst, R. E., Rodygin, S. A., & Grinev, O. M. (2020). Age correlation of Large Igneous Provinces with Devonian biotic crises. *Global and Planetary Change*, 185, 103097.

Filippelli, G. M. (1997). Controls on phosphorus concentration and accumulation in oceanic sediments. *Marine Geology*, 139(1-4), 231-240.



Filippelli, G.M., and Souch, C., 1999, Effects of climate and landscape development on the terrestrial phosphorus cycle: *Geology*, v. 27, p. 171.

Filippelli, G.M., 2002, The Global Phosphorus Cycle: Reviews in mineralogy and geochemistry, v. 48, p. 391–425.

Franks, P. J., Royer, D. L., Beerling, D. J., Van de Water, P. K., Cantrill, D. J., Barbour, M. M., & Berry, J. A. (2014). New constraints on atmospheric CO<sub>2</sub> concentration for the Phanerozoic. *Geophysical Research Letters*, 41(13), 4685-4694.

House, M. R. (1985). Correlation of mid-Palaeozoic ammonoid evolutionary events with global sedimentary perturbations. *Nature*, 313(5997), 17-22.

Huang, C., Joachimski, M. M., & Gong, Y. (2018). Did climate changes trigger the Late Devonian Kellwasser Crisis? Evidence from a high-resolution conodont  $\delta^{18}\text{OPO}_4$  record from South China. *Earth and Planetary Science Letters*, 495, 174-184.

Joachimski, M. M., & Buggisch, W. (1993). Anoxic events in the late Frasnian—Causes of the Frasnian-Famennian faunal crisis? *Geology*, 21(8), 675-678.

Joachimski, M. M., & Buggisch, W. (2002). Conodont apatite  $\delta^{18}\text{O}$  signatures indicate climatic cooling as a trigger of the Late Devonian mass extinction. *Geology*, 30(8), 711-714.

Joachimski, M. M., Pancost, R. D., Freeman, K. H., Ostertag-Henning, C., & Buggisch, W. (2002). Carbon isotope geochemistry of the Frasnian–Famennian transition. *Palaeogeography, Palaeoclimatology, Palaeoecology*, 181(1-3), 91-109.

Joachimski, M. M., Breisig, S., Buggisch, W., Talent, J. A., Mawson, R., Gereke, M., ... & Weddige, K. (2009). Devonian climate and reef evolution: insights from oxygen isotopes in apatite. *Earth and Planetary Science Letters*, 284(3-4), 599-609.

Larsen, P. H., Olsen, H., & Clack, J. A. (2008). The Devonian basin in East Greenland—Review of basin evolution and vertebrate assemblages. *The Greenland Caledonides: Evolution of the Northeast Margin of Laurentia: Geological Society of America Memoir*, 202, 273-292.

Laskar, J., Fienga, A., Gastineau, M., & Manche, H. (2011). La2010: a new orbital solution for the long-term motion of the Earth. *Astronomy & Astrophysics*, 532, A89.

Lenton, T.M., Dahl, T.W., Daines, S.J., Mills, B.J.W., Ozaki, K., Saltzman, M.R., Porada, P., 2016. Earliest land plants created modern levels of atmospheric oxygen. *Proc. Natl Acad. Sci. USA* 113, 9704-9709.

Lenton, T. M., Daines, S. J., & Mills, B. J. (2018). COPSE reloaded: an improved model of biogeochemical cycling over Phanerozoic time. *Earth-Science Reviews*, 178, 1-28.

Lu, M., Lu, Y., Ikejiri, T., Sun, D., Carroll, R., Blair, E. H., ... & Sun, Y. (2021). Periodic oceanic euxinia and terrestrial fluxes linked to astronomical forcing during the Late Devonian Frasnian–Famennian mass extinction. *Earth and Planetary Science Letters*, 562, 116839.

McGhee Jr, G. R., Clapham, M. E., Sheehan, P. M., Bottjer, D. J., & Droser, M. L. (2013). A new ecological-severity ranking of major Phanerozoic biodiversity crises. *Palaeogeography, Palaeoclimatology, Palaeoecology*, 370, 260-270.

McGhee Jr, G. R. (2001). The ‘multiple impacts hypothesis’ for mass extinction: a comparison of the Late Devonian and the late Eocene. *Palaeogeography, Palaeoclimatology, Palaeoecology*, 176(1-4), 47-58.

Meyer-Berthaud, B., Scheckler, S. E., & Wendt, J. (1999). *Archaeopteris* is the earliest known modern tree. *Nature*, 398(6729), 700-701.

Meyer-Berthaud, B., Soria, A., & Decombeix, A. L. (2010). The land plant cover in the Devonian: a reassessment of the evolution of the tree habit. *Geological Society, London, Special Publications*, 339(1), pp.59-70.

Meyers, S. R. (2015). The evaluation of eccentricity-related amplitude modulation and bundling in paleoclimate data: An inverse approach for astrochronologic testing and time scale optimization. *Paleoceanography*, 30(12), 1625-1640.

Meyers, S. R. (2019). Cyclostratigraphy and the problem of astrochronologic testing. *Earth-Science Reviews*, 190, 190-223.

Ozaki, K., Reinhard, C.T., 2021. The future lifespan of Earth's oxygenated atmosphere. *Nature Geoscience* 14, 138-142.

Percival, L. M. E., Selby, D., Bond, D. P. G., Rakociński, M., Racki, G., Marynowski, L., ... & Föllmi, K. B. (2019). Pulses of enhanced continental weathering associated with multiple Late Devonian climate perturbations: Evidence from osmium-isotope compositions. *Palaeogeography, Palaeoclimatology, Palaeoecology*, 524, 240-249.

Percival, L. M. E., Bond, D. P. G., Rakociński, M., Marynowski, L., Hood, A. V. S., Adatte, T., ... & Föllmi, K. B. (2020). Phosphorus-cycle disturbances during the Late Devonian anoxic events. *Global and Planetary Change*, 184, 103070.

Racki, G., Rakociński, M., Marynowski, L., & Wignall, P. B. (2018). Mercury enrichments and the Frasnian-Famennian biotic crisis: A volcanic trigger proved? *Geology*, 46(6), 543-546.

Racki, G. (2020). A volcanic scenario for the Frasnian–Famennian major biotic crisis and other Late Devonian global changes: More answers than questions? *Global and Planetary Change*, 189, 103174.

Raup, D. M., & Sepkoski, J. J. (1982). Mass extinctions in the marine fossil record. *Science*, 215(4539), 1501-1503.

Retallack, G. J., & Huang, C. (2011). Ecology and evolution of Devonian trees in New York, USA. *Palaeogeography, Palaeoclimatology, Palaeoecology*, 299(1-2), 110-128.

Royer, D. L., Berner, R. A., & Park, J. (2007). Climate sensitivity constrained by CO<sub>2</sub> concentrations over the past 420 million years. *Nature*, 446(7135), 530-532.

Royer, D. L. (2014). Atmospheric CO<sub>2</sub> and O<sub>2</sub> during the Phanerozoic: Tools, patterns, and impacts. *Treatise on Geochemistry (Second Edition)*, 6.

Scotese, C. R., Song, H., Mills, B. J., & van der Meer, D. G. (2021). Phanerozoic paleotemperatures: The earth's changing climate during the last 540 million years. *Earth-Science Reviews*, 103503.

Scotese, C. R. (2016). Tutorial: PALEOMAP paleoAtlas for GPlates and the paleoData plotter program.

Smart, M. S., Filippelli, G., Gilhooly III, W. P., Marshall, J. E., & Whiteside, J. H. (2022). Enhanced terrestrial nutrient release during the Devonian emergence and expansion of forests: Evidence from lacustrine phosphorus and geochemical records. *GSA Bulletin*. In Press.

Stein, W. E., Berry, C. M., Morris, J. L., Hernick, L. V., Mannolini, F., Ver Straeten, C., ... & Leake, J. R. (2020). Mid-Devonian *Archaeopteris* roots signal revolutionary change in earliest fossil forests. *Current Biology*, 30(3), 421-431.

Thompson, J. B., & Newton, C. R. (1988). Late Devonian mass extinction: episodic climatic cooling or warming? Complete this reference.

Ueyama, M., Ichii, K., Kobayashi, H., Kumagai, T. O., Beringer, J., Merbold, L., ... & Yasuda, Y. (2020). Inferring CO<sub>2</sub> fertilization effect based on global monitoring land-atmosphere exchange with a theoretical model. *Environmental Research Letters*, 15(8), 084009.

Wang, X., Liu, S. A., Wang, Z., Chen, D., & Zhang, L. (2018). Zinc and strontium isotope evidence for climate cooling and constraints on the Frasnian-Famennian (~ 372 Ma) mass extinction. *Palaeogeography, Palaeoclimatology, Palaeoecology*, 498, 68-82.

Xu, B., Gu, Z., Wang, C., Hao, Q., Han, J., Liu, Q., ... & Lu, Y. (2012). Carbon isotopic evidence for the associations of decreasing atmospheric CO<sub>2</sub> level with the Frasnian-Famennian mass extinction. *Journal of Geophysical Research: Biogeosciences*, 117(G1).

Zhang, L., Chen, D., Huang, T., Yu, H., Zhou, X., & Wang, J. (2020). An abrupt oceanic change and frequent climate fluctuations across the Frasnian–Famennian transition of Late Devonian: constraints from conodont Sr isotope. *Geological Journal*, 55(6), 4479-4492.

## CHAPTER 4. LINKING LAND PLANT EXPANSION TO EPISODIC ANOXIA IN A DEVONIAN LAKE

### 4.1. Introduction

The evolution and expansion of land plants in the Devonian was arguably one of the most important events in Earth's past. Its significance with respect to the diversification and proliferation of vascular land plants is surpassed only by its cascading impacts on global biogeochemical cycling and subsequent impacts on Earth's biosphere. The stepwise evolution of root systems resulted in the initiation of modern soil formation and weathering processes (Algeo et al., 1995; Algeo and Scheckler, 1998; Stein et al., 2012; Giesen and Berry, 2013; Berry and Marshall, 2015; Morris et al., 2015; Lenton et al., 2016; Stein et al., 2020; Davies et al., 2021) which likely had a significant impact on terrestrial nutrient flux (Algeo et al., 1995; Percival et al. (2020); Smart et al., 2022a; Smart et al., 2022b). The evolution of root systems combined with other innovations such as arborescence and the propensity for plants to bear seeds allowed plants to colonize a significant portion of the Earth's surface which had previously been relatively bereft of vegetation (Algeo et al., 1995; Algeo and Scheckler, 1998). The timing and impact of plant expansion has been widely debated (e.g., Algeo et al., 1995; Algeo and Scheckler, 1998; D'Antonio et al., 2020; Pawlik et al., 2020; Smart et al., 2022a), but some theorize that land plant evolution and expansion in the Middle to Late Devonian perturbed terrestrial nutrient flux to a large enough extent to cause (Algeo et al., 1995; Algeo and Scheckler, 1998), or at least exacerbate (Smart et al., 2022a; Smart et al., 2022b), some of the multiple marine extinctions which occurred during that interval.



Although evidence directly tying land plant expansion to global biogeochemical perturbations has generally been circumstantial, recent studies of Devonian lacustrine sequences have uncovered direct evidence of enhanced terrestrial nutrient export concurrent with land plant expansion (see Smart et al., 2022a; Smart et al., 2022b). In the case of the Devonian's most devastating mass extinctions, the Frasnian-Famennian extinction, the magnitude of nutrient export would have been sufficient to induce significant anoxia in the shallow and epeiric seas prevalent in the Period (Smart et al., 2022b). As land plant expansion occurred gradually between the Middle to Late Devonian (Algeo et al., 1995; Meyer-Berthaud et al., 1999; Meyer-Berthaud et al., 2010; Stein et al., 2020) and in an episodic fashion as suggested by some authors (Retallack and Huang, 2011; Smart et al., 2022a; Smart et al., 2022b), the implications of this are profound given the presence of five significant marine extinctions during the same timeframe (House, 1985; House, 2002). A limitation with terrestrial-based evidence, however, is its reliance on total phosphorus data as a primary gauge of terrestrial nutrient flux and internal nutrient dynamics (e.g., Smart et al., 2022a; Smart et al., 2022b). Isotopic analysis of nitrogen and carbon combined with phosphorus data and other geochemical proxies would greatly reduce uncertainty as to the source of the recorded nutrient influx whilst simultaneously providing insight into internal lake nutrient dynamics.

Here we present additional analyses of a high-resolution Middle Devonian lacustrine sequence temporally aligned with the Kačák extinction event. We integrate nitrogen isotopes ( $\delta^{15}\text{N}$ ) and carbon isotopes ( $\delta^{13}\text{C}$ ) with previously reported total phosphorus and multi-proxy geochemical data to further corroborate the evolution of land

plants as a causal or contributing factor to episodic lacustrine anoxia and subsequently, the Kačák extinction event. Principal component analyses are also performed on the body of geochemical data available for this Devonian lake to establish relational links between various geochemical proxies.

## 4.2. Materials and Methods

### 4.2.1. Sample Location and Background

The sample site is a locality known as Geanies near Tain, Easter Ross, Scotland (Fig 4.1.). The Geanies locality is the site of a series of cyclic Devonian lacustrine deposits located in what was once the Orcadian Basin, an area containing numerous Devonian lakes formed in extensional half graben basins (Marshall and Hewitt, 2003). The formation of the cyclic lacustrine deposits found at Geanies, and throughout the Orcadian Basin, is tied to astronomically forced climate perturbations (Astin, 1990; Kelly, 1992; Marshall 1996; Andrews and Trewin, 2010; Andrews et al., 2016). Specifically, a cycle of lake shallowing followed by deepening and subsequent shallowing recurred within the short eccentricity parameter (approximately every 100 kyr; Astin, 1990; Kelly, 1992). Such was this sedimentary chronometer that sequences in the Orcadian Basin are generally able to be relatively dated via counting the number of shallow-deep-shallow cycles, or lake cycles (e.g., Smart et al., 2022a and references contained therein). Our focus at Geanies is 12 of these lake cycles, covering approximately 1.2 Myr. Sample coverage begins in the Balintore Formation, extends into the Jesse Port Formation (Kačák event equivalent) in the latest Eifelian, and terminates in

the Geanies Formation in the earliest Givetian (Marshall et al., 2007; Marshall et al., 2011). Sampling methodology was every 10 cm from deep lake facies of each lake cycle.



Figure 4.1. Location of the Geanies sample site (annotated with a red star in the inset).

#### 4.2.2. Sample Preparation and Analysis

All samples were collected from the archives at the University of Southampton and were subsequently processed for geochemical analysis (see Smart et al. 2022a for detailed description of sample preparation). Samples were analyzed for total nitrogen (TN), bulk nitrogen isotopes  $\delta^{15}\text{N}_{\text{tot}}$  and organic carbon isotopes ( $\delta^{13}\text{C}_{\text{org}}$ ) using a Thermo EAIsolink elemental analyzer (EA) and a Thermo Delta V Plus isotope ratio mass spectrometer (IRMS). For  $\delta^{15}\text{N}_{\text{tot}}$  analyses, 60 mg of powdered sample was utilized. Five acetanilide standards were employed to obtain a reference curve and  $\delta^{15}\text{N}$  values were

normalized to USGS 40, Buffalo River Sediment and IAEA N1. Samples with amplitudes below the lowest acetanilide standard were rerun or discarded. Precision for the reference material was within 0.01 ‰. No more than 50 samples were run in succession (samples plus standards) to minimize drift. A blank was run with each set and  $\delta^{15}\text{N}_{\text{tot}}$  values were corrected utilizing the blank. For  $\delta^{13}\text{C}_{\text{org}}$  analyses, powdered samples were first acidified with phosphoric acid to remove inorganic C, with the remaining residue being representative of the organic fraction. The residue was rinsed, dried and homogenized. Average sample weight was approximately 10 mg but varied based on the organic C content. Samples were analyzed using a similar method as described above for  $\delta^{15}\text{N}$ , however  $\delta^{13}\text{C}_{\text{org}}$  values were normalized to USGS 40, Buffalo River Sediment and Bovine Liver. Precision for the reference material for  $\delta^{13}\text{C}_{\text{org}}$  analyses was within 0.1 ‰.

#### 4.2.3. Utility of Isotopic and Elemental Data

Nitrogen isotopes can record a great deal of information regarding geochemical cycling within a lake as well as the dominant source of organic matter.  $\delta^{15}\text{N}$  values of bulk lake sediments are generally reflective of the isotopic composition of the initial source of inorganic N. Lacustrine algae utilize dissolved nitrate as their primary inorganic N source. The  $\delta^{15}\text{N}$  values of dissolved nitrate found in lacustrine environments typically fall between +7-10 ‰, thus lacustrine algae have  $\delta^{15}\text{N}$  values of ~8.6‰ (Peters et al., 1978; Meyers, 1994; Meyers, 2003). In contrast, land plants utilize atmospheric  $\text{N}_2$ , which has an isotopic value of 0 ‰ and fractionation during biologic uptake is minimal, resulting in  $\delta^{15}\text{N}$  values of ~0.5 ‰ for land plants which use the C3 metabolic pathway (Peters et al., 1978; Meyers, 1994 and references contained therein), although values

ranging from -5 to +8 ‰ have been reported in various studies (Faure and Mensing, 2005; Leng et al., 2006). While fractionation varies for plants which utilize C4 and Crassulacean acid metabolism (CAM) pathways, those evolutionary advancements did not occur until well after the Devonian with the first appearance of C4 plants in the Oligocene and CAM plants in the Mesozoic (see Sage, 2004; Keeley and Rundel, 2003). Sedimentary  $\delta^{15}\text{N}$  values can also be impacted by factors such as water level changes and redox conditions within a lake. Water level changes can result in fractionation of up to +/- 2 ‰ (Cline and Kaplan, 1975; Meyers, 1997). Under anoxic or suboxic conditions, denitrification of dissolved nitrate results in the selective release of the lighter  $^{14}\text{N}$  isotope, leaving the remaining nitrate enriched in  $^{15}\text{N}$  (Cline and Kaplan, 1975; Mariotti et al., 1982; Meyers, 1997; Leng et al., 2006).

As  $\delta^{15}\text{N}$  values can be complicated by water level and redox changes, they cannot be relied upon as a sole method to determine the source of organic matter in lake sediments. The ratio of TOC to organic N (TON), referred to henceforward as C/N, offers an additional method to distinguish between allochthonous and autochthonous organic matter. The fundamental absence of cellulose in algae and its relative abundance in vascular land plants results in dramatically different C/N ratios for each. Algae typically have C/N ratios of between 4-10, while vascular land plants are typically > 20 (Meyers, 1994; Meyers, 2003). As with  $\delta^{15}\text{N}$  values, C/N ratios are not without limitations. In situ degradation of algae during sinking can sometimes result in elevated C/N ratios while ammonia absorption from the decomposition of organic matter in lake and ocean sediments can result in the remineralization and release of C, thereby lowering the C/N ratio (Meyers, 1994; Filley et al., 2001). Additionally, as indicated above, the ideal

comparison is that of TOC to TON. TOC values utilized are those from Smart et al. (2022a), however we use TN as an approximation for TON. This is done primarily because in most cases, the concentration of total inorganic N is small and methods to extract organic N are extremely laborious and often yield results very similar to or often indistinguishable from those which utilize TN. In some cases, however (see Müller, 1977; Sollins et al., 1984), ammonium can have a significant influence on the  $\delta^{15}\text{N}$  total value, but this can be tested for post-analysis and will be discussed in section 3.5. Additionally, the combination N isotopes and C/N ratios offers an additional approach to attributing the source of organic matter to our study lakes, whether algal or vascular land plant material (Meyers, 1994; Meyers, 2003).

Carbon isotopes offer a third method to assist in identifying the source of organic material within a lake but require an additional layer of analysis in order to be informative in that regard. Like  $\delta^{15}\text{N}$  values,  $\delta^{13}\text{C}_{\text{org}}$  values of lake sediments are determined by the source of C as well as fractionation associated with biological uptake. Isotopic fractionation during  $\text{CO}_2$  fixation by land plants varies according to which metabolic pathway they utilize (i.e., C3, C4 or CAM), with C3 plants producing a fractionation of approximately -20 ‰ relative to the  $\delta^{13}\text{C}$  of atmospheric  $\text{CO}_2$ . This results in a combined average  $\delta^{13}\text{C}_{\text{org}}$  value of -27‰ for C3 land plants (Orem et al., 1991; Meyers, 2003; Meyers, 1994; Tipple and Pagani, 2010). Complicating interpretations however, freshwater algae utilize dissolved  $\text{CO}_2$ , which is isotopically indistinguishable from atmospheric  $\text{CO}_2$ . Preferential uptake of  $^{12}\text{C}$  results in further fractionation of approximately -20 ‰ and a  $\delta^{13}\text{C}$  value of preserved sediment between -20 and -30 ‰, often making it difficult to distinguish from land plants (Orem et al., 1991;

Meyers, 2003). It is for this reason that a comparison of  $\delta^{13}\text{C}_{\text{org}}$  vs C/N ratios is often utilized to differentiate allochthonous or autochthonous sources (e.g., Meyers, 1994; Meyers, 2003). Thus, combined analyses of  $\delta^{13}\text{C}_{\text{org}}$ , C/N and  $\delta^{15}\text{N}$  can provide a robust estimate of the organic matter sources. Additional factors which can impact  $\delta^{13}\text{C}_{\text{org}}$  values include the anaerobic decomposition of organic matter due to methanogenesis and oxidation of methane which can result in low  $\delta^{13}\text{C}_{\text{org}}$  values ( $< -69\text{‰}$ ) (e.g., Yamaguchi et al., 2009; Blaser and Conrad, 2016).

We also utilize principal component analysis (PCA) conducted in Graphpad Prism in order to reveal trends amongst the geochemical parameters analyzed here and in combination with those of previous studies on this sample sequence. PCA is advantageous for large data sets as it serves to reduce dimensionality among the different variables whilst simultaneously preserving the original information. While there are various methods utilized to identify principal components, we utilize parallel analysis here which is a method that accounts for data variance due to noise. We incorporate  $\delta^{15}\text{N}$ ,  $\delta^{13}\text{C}_{\text{org}}$  and C/N ratios determined in this study with numerous proxies using data from Smart et al. (2022a). Additional proxies selected for PCA include those for terrestrial phosphorus (P) input such as P/Al, P/Fe and P/Ti (e.g., Filippelli and Souch, 1999; Smart et al., 2022a); the paleoclimate proxy Sr/Cu (e.g., Vosoughi Moradi et al., 2016; Tang et al., 2019; Li et al., 2020; Pan et al., 2020); the chemical weathering proxy Rb/Sr (e.g., Xu et al., 2010); physical weathering proxies Mg/Al, Nb/Al, Sr/Al, Th/Al and Y/Al (e.g., Wei and Algeo, 2020); silt to clay ratio proxy Ti/Al (see Calvert and Pedersen, 2007; Wei and Algeo, 2020); and redox proxies Cu/Al (expressed as an enrichment factor,  $\text{Cu}_{\text{EF}}$ , relative to reference values for upper continental crust established by McLennan (2001);

see Algeo and Liu, 2020; Smart et al., 2022a) and the ratios of TOC to total P ( $C_{org}:P_{tot}$ ) (e.g., Algeo and Ingall, 2007). Multiple proxies were selected wherever possible, but in the case of paleoclimate and chemical weathering proxies, only one was possible for each based on the limitation in elemental data from the source data set. Smart et al. (2022a) utilized seven distinct redox proxies in their study, but we limit our analyses to  $Cu_{EF}$  and  $C_{org}:P_{tot}$  for clarity as all seven were equally efficacious in the original study. We employ five distinct physical weathering proxies as covariation of all five is generally indicative of a lack of secondary alteration amongst our samples (e.g., Wei and Algeo, 2020), something which would be abundantly clear in a plot of PCA loadings. While PCA was performed on the entire sample sequence, as noted by Smart et al. (2022a) there appears to be a distinction between the lower lakes (9-13) and the upper lakes (14-20), thus additional and separate PCAs were performed on the samples using this division.

### 4.3. Results

#### 4.3.1. Isotopic and Elemental Analyses

Results for  $\delta^{15}N$ ,  $\delta^{13}C_{org}$  and C/N are shown in Fig. 4.2. Ratios of C/N were generally high for the sequence with a median value of 19.1. While there are no defined periods of particularly low C/N ratios, lake 14 has the overall lowest values (except for the top of the lake) with a median value of 12.8. The highest values are observed in lakes 10, 11, 16 and 19 with maxima  $>100$  in all but lake 16. Maxima in lake 16 is  $\sim 60$  with a median value of 43.2.



$\delta^{15}\text{N}$  appears to generally trend with C/N ratios and varies between 3.6 and 17.0 ‰, with a median value of 6.1 ‰. Higher values ( $> 7$  ‰) are prevalent in lakes 10, 12, 16 and 19 with overall lower values ( $< 7$  ‰) in lakes 9, 11, 13-15, 17, 18 and 20.

The  $\delta^{13}\text{C}_{\text{org}}$  values are antithetic to those of  $\delta^{15}\text{N}$ . Values range between -33.7 to -25.7 ‰, with a median value of -28.3 ‰. Lower values ( $< -30$  ‰) are observed in lakes 10, 12 (upper portion), 16 (upper portion) and 19 (middle). Higher values ( $> -30$  ‰) are observed in lakes 11, 12 (lower portion), 13-15, 16 (lower portion), 17, 18 and 20.

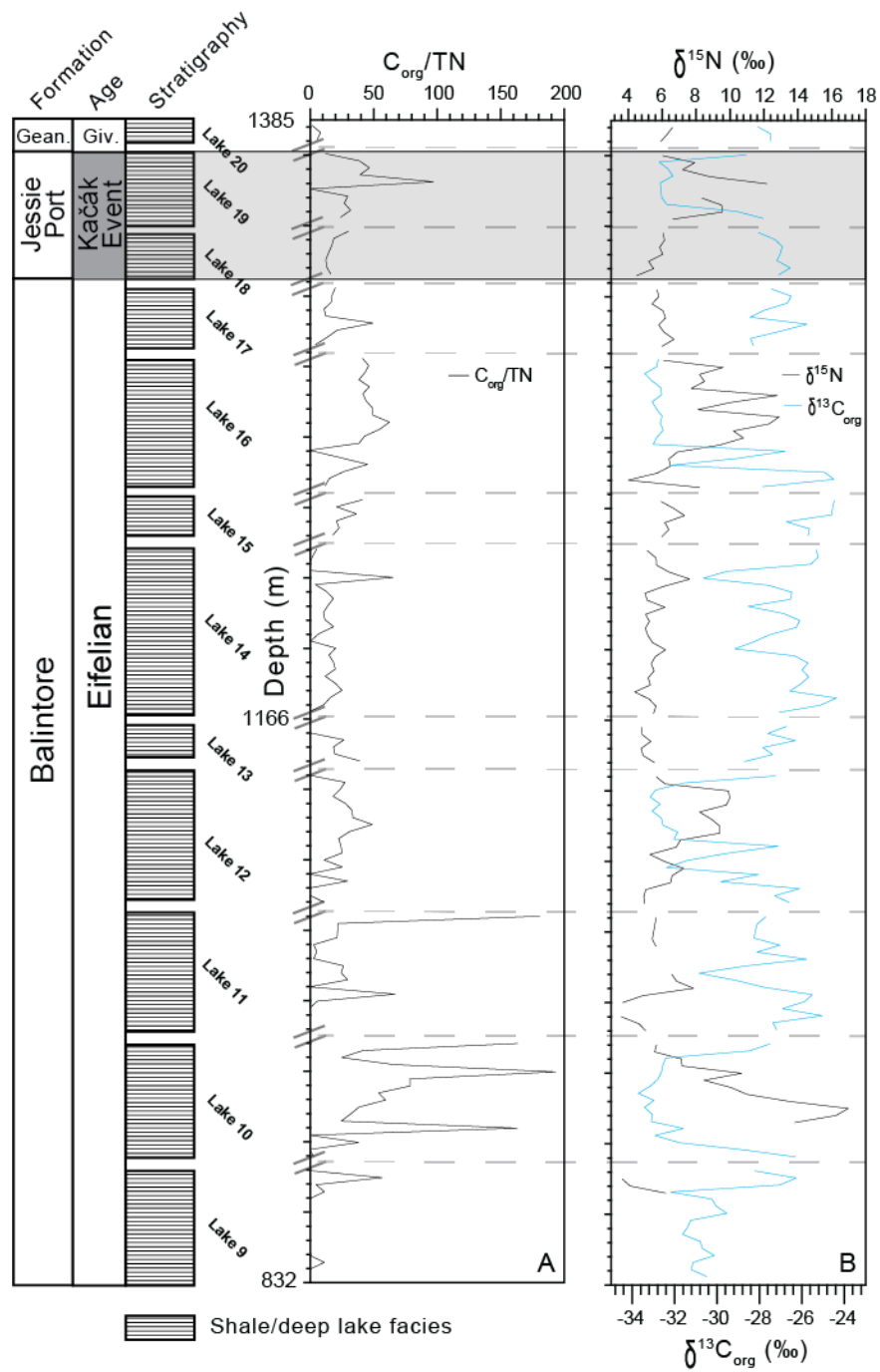


Figure 4.2. Results for EA-IRMS analyses of the Geanies sequence plotted against depth (m). Formation, age and general stratigraphy are shown on the left. Gray dashed lines show lake cycle boundaries. Gray shaded region represents the interval concurrent with the Kačák extinction event. A. Ratio of  $C_{org}/TN$  with  $C_{org}$  data derived from Smart et al. (2020a). B.  $\delta^{15}N$  results shown in black and  $\delta^{13}C_{org}$  results shown in blue.

#### 4.3.2. Principal Component Analysis – Entire Sequence

Results for PCA for the combined sequence are shown in Fig. 4.3. The first principal component (PC1) accounted for 44.27% of the total variance in the dataset, followed by 16.18% for the second principal component (PC2) and 11.00% for the third principal component (PC3). Together, these three PCs accounted for 71.45% of the total dataset variance. While additional PCs were calculated, their proportion of the total variance was significantly less than the first three and thus will not be considered here. A cross plot for the first two PCs (Fig. 3) shows relationships between the proxies analyzed. Notably, all proxies seem to fit within four relative groupings: (1) P/Fe, P/Al, P/Ti, C/N and  $C_{org}$ ; (2)  $Cu_{EF}$ ,  $C_{org}:P_{tot}$  and  $\delta^{15}N$ ; (3) Ti/Al, Sr/Cu, Nb/Al, Mg/Al, Y/Al, Th/Al and Sr/Al; and (4)  $\delta^{13}C_{org}$  and Rb/Sr. Additionally, within those four groupings, related proxies further group together. Specifically, those indicative of terrestrial nutrient flux (P/Fe, P/Al and P/Ti), organic matter content/influx (C/N and  $C_{org}$ ) and those associated with physical weathering (Nb/Al, Mg/Al, Y/Al, Th/Al and Sr/Al). The strongest loadings are associated with PC1 and include all the physical weathering proxies (ranging between -0.87 and -0.90),  $C_{org}:P_{tot}$  (0.80),  $\delta^{15}N$  (0.76), Rb/Sr (-0.70) and  $\delta^{13}C_{org}$  (-0.66). Additionally, Sr/Cu and  $Cu_{EF}$  both have loadings  $> 0.50$ . While the loadings for PC2 are less in magnitude, C/N,  $C_{org}$ , P/Ti and P/Fe are all  $> 0.50$ . Notably,  $C_{org}$  seems to be strongly associated with both PC1 and PC2 with loadings of 0.58 and 0.65, respectively. C/N appears to also be associated with both PC1 and PC2 with loadings of 0.46 and 0.50, respectively. The remaining proxies, P/Al and Ti/Al have the weakest loadings. P/Al is associated with PC2 and comes in slightly lower than the other proxies associated with PC2 at 0.49. Ti/Al is most strongly associated with PC1 with a loading of 0.46, but also

shows some association with PC2 with a loading of -0.39. The majority of PC3 loadings are weak, excepting P/Al (0.76) and P/Fe (0.67).  $C_{uEF}$ ,  $C_{org}$  and  $C_{org}:P_{tot}$  show some association with PC3, but their loadings range between 0.37-0.40.

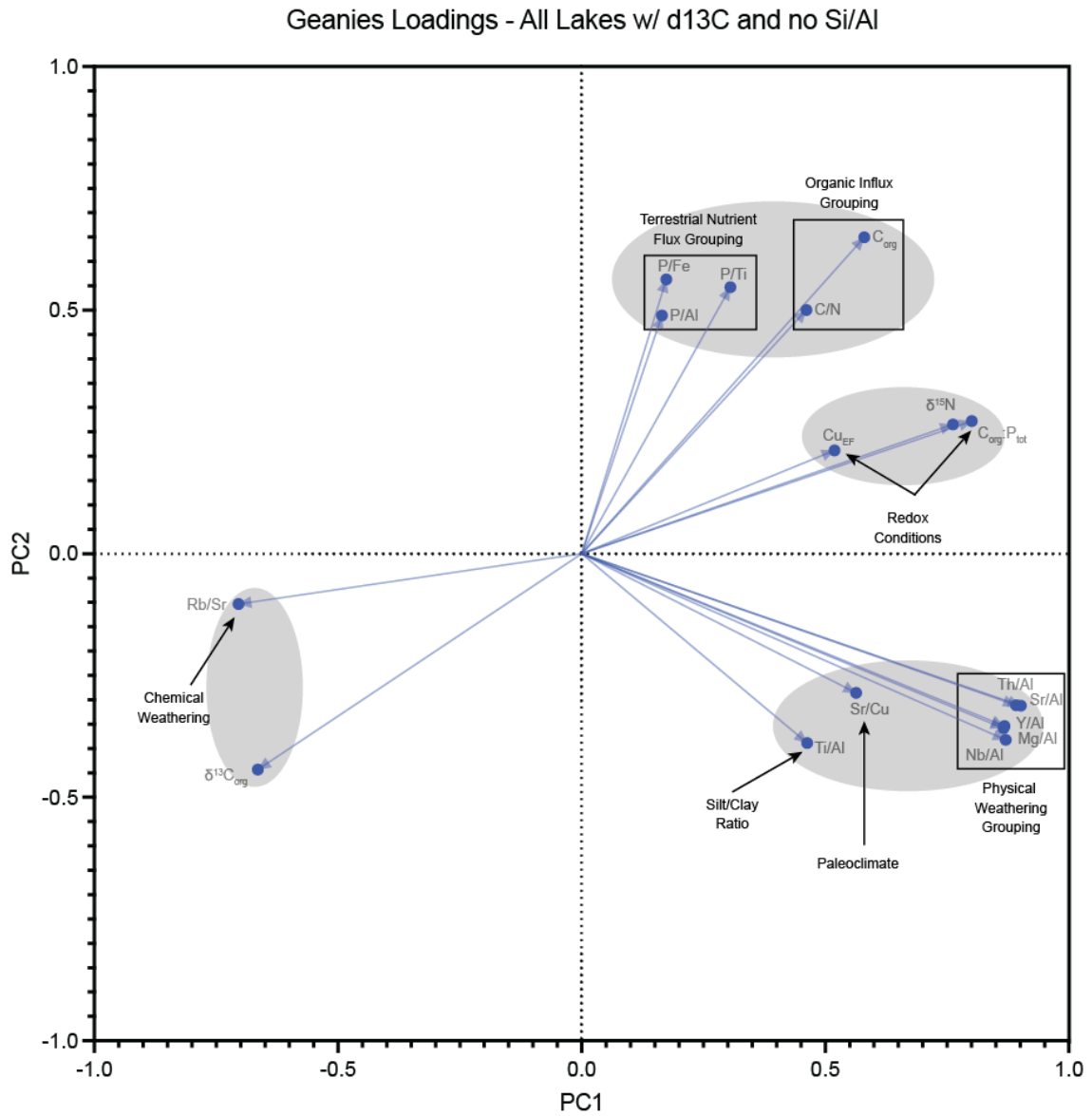


Figure 4.3. Cross plot of PCA results for PC1 and PC2 for the entire Geanies sequence (lakes 9-20). Significant groupings are highlighted in gray. Black boxes denote related proxies which group closely (e.g., terrestrial nutrient flux, organic matter influx and physical weathering proxies).

#### 4.3.3. Principal Component Analysis – Lower Geanies

Results for the PCA for the lower portion of the Geanies sequence (lakes 9-13) are shown in Fig. 4.4. Utilizing parallel analysis, only two principal components were selected, PC1 and PC2. This is based on the principal behind parallel analysis used in Graphpad Prism whereby Monte Carlo simulations are performed on random data similar to the sample data and assigned eigenvalues. The mean of these eigenvalues is compared with those of the sample data and only sample PCs with eigenvalues greater than the 95th percentile of the simulated eigenvalues are selected. In this case, there were only two. PC1 accounted for 40.31% of the total variance in the data set and PC2 accounted for 20.10%, for a combined total of 60.42%. Similar groupings of related proxies are again observed in the lower lakes. Notably, the physical weathering proxies again group tightly and have strong loadings associated with PC1 (0.90 – 0.93). The terrestrial nutrient flux proxies P/Ti and P/Al group together, but P/Fe is notably separate and displays a relatively weak loading (0.17 for PC1 and 0.23 for PC2). The organic influx proxies C<sub>org</sub> and C/N again group together and display some of the strongest loadings on PC1 at 0.94 and 0.78, respectively. Significant differences from the previous PCA include the notable separation of redox proxies, the grouping of  $\delta^{15}\text{N}$  with the terrestrial nutrient flux proxies and the weak loadings for Sr/Cu and Cu<sub>EF</sub> (0.18 and 0.26 for PC2, respectively).

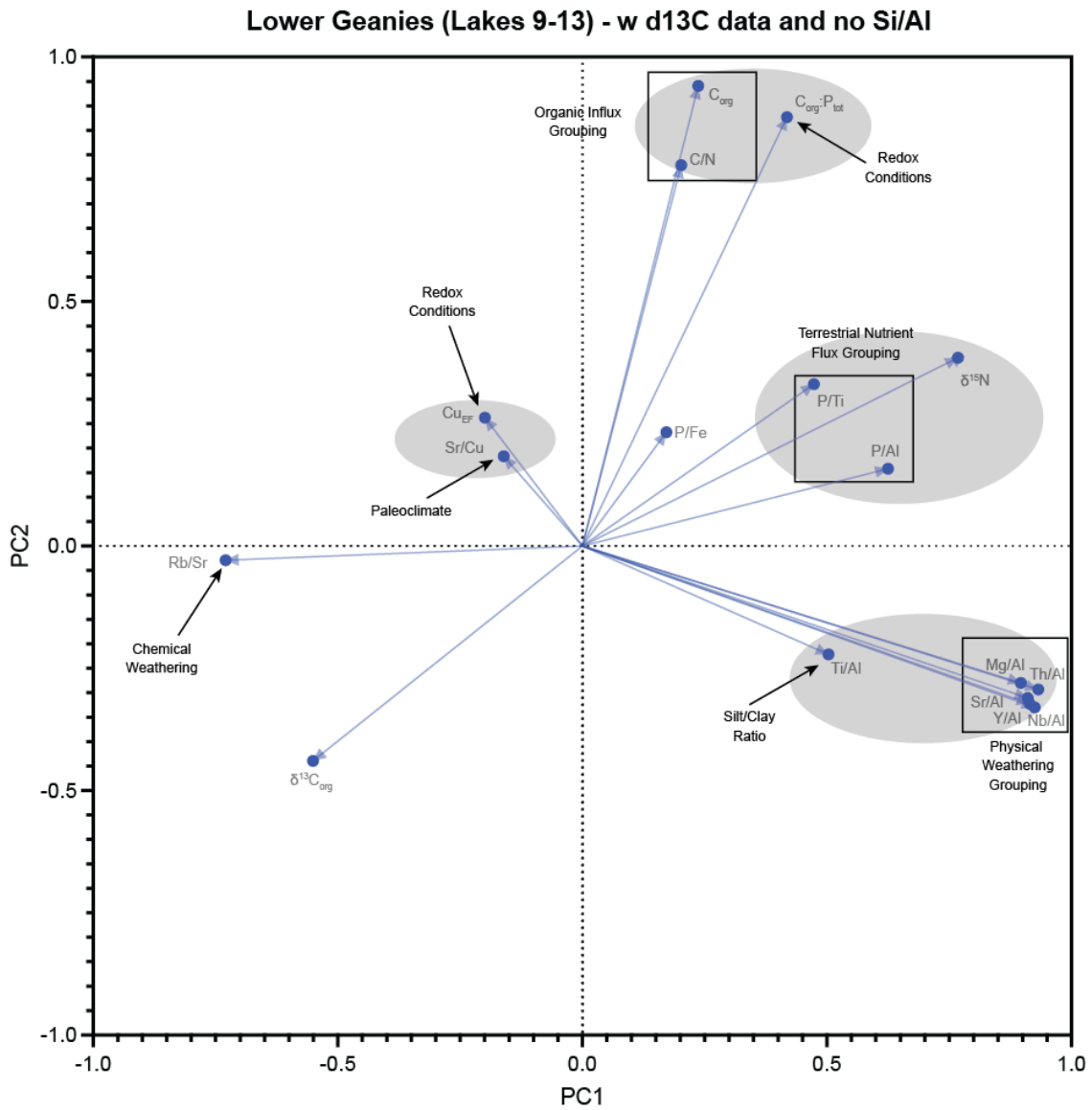


Figure 4.4. Cross plot of PCA results for PC1 and PC2 for the lower lakes at Geanies (lakes 9-13). Significant groupings are highlighted in gray. Black boxes denote related proxies which group closely (e.g., terrestrial nutrient flux, organic matter influx and physical weathering proxies).

#### 4.3.4. Principal Component Analysis – Upper Geanies

Results for the PCA on the upper lakes at Geanies, lakes 14-20, are given in Fig.

4.5. Similar to the PCA on the entire sequence, three PCs were identified. PC1 accounted for 55.43% of the total variance, PC2 14.04% and PC3 11.00% for a combined total of 80.47%. All loadings are relatively strong (the lowest being P/Ti at 0.52 and Ti/Al at 0.54). Related proxies group in a similar fashion here as well. The most notable difference is the relative isolation of the terrestrial nutrient flux grouping. Whereas in the PCA for the entire sequence the terrestrial nutrient flux proxies grouped closely with the organic influx proxies, here the organic influx proxies are separated from both the terrestrial nutrient flux grouping and each other. The organic influx proxies instead group closely with both redox proxies as well as  $\delta^{15}\text{N}$ , all of which are strongly associated with PC1 having loadings of between 0.80 – 0.89. The physical weathering proxies again group together here and display the largest loadings associated with PC1 of between 0.88 – 0.93. They also appear more strongly associated with Sr/Cu than in the PCA for the entire sequence with Sr/Cu reflecting a loading on PC1 of 0.75 (compared with 0.56 in the first scenario). Rb/Sr and  $\delta^{13}\text{C}_{\text{org}}$  again group closely here and have similar magnitudes associated with PC1 as in the first scenario (-0.71 and -0.72, respectively). Loadings for PC3 are weak here as well, apart from Ti/Al, P/Fe and P/Al (0.53, 0.65 and 0.68 respectively).

#### 4.3.5. Potential Influences on Elemental and Isotopic Data

Based on the variation observed in both the elemental and isotopic data, the lakes at Geanies appear to present an extremely dynamic environment. C/N ratios vary significantly not only from lake to lake, but in many cases within the lakes themselves

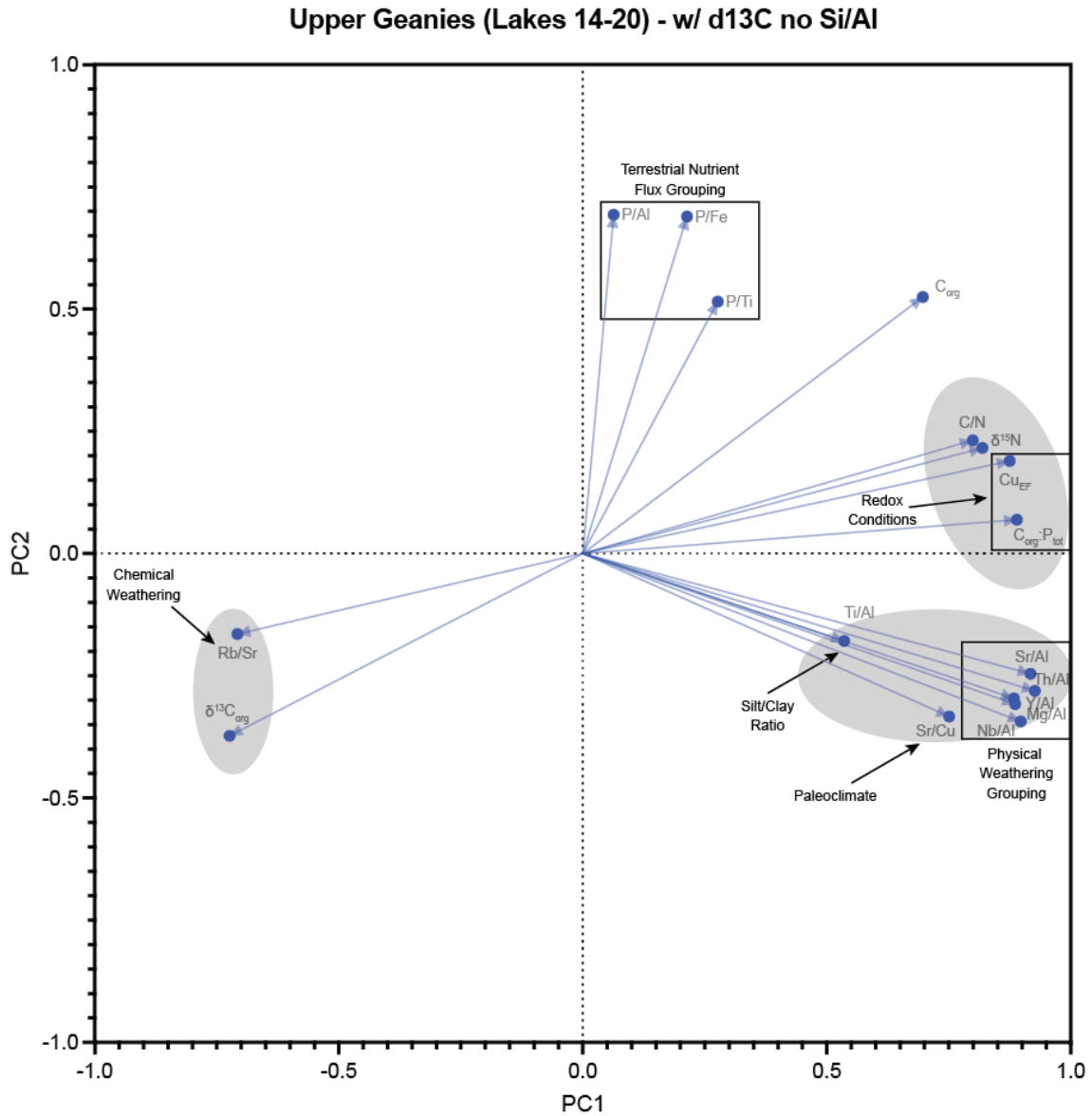


Figure 4.5. Cross plot of PCA results for PC1 and PC2 for the upper lakes at Geanies (lakes 14-20). Significant groupings are highlighted in gray. Black boxes denote related proxies which group closely (e.g., terrestrial nutrient flux, organic matter influx and physical weathering proxies).

(e.g., lakes 10, 11, 16, 17 and 19). This is also true for both  $\delta^{13}\text{C}_{\text{org}}$  and  $\delta^{15}\text{N}$  and generally during the same intervals that C/N experiences large in-lake variations. What's



more, the antithetic relationship observed between  $\delta^{13}\text{C}_{\text{org}}$  and  $\delta^{15}\text{N}$  (Fig. 4.2) results in a statistically significant negative correlation ( $r^2=0.55$ ,  $p<0.0001$ ). This relationship is suggestive of geochemical changes occurring within these lake cycles driven by external stimuli.

Herein, the C/N ratio is utilized to differentiate vascular plant contributions to the lake record, where values greater than 20 are generally considered consistent with vascular land plant material (Meyers, 1994; Meyers, 2003). The utility of this ratio assumes a comparison between organic sources of C and N. Utilizing bulk TN as an approximation for organic N may alter data interpretations (see section 4.2.3) if there is a significant fraction of inorganic N. C/N ratios containing inorganic N would result in artificially low values that potentially mask contributions from vascular plant material. For a portion of the dataset, the median C/N value of 19.1 could indicate a conservative estimate of plant derived organic matter; however, lakes with relatively lower C/N ratios, such as lake 14 with a median value of 12.8, an admixture of inorganic N would shift the ratios to lower values and mischaracterize the organic matter sources. To address this, a cross-plot of TOC vs TN can be used to determine the relative contribution of inorganic N to the bulk sedimentary N concentrations (Schubert and Calvert, 2001; Calvert, 2004).

Correlation between TOC and TN for the entire Geanies sequence is high ( $r^2=0.6117$ ,  $p<0.0001$ ), however linear regression reveals a non-zero x-intercept of 0.012, indicating that inorganic N is present (Fig. 4.6). This could potentially be a result of the presence of clay-bound ammonium in these lacustrine sediments, however this value is small and unlikely to significantly bias the overall interpretations (Calvert, 2004 and references contained therein). Additionally, as there are 12 distinct lake cycles in the Geanies sequence, it is possible to further refine this analysis down to individual lake cycles. Performing individual regressions on each lake cycle independently reveals that most lake cycles are unaffected and only lakes 12, 16 and 19 have non-zero intercepts (0.016, 0.014 and 0.006 respectively). Nevertheless, these values are quite low and very close to zero, especially for lake 19, so the impact of inorganic N is assessed as minimal.

Furthermore, lakes 12, 16 and 19 have median C/N ratios of 24.6, 43.2 and 31.1

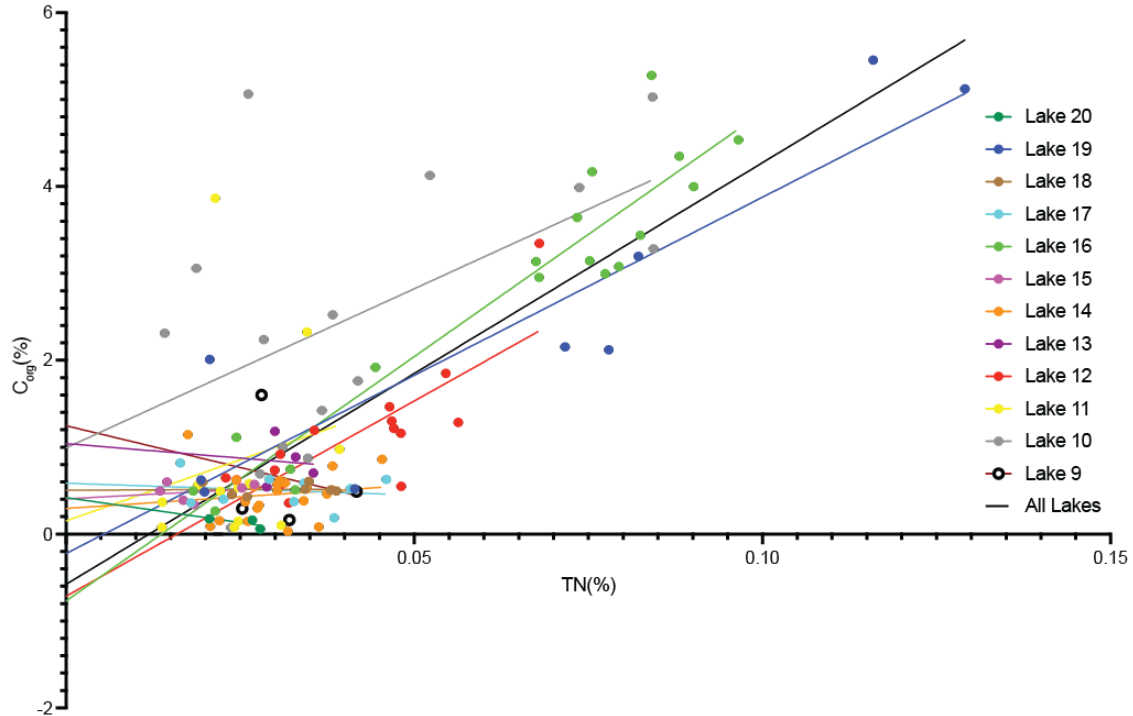


Figure 4.6. Cross-plot of  $C_{org}$  and TN. Individual lake cycles are color-coded (see legend). Linear regressions were performed on each lake cycle individually and on the entire data set (black line).

respectively, so even if the presence of inorganic N has decreased the C/N ratios, they are still well within those consistent with C3 land plants. Thus, the data are highly robust, lending confidence to our interpretations.

Another potential concern could be diagenetic changes due to N renewal during decomposition (see section 4.2.3) which could lower C/N ratios. This concern can similarly be addressed by a cross-plot of  $\delta^{15}\text{N}$  and C/N. A linear regression showing strong correlation between the two would be suggestive of diagenetic changes. While some correlation is observed in our data (Fig. 4.7a), it is fairly weak ( $r^2=0.1143$ ,  $p<0.0002$ ) suggesting that diagenetic impacts are possible, but likely not strongly biasing the data.

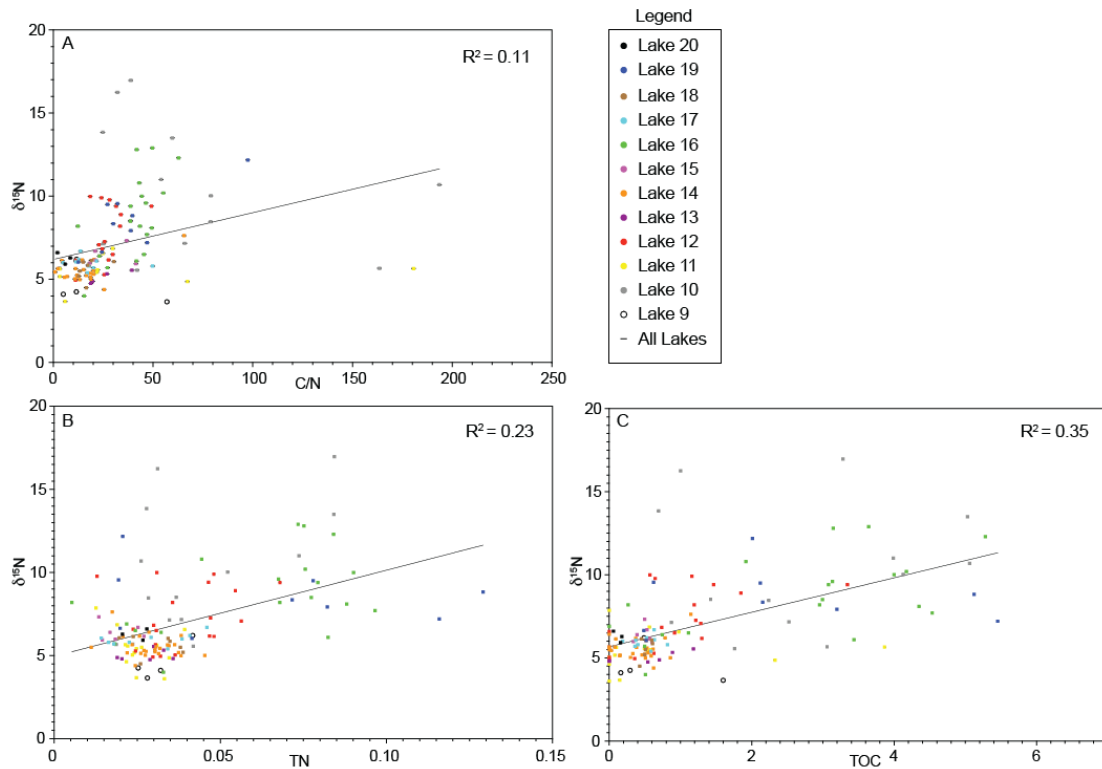


Figure 4.7. Cross-plots for the Geanies sequence. Data is plotted by lake cycle and color coded (see legend). Linear regression for the entire data set is indicated by the black line and correlation is noted in the upper right corner. (A)  $\delta^{15}\text{N}$  vs C/N; (B)  $\delta^{15}\text{N}$  vs TN and (C)  $\delta^{15}\text{N}$  vs  $\text{C}_{\text{org}}$ .

Finally, it is also essential to consider the impact any potential lithological changes could have on the data. Changes in lithology can result in the varying delivery of N bound to clay minerals (i.e., ammonium), which has the potential to alter bulk  $\delta^{15}\text{N}$  values. Given that the sequence spans approximately 1.2 Myr and is marked by climate oscillations which impacted terrestrial influx (see Smart et al., 2022a), this is a significant concern, especially given the large variations observed in  $\delta^{15}\text{N}$  throughout the sequence. Strong correlation between  $\delta^{15}\text{N}$  and both TOC and TN can indicate whether lithological changes are driving variation in the data (Percival et al., 2022). Cross-plots from the Geanies sequence for both are shown in Fig. 4.7b,c. While statistically significant correlations do exist for both  $\delta^{15}\text{N}$  vs TOC ( $r^2=0.35$ ,  $p<0.0001$ ) and  $\delta^{15}\text{N}$  vs TN ( $r^2=0.23$ ,  $p<0.0001$ ), they are relatively weak, especially given the climate fluctuations referenced above which could catalyze such changes. While lithological variations likely influenced the data to some degree, they are unlikely to have been significant enough to overprint the isotopic signature. It is more likely that internal lake geochemistry is the dominant factor and the  $\delta^{15}\text{N}$  values observed at Geanies are reflective of true nitrogen cycle perturbations. Furthermore, regressions performed on individual lake cycles for  $\delta^{15}\text{N}$  vs TOC data reveal that only lakes 12, 13 and 16 have statistically significant correlations ( $r^2=0.34$ ,  $p<0.0091$ ;  $r^2=0.67$ ,  $p<0.046$ ;  $r^2=0.36$ ,  $p<0.0064$  respectively). Separate lake cycle regressions for the  $\delta^{15}\text{N}$  vs TN data return a statistically significant correlation for lake 16 only ( $r^2=0.24$ ,  $p<0.033$ ). This points to the conclusion that lithological variations occurred during this 1.2 Myr period, but they were likely only significant during specific lake cycles (most likely lake 16, based on both results).

While clearly there are some influences on the data which must be considered, based on the examination above it is reasonable to conclude that the elemental and isotopic data from Geanies is minimally biased. The nitrogen cycle perturbations and C/N ratios recorded are likely generally reflective of true geochemical cycling within the lakes and allochthonous input of C3 plant material, respectively.

#### 4.4. Discussion

##### 4.4.1. Evidence for the Presence of Vascular Land Plants

One of the primary objectives of this study is to determine if there is a real link between terrestrial soil development and marine anoxia associated with Devonian marine extinctions. A corollary objective being to uncover data linking these biogeochemical perturbations to the Kačák extinction event. The elemental and isotopic composition of organic carbon and nitrogen suggest vascular land plant material was mobilized into the lakes at Geanies. Of the 123 samples for which C/N ratios could be determined, 17 had C/N ratios < 10 corresponding to a system dominated by lacustrine algae, 29 had C/N ratios between 10-20 corresponding to a mixed input system, and 77 had C/N ratios > 20 corresponding to a system dominated by C3 land plant organic matter.

The range in C/N for algae and C3 plant material compared to their respective  $\delta^{13}\text{C}_{\text{org}}$  values (Meyers 1994) further illustrates the contribution of vascular plant matter to most of the lakes (Fig. 4.8). Assuming the intrinsic carbon isotope fractionations during photosynthesis has not changed through the Phanerozoic (e.g., Kędzior et al., 2022; Wan et al., 2019), the  $\delta^{13}\text{C}_{\text{org}}$  ranges associated with modern C3 plants are also

applicable in the Devonian. Nearly every lake contains samples which contain organic matter from C3 land plants, including lakes 18 and 19 which are temporal correlatives with the Kačák event. A minority of lakes appear to record at least some periods where they were dominated by lacustrine algae, specifically lakes 9, 14, 17 and 20 (adopting a slightly wider window allows the inclusion of lakes 10 and 12 as well). There are numerous samples which fall outside either the isotopic or the C/N window. Most samples fall within the end member elemental and isotopic compositions for lacustrine algae and C3 land plants, but a significant number are  $^{13}\text{C}$  depleted. These samples represent portions of lakes 9, 10, 11, 12, 14, 16 and 19 (notably, samples for each of these lakes fall within the established windows as well). However, most of these samples come from four lakes: 10, 12, 16 and 19. Conversely, C/N ratios are nearly all inside the range for lacustrine algae and C3 land plants (or somewhere in-between). Only seven samples fall outside this range and include lakes 10, 11, 14 and 20. Reasons for these deviations will be explored below, but with those exceptions noted, the data overwhelmingly support the presence of C3 land plant material within the lakes at Geanies. This confirmation supports the conclusions of Smart et al. (2022a) that land plants were present throughout the entire Geanies sequence, and leaves open the possibility that they did indeed influence geochemical cycling at Geanies. The extent of their influence however has yet to be fully corroborated and will be further investigated.

#### 4.4.2. A Multi-proxy Approach

Based on the body of evidence presented here, terrestrial land plants were present in the drainage basin and were the dominant source of organic matter at Geanies. The

concurrency of both the isotopic and elemental data provide a significant and robust characterization of the linkages between early soil formation and influx to the lakes. There is also strong cause to suggest that land plant expansion was indeed episodic here (Smart et al., 2022a). This is particularly apparent in lakes 10, 16 and 19 which are explored in detail in this section.

Combining data from Smart et al. (2022a) with those presented here provides an opportunity for a highly robust analysis of lake dynamics. Fig. 4.9 is a plot which combines C and N data from this study with proxies from Smart et al. (2022a) that include P/Ti for terrestrial input;  $C_{org}$ ; the paleoredox proxy  $C_{org}:P_{tot}$ ; physical weathering proxies Sr/Al, Nb/Al and Y/Al; the paleoclimate proxy Sr/Cu; and the chemical weathering proxy Rb/Sr. P/Ti and C/N appear to covary throughout the record (with the singular exception being lake 9), and specifically during intervals where both are elevated (e.g., lakes 10, 16 and 19). They also both attain maxima in lake 10 and decrease steadily through lake 14. Smart et al. (2022a) attribute this pattern in P/Ti to the stabilization of phosphorus (P) in a young landscape over time (e.g., Filippelli and Souch, 1999; Filippelli, 2002). Notably, during the intervals where P/Ti and C/N both exhibit elevated values (lakes 10, 16 and 19), concurrent maxima are observed in  $\delta^{15}N$ ,  $C_{org}$ ,  $C_{org}:P_{tot}$  and amongst the physical weathering proxies. Conversely, minima are observed in  $\delta^{13}C_{org}$  during those intervals. A possible explanation for these trends could be elevated terrestrial P export due to land plant proliferation adjacent to the lake or within the drainage basin (Smart et al., 2022a). Elevated P/Ti values in combination with high C/N and low  $\delta^{13}C_{org}$  values suggest a greater proportion of incoming C3 plant material concurrent with increased terrestrial P export into the lakes. The high  $C_{org}$  (> 4% for lake

16 and > 5% for lake 19) recorded in this interval is likely the result of carbon exported into the lake combined with increased deposition of autochthonous organic matter due to elevated in situ production stimulated by increased P influx. Terrestrial P export of a similar magnitude has been shown to be sufficient to cause widespread anoxia in a similar Devonian sequence (Smart et al., 2022b) and the combined elemental and isotopic data appear to support that here as well.

The striking concurrence amongst the geochemical parameters indicate that the above scenario is exactly what is occurring here, and this conclusion is further supported by the carbon isotope data.  $\delta^{13}\text{C}_{\text{org}}$  values attain minima during these anoxic intervals (between approximately -32.5 and -33.5 ‰) which as noted in section 4.4.1, is below that typically associated with land plants or lacustrine algae. There are several possible

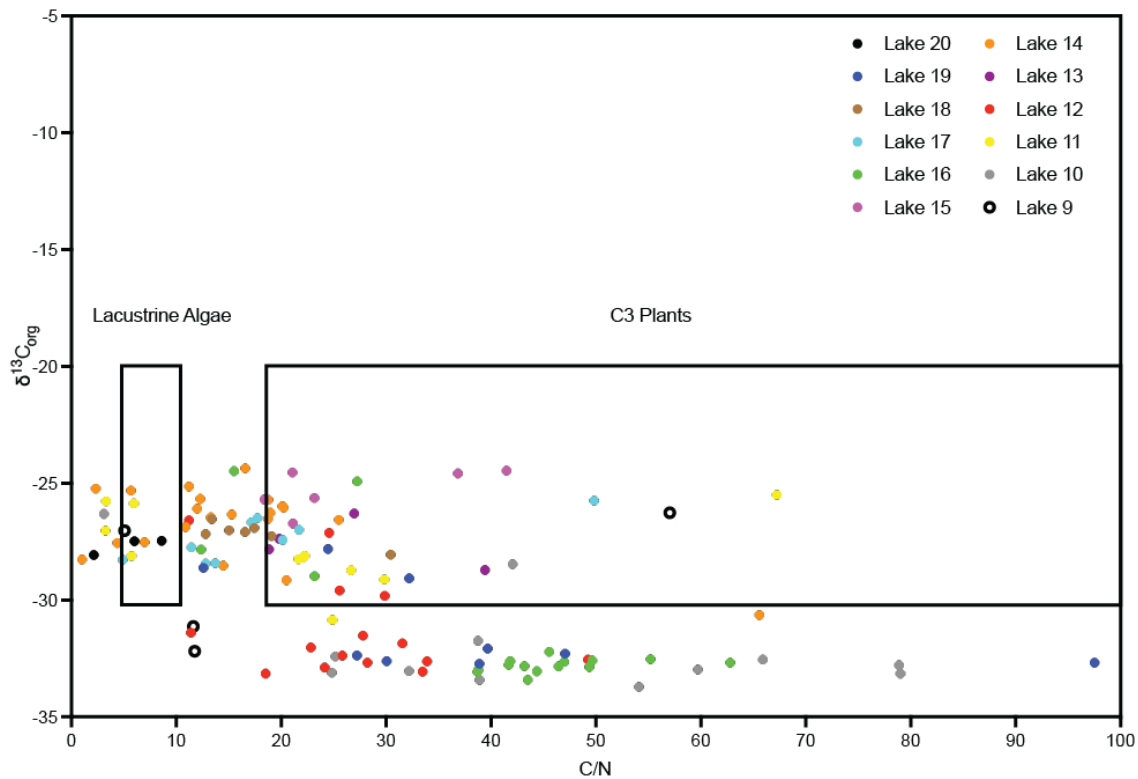


Figure 4.8. Cross-plot of  $\delta^{13}\text{C}_{\text{org}}$  and C/N. Samples are color coded by lake cycle (see legend). Boxed regions represent typical windows for lacustrine algae and C3 land plants (Orem et al., 1991; Meyers, 2994; Meyers, 2003).



explanations for this. The first is the occurrence of methanogenesis, or anaerobic respiration carried out by methanogens. As methanogens do not grow in the presence of O<sub>2</sub>, they are common in anoxic environments and thus it is likely they were present, at the very least, during the anoxic intervals in the lakes at Geanies. Isotopic fractionation associated with methanogens can result in  $\delta^{13}\text{C}_{\text{org}}$  values as low as -69 ‰ (Conrad, 2005; Faure and Mensing, 2005; Blaser and Conrad, 2016 and references contained therein). Even a minimal amount of methanogenesis in the lake could lower the  $\delta^{13}\text{C}_{\text{org}}$  of the sediments. This interpretation is supported by evidence of anoxia given by the redox proxy data. In each case where anoxia is likely (lakes 10, 12, 16 and 19),  $\delta^{13}\text{C}_{\text{org}}$  values attain their lowest levels. Outside of these anoxic intervals,  $\delta^{13}\text{C}_{\text{org}}$  values are up to 6 ‰ higher. While the above scenario is highly plausible, another possible explanation for the low  $\delta^{13}\text{C}$  values is that atmospheric composition during the Devonian may have resulted in changes to metabolic fractionation in C3 land plants compared with those of modern plants (e.g., Beerling et al., 1993). Atmospheric pCO<sub>2</sub> values in the Devonian were still extremely high, especially in the Middle Devonian with estimates ranging from 500-3000 ppm (Franks et al., 2014; Royer, 2014; Lenton et al., 2018). It has been estimated that isotopic composition of atmospheric pCO<sub>2</sub> likely ranged between -9.7 to -16.7 ‰ based on the pCO<sub>2</sub> estimates above (Schubert et al., 2012). Compared with modern pCO<sub>2</sub> isotopic composition values of -7 ‰, this a difference of -2.7 to -9.7 ‰ and could potentially result in final  $\delta^{13}\text{C}$  values of Devonian land plants lower than that observed in modern C3 land plants. Despite this difference however, a study by Wan et al. (2019) on 190 fossil plant specimens from the Devonian and Early Carboniferous concluded that  $\delta^{13}\text{C}$  values of ancient plants are similar to modern C3 plants with a reported range of

between -20.3 and -30.5 ‰. Thus, it is unlikely differences in  $\delta^{13}\text{C}$  values between modern and ancient C3 land plants can account for the observed low  $\delta^{13}\text{C}$  values in lakes 10, 12, 16 and 19. An additional possibility is that the low  $\delta^{13}\text{C}_{\text{org}}$  values are simply associated with the type of lacustrine algae prevalent at the time. Studies of similar Devonian lacustrine sequences in the Orcadian Basin report  $\delta^{13}\text{C}_{\text{org}}$  values of as low as -33 ‰ associated with algal material (see Stephenson et al., 2006; Wilson, 2012), although it is worth noting that simultaneously high C/N ratios were not noted in those studies as they were in the Geanies sequence. Eutrophication catalyzed by increased terrestrial nutrient influx would be expected to result in increased deposition of autochthonous organic matter. This possibility is unlikely however, as C/N ratios in each case suggest the presence of a much greater proportion of plant derived organic matter. Also of note,  $\delta^{13}\text{C}_{\text{org}}$  values during periods of relative geochemical stability (e.g., lakes 13-15) are enriched in  $^{13}\text{C}$  isotope (ranging between -30.6 and -24.4 ‰) and consistent with values common amongst modern algae and C3 land plants (see section 4.2.3). Thus, it is reasonable to conclude that the isotopic values observed at Geanies are generally consistent with lacustrine algae and land plant material and that the lower  $\delta^{13}\text{C}_{\text{org}}$  values are easily explained by invoking methanogenesis occurring during the anoxic periods in the lake. The overall consistency of the  $\delta^{13}\text{C}_{\text{org}}$  values with respect to the other geochemical parameters reviewed are corroborative of land plants as a causal factor in the nutrient fluxes in lakes 10, 16 and 19.

The  $\delta^{15}\text{N}$  values observed in lakes 10, 16 and 19 also appear to track redox conditions and thus are corroborative of the body of geochemical data (Fig. 4.9). Denitrification under anoxic or suboxic conditions (see section 4.2.3) results in an

increase in  $\delta^{15}\text{N}$  values of  $> 10 \text{ ‰}$  (Leng et al., 2006) which is observed in all three intervals where anoxia is indicated by redox proxies ( $\text{C}_{\text{org}}:\text{P}_{\text{tot}}$ ). High  $\text{C}_{\text{org}}:\text{P}_{\text{tot}}$  values suggest anoxic conditions in lakes 10, 16 and 19, all of which correspond to  $\delta^{15}\text{N}$  values  $> 10 \text{ ‰}$ . Additionally, during oxic intervals (as indicated by low  $\text{C}_{\text{org}}:\text{P}_{\text{tot}}$  values) and when the C/N ratio is biased more towards the dominance of algae and  $\delta^{13}\text{C}_{\text{org}}$  values are higher (lakes 13-15, for example),  $\delta^{15}\text{N}$  values are more consistent with those of modern lacustrine algae (varying between  $+5$  to  $+8 \text{ ‰}$ ) (Peters et al., 1978; Meyers, 1994; Meyers, 2003). While the  $\delta^{15}\text{N}$  values are generally not reflective of those associated with

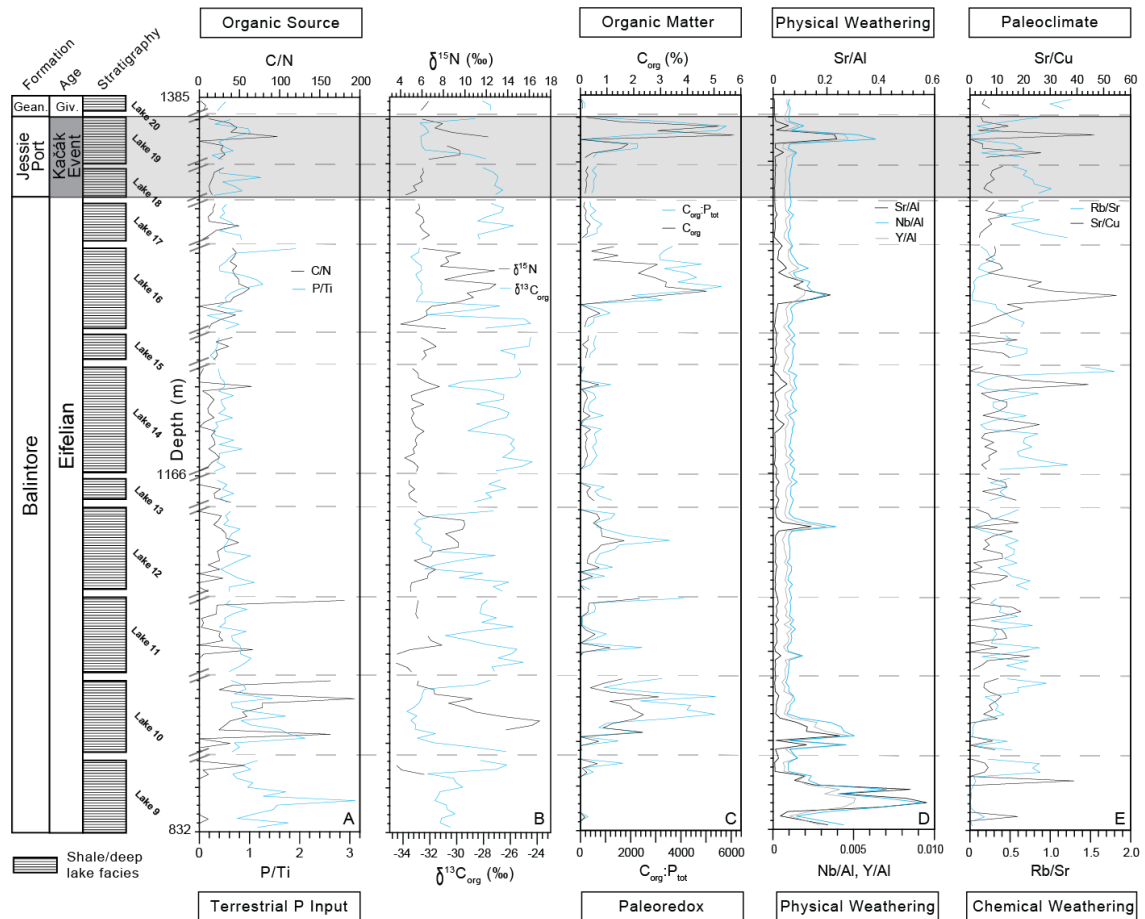


Figure 4.9. Combined plot featuring N and C isotopic and elemental data combined with data from a previous study on the Geanies sequence (Smart et al., 2022a). Data is plotted with depth. Gray shaded region represents sedimentary layers concurrent with the Kačák Event. (A) Terrestrial nutrient flux proxy P/Ti plotted with organic matter source proxy C/N. (B)  $\delta^{15}\text{N}$  plotted with  $\delta^{13}\text{C}_{\text{org}}$ . (C)  $\text{C}_{\text{org}}$  plotted with redox proxy  $\text{C}_{\text{org}}:\text{P}_{\text{tot}}$ . (D) Physical weathering proxies Sr/Al, Nb/Al and Y/Al. (E) Paleoclimate proxy Sr/Cu plotted with chemical weathering proxy Rb/Sr.

organic material from modern land plants, as referenced above, applying proxies developed for modern lakes to ancient ones should be done with care. Even modern plants can have a range of values (see section 4.2.3). In general, the behavior of  $\delta^{15}\text{N}$  with respect to oxic and anoxic/suboxic environments is consistent with expectations and serves to further support conclusions based on other geochemical parameters reviewed here.

While the similarities between lakes 10, 16 and 19 have been discussed, there are some notable differences. The presence of strong aridity as suggested by the elevated Sr/Cu values in lakes 16 and 19 is not present in lake 10. Strong aridity allows for the possibility of the development of meromixis, or semi-permanent stratification (Leng et al., 2006), which would favor the development of anoxia independent of eutrophication and serve to make lakes 16 and 19 more prone to anoxia from a smaller nutrient perturbation (Smart et al., 2022a). Notably, this possibility seems unlikely for lake 10 as indicated by the low Sr/Cu values indicative of wetter conditions (Smart et al., 2022a). This observation allows distinction between lake 10 and lakes 16 and 19. A further distinction can be made by analysis of the physical weathering proxies which suggests a substantial increase in physical weathering preceding the onset of anoxia in lake 10 (concurrent with wetter conditions). Similar increases in physical weathering are also present in lakes 16 and 19, however they appear to generally coincide with the onset of anoxia, vice lead it. This is significant because lake 10 returned the highest C/N ratios of the entire sequence and P/Ti maxima second only to lake 9. A well-mixed, or holomictic, lake would presumably require a more substantial nutrient influx to induce anoxia than would a meromictic lake. Both the P/Ti values and the C/N values for lake 10 are of a

greater magnitude than those in both lake 16 and lake 19, yet both have larger  $C_{org}$  values and more pronounced anoxia than lake 10. As discussed previously, isotopic compositions are also very similar for all three (although lake 19 has a slightly greater maximum  $\delta^{13}C_{org}$  value). A possible explanation for these variations could be the episodic expansion of land plants (Retallack and Huang, 2011; Smart et al., 2022a; Smart et al., 2022b). Given the significant geochemical perturbations present early in the Geanies sequence, evidence suggests a large and sustained nutrient influx occurred in lake 10, with the source of the nutrient flux likely proximal to the lake itself based on the magnitude and duration of the P/Ti perturbations. The landscape then stabilized over time (see Filippelli and Souch, 1999; Filippelli, 2002; Smart et al., 2002a) and remained stable between lakes 13 and 15. A smaller, but still significant nutrient influx occurred in lake 16, possibly in a more distant portion of the drainage basin explaining the decreased P/Ti magnitude, but that ultimately impacted the lake at Geanies (Smart et al., 2022a). Based on the Sr/Cu data, this could have been driven by the beginnings of a shift in climate to wetter conditions as aridity began to fade in the middle of lake 16 (Smart et al., 2022a). A period of stability returned during lake 17, but climate conditions remained relatively wet through lake 18, which marks the beginning of the Kačák event. During lake 19, there is again a large influx of terrestrial nutrients concurrent with a shift to the predominance of allochthonous organic matter. While this perturbation appears muted in comparison with lake 10, it resulted in the largest deposition of organic matter and the most significant anoxia in the entire sequence (Smart et al., 2022a). The presence of these trends during the Kačák Event is unlikely to be coincidental and if significant anoxia was induced in the lakes at Geanies during an extinction event, this likely occurred elsewhere (Smart et

al., 2022a; Smart et al., 2022b). A final item of comparison is that of chemical weathering to physical weathering. In each of the three lakes, large increases in physical weathering gave way to subsequent increases in chemical weathering. This is most apparent in lakes 10 and 19, but there is a small increase in Rb/Sr in the latter half of lake 16 followed by a larger increase in lake 17. The increase in Rb/Sr in lake 19 is sustained through the latter half of the lake and through lake 20. This type of transition from physical to chemical weathering would be expected as young landscapes are colonized by land plants (Smart et al., 2022a). Linear regressions performed on Rb/Sr show a positive trend in values from lake 9 to lake 20 of 0.28 to 0.62. An antithetic trend is observed in the physical weathering data, with an overall decrease in values of all proxies from lake 9 to lake 20.

#### 4.4.3. Integrating Principal Component Analysis

The results from the principal component analyses serve as additional evidence linking the evolution and expansion of land plants to geochemical perturbations at Geanies. Although PCAs were performed on the entire sequence (Fig. 4.3) as well as the lower (Fig. 4.4) and upper halves (Fig. 4.5), the PCA for the entire sequence does not vary significantly from that of the other two and serves to reinforce conclusions drawn from interpretations of the isotopic and elemental data. Specifically, the PCA performed on the broader sequence results in the general grouping of all terrestrial nutrient flux proxies with TOC and C/N. This strong affiliation would be expected if terrestrial nutrient influx was driven by the expansion of land plants. Additionally, redox proxies  $Cu_{EF}$  and  $C_{org}:P_{tot}$  group tightly with  $\delta^{15}N$ . The correlation between these three proxies suggests two conclusions. The first conclusion is that denitrification under anoxic

conditions is the correct interpretation of the lowest  $\delta^{15}\text{N}$  values. The second is that  $\delta^{15}\text{N}$  and redox conditions are closely associated with the influx of allochthonous organic matter (all which group in relative proximity in the upper right quadrant).

Conversely,  $\delta^{13}\text{C}_{\text{org}}$  values appear in the opposite quadrant. Interpretations of this trend are more complex, but the inverse variation between  $\delta^{13}\text{C}_{\text{org}}$  and redox proxies suggest that methanogenesis associated with anoxia is a valid explanation. However,  $\delta^{13}\text{C}_{\text{org}}$  also varies inversely with the terrestrial nutrient influx and organic influx groupings, suggesting that low  $\delta^{13}\text{C}_{\text{org}}$  values could be driven by the influx of land plant material due to terrestrial plant expansion (assuming a more negative fractionation at higher Devonian  $\text{pCO}_2$  levels). Unfortunately, it is also just as likely based on the PCA that lacustrine algae with lower values than modern algae are to blame, as algal blooms would be driven by elevated nutrient influx. At a minimum, these results indicate that each of the three possibilities is plausible.

It was expected that the multiple different physical weathering proxies ( $\text{Mg}/\text{Al}$ ,  $\text{Nb}/\text{Al}$ ,  $\text{Sr}/\text{Al}$ ,  $\text{Th}/\text{Al}$  and  $\text{Y}/\text{Al}$ ) would group tightly on the PCA cross plot and that was indeed the case in our results. Had they not grouped together, or if there were significant variation amongst those proxies, that would suggest the possibility of secondary alteration of these elements post burial (see Wei and Algeo, 2020). Additionally, the physical weathering proxies appear in adjacent quadrants with both the terrestrial nutrient proxies and the organic influx grouping, indicating they have no functional correlation with one another. This discounts the possibility that elevated terrestrial input is tied to increases in physical weathering. This conclusion is not surprising as the function of normalizing P to both Ti and Al is to separate variations due to changes in sedimentation

rates, but the results are nonetheless confirming regarding the data. The paleoclimate proxy Sr/Cu also groups tightly with the physical weathering proxies and thus is not correlated with the terrestrial nutrient grouping nor the organic influx grouping. While this suggests climate changes are not linked to the amount of allochthonous organic matter entering the lake, it simultaneously challenges the hypothesis that climate fluctuations drove land plant expansion in the Orcadian Basin (e.g., Smart et al., 2022a). Similarly, the grouping of the silt/clay ratio proxy Ti/Al with the paleoclimate and physical weathering proxies suggests no correlation with the terrestrial nutrient flux proxies and instead a correlation with physical weathering rates. This conclusion is inconsistent with what would be expected with landscape evolution as land plants proliferate and weather soil profiles (thus creating a positive correlation between terrestrial nutrient flux and silt to clay ratio). This relationship remains relatively unchanged in both additional PCAs. Linear regression performed on the Ti/Al data alone returned no significant slope. Based on the associations discussed above, it is possible Ti/Al is not an effective proxy for silt to clay ratio in this formation. As has been noted in previous studies on Devonian sequences, the uncritical application of proxies to outcrops of varying geochemical makeup may yield incorrect results (Algeo and Liu, 2020). While the authors were aware of this potential limitation, the inclusion of multiples for each proxy would have greatly increased the difficulty in interpreting the PCA, thus the drawbacks of utilizing only one proxy for silt to clay ratio were accepted during study design. However, results from the broader PCA were generally confirmational of conclusions drawn from analysis of the geochemical data.



As briefly mentioned above, the PCAs for the lower and upper lakes at Geanies did not vary significantly from those of the broader PCA. In the case of the PCA for the lower lakes however (Fig. 4.4), there were significant shortcomings, not the least of which were the very weak loadings for Sr/Cu, Cu<sub>EF</sub> and P/Fe. Additionally, the organic flux grouping was less associated with the terrestrial nutrient flux grouping and  $\delta^{15}\text{N}$ . The redox proxies plotted in separate quadrants as well. The PCA for the upper lakes (Fig. 4.5) was more closely aligned with the broader PCA and had strong loadings. It is possible that the differences in the PCA for the lower lakes suffered due to a sampling bias unintentionally introduced when the data set was divided. Due to the lack of C and N data points for much of lake 9, only 59 data points were available for the lower lakes while 78 were available for the upper lakes. This may explain why the PCA for the upper lakes is more reflective of the broader PCA. The number of samples used for the broader PCA would generally result in a more robust analysis either way, thus further analysis of the individual PCAs is not warranted.

Based on the findings discussed above, additional PCAs were performed separating the Geanies data into two groups according to C/N ratio. All samples having C/N ratios  $> 19$  were sequestered from those with C/N ratios  $< 19$  so as to determine if the overall loadings varied significantly based on the dominance of allochthonous organic matter vice autochthonous, respectively. A C/N value of 19 vice 20 was chosen to incorporate more of the mixed input system that was still dominated by terrestrial organic matter (this resulted in an additional six samples being grouped with the allochthonous organic matter subdivision). The cross plot of loadings for the PCA performed on data from the allochthonous group (Fig. 4.10) was nearly identical to that of the overall PCA

(Fig. 4.3). Conversely, the cross plot of loadings for the PCA performed on data from the autochthonous group (Fig. 4.11) was significantly different with terrestrial nutrient flux, organic influx and physical weathering proxies plotting in different quadrants than that of the overall PCA. Significantly, the terrestrial nutrient flux and organic matter influx proxies show no significant relationship as they do in the overall PCA. The fact that the PCA loadings for the overall data set and those data with C/N ratios  $> 19$  are in such close agreement whilst those data associated with C/N ratios  $< 19$  are not, further support the conclusion that land plants are directly responsible for the elevated terrestrial nutrient influx observed at Geanies.

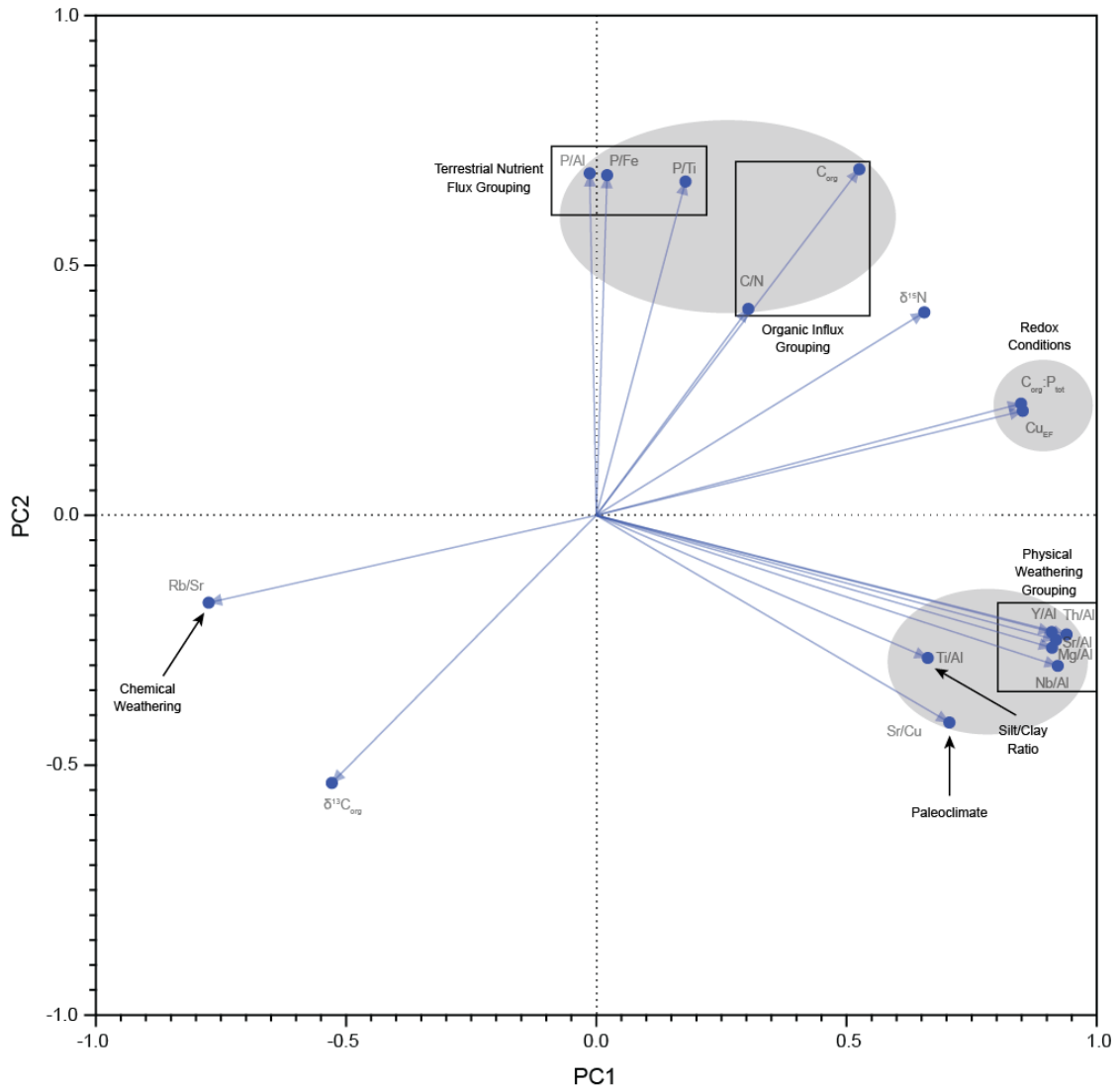


Figure 3.10. PCA cross plot utilizing data in which the C/N ratio was greater than 19, indicating organic matter input dominated by terrestrial land plant material.

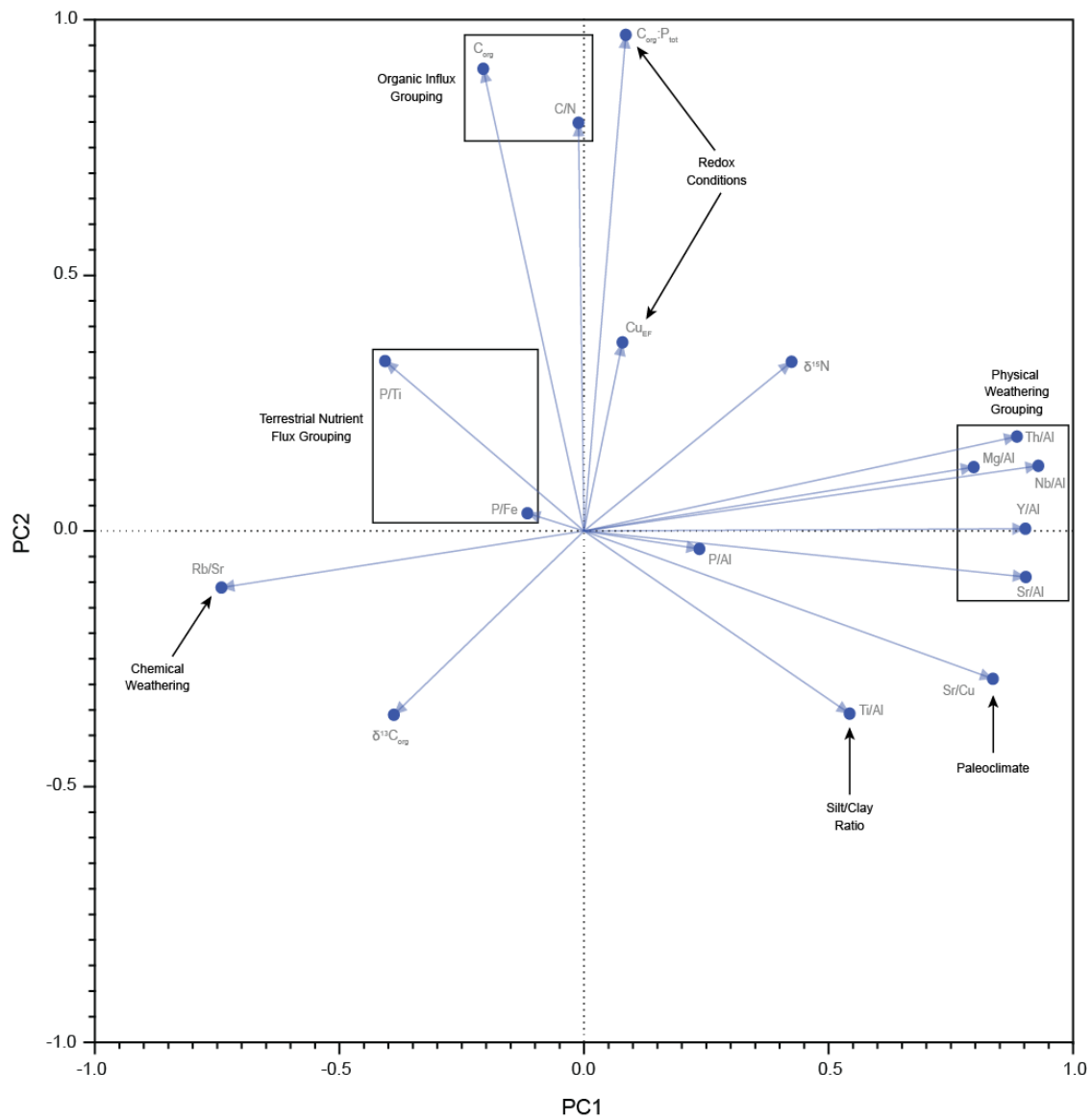


Figure 4.11. PCA cross plot utilizing data for which the  $C/N$  ratio was  $< 19$ , indicating organic matter input was mixed or dominated by lacustrine algae.

#### 4.5. Conclusions

There are inevitably shortcomings associated with any analysis of parameters in deep time. The variables introduced by the slow passage of geologic time introduce many complexities which must be accounted for when interpreting data. Those complexities can be mitigated by methodical and robust analysis of a wide range of paleo proxies. The combination of C and N isotopic and elemental data presented here with the suite of elemental geochemical data from previous studies available for the lakes at Geanies has decreased the uncertainty related to the factors impacting their internal geochemical cycling. The addition of complex statistical analyses in the form of principal component analysis further reduces that uncertainty.

Results using these methods demonstrate that land plants were implicated in nearly the entirety of the 1.2 Myr lacustrine record at Geanies. Furthermore, the most severe periods of geochemical perturbations which resulted in the development of significant anoxia in three lake cycles, to include during the Kačák extinction event, occurred during periods where allochthonous organic matter influx was at its greatest extent and were concurrent with elevated levels of terrestrial export of the nutrient P. This nutrient influx was sufficient to induce anoxia during periods when the lakes were likely well-mixed, as well as during arid periods when they were likely more stratified. The magnitude of allochthonous organic matter varied during each anoxia-inducing nutrient pulse, but the outcome was identical in each of the three cases discussed here. This suggests not only that land plant expansion was episodic in the drainage basin at Geanies, where periods of P mobilization and export were followed by periods of stability which lasted up to 300 kyr, but also each episode of plant expansion produced a

nutrient pulse of varying magnitudes that was sufficient to drive anoxia. While attribution of land plants as a causal factor in the Kačák Event is not possible based on analysis of a single lacustrine sequence, robust analyses of this type should be repeated elsewhere to further support or refute the connection of land plants with the Kačák Event and other extinction events within the Devonian.

#### 4.6. References

Algeo, T.J., and Ingall, E., 2007, Sedimentary  $C_{org}:P$  ratios, paleocean ventilation, and Phanerozoic atmospheric  $pO_2$ : *Palaeogeography, Palaeoclimatology, Palaeoecology*, v. 256, p. 130–155.

Algeo, T.J., and Liu, J., 2020, A re-assessment of elemental proxies for paleoredox analysis: *Chemical Geology*, v. 540, p. 119549.

Algeo, T.J., and Scheckler, S.E., 1998, Terrestrial-marine teleconnections in the Devonian: links between the evolution of land plants, weathering processes, and marine anoxic events: *Philosophical transactions of the Royal Society of London. Series B, Biological Sciences*, v. 353, p. 113–130.

Andrews, S.D., Cornwell, D.G., Trewin, N.H., Hartley, A.J., and Archer, S.G., 2016, A 2.3 million year lacustrine record of orbital forcing from the Devonian of northern Scotland: *Journal of the Geological Society*, v. 173, p. 474–488.

Andrews, S.D., and Trewin, N.H., 2010, Periodicity determination of lacustrine cycles from the Devonian of Northern Scotland: *Scottish Journal of Geology*, v. 46, p. 143–155.

Astin, T.R., 1990, The Devonian lacustrine sediments of Orkney, Scotland; implications for climate cyclicity, basin structure and maturation history: *Journal of the Geological Society*, v. 147, p. 141–151.

Beerling, D. J., & Woodward, F. I. (1993). Ecophysiological responses of plants to global environmental change since the Last Glacial Maximum. *New Phytologist*, 125(3), 641-648.

Berry, C.M., and Marshall, J.E.A., 2015, Lycopoid forests in the early Late Devonian paleoequatorial zone of Svalbard: *Geology*, v. 43, p. 1043–1046.

Calvert, S. E. (2004). Beware intercepts: interpreting compositional ratios in multi-component sediments and sedimentary rocks. *Organic Geochemistry*, 35(8), 981-987.

Cline, J. D., & Kaplan, I. R. (1975). Isotopic fractionation of dissolved nitrate during denitrification in the eastern tropical North Pacific Ocean. *Marine Chemistry*, 3(4), 271-299.

Conrad, R. (2005). Quantification of methanogenic pathways using stable carbon isotopic signatures: a review and a proposal. *Organic geochemistry*, 36(5), 739-752.

D'Antonio, M. P., Ibarra, D. E., & Boyce, C. K. (2020). Land plant evolution decreased, rather than increased, weathering rates. *Geology*, 48(1), 29-33.

Davies, N. S., Berry, C. M., Marshall, J. E., Wellman, C. H., & Lindemann, F. J., 2021, The Devonian Landscape Factory: plant-sediment interactions in the Old Red Sandstone of Svalbard and the rise of vegetation as a biogeomorphic agent: *Journal of the Geological Society*, v. 178, p. 202–225.

Degens, E. T., Guillard, R. R. L., Sackett, W. M., & Hellebust, J. A. (1968, February). Metabolic fractionation of carbon isotopes in marine plankton—I. Temperature and respiration experiments. In *Deep Sea Research and Oceanographic Abstracts* (Vol. 15, No. 1, pp. 1-9). Elsevier.

Deleens, E., Treichel, I., & O'Leary, M. H. (1985). Temperature dependence of carbon isotope fractionation in CAM plants. *Plant physiology*, 79(1), 202-206.

Faure, G., & Mensing, T. M. (2005). *Isotopes: Principles and Applications* (p. 897). John Wiley & Sons, Inc.

Filippelli, G.M., and Souch, C., 1999, Effects of climate and landscape development on the terrestrial phosphorus cycle: *Geology*, v. 27, p. 171.



Filippelli, G.M., 2002, The Global Phosphorus Cycle: Reviews in Mineralogy and Geochemistry, v. 48, p. 391–425.

Filley, T. R., Freeman, K. H., Bianchi, T. S., Baskaran, M., Colarusso, L. A., & Hatcher, P. G. (2001). An isotopic biogeochemical assessment of shifts in organic matter input to Holocene sediments from Mud Lake, Florida. *Organic Geochemistry*, 32(9), 1153-1167.

Franks, P. J., Royer, D. L., Beerling, D. J., Van de Water, P. K., Cantrill, D. J., Barbour, M. M., & Berry, J. A. (2014). New constraints on atmospheric CO<sub>2</sub> concentration for the Phanerozoic. *Geophysical Research Letters*, 41(13), 4685-4694.

Garcia, A. K., Cavanaugh, C. M., & Kacar, B. (2021). The curious consistency of carbon biosignatures over billions of years of Earth-life coevolution. *The ISME Journal*, 15(8), 2183-2194.

Giesen, P., and Berry, C.M., 2013, Reconstruction and growth of the early tree calamophyton (pseudosporochnales, cladoxylopsida) based on exceptionally complete specimens from Lindlar, Germany (mid-Devonian): Organic connection of calamophyton branches and duisbergia trunks: *International Journal of Plant Sciences*, v. 174, p. 665–686.

Hinga, K. R., Arthur, M. A., Pilson, M. E., & Whitaker, D. (1994). Carbon isotope fractionation by marine phytoplankton in culture: the effects of CO<sub>2</sub> concentration, pH, temperature, and species. *Global Biogeochemical Cycles*, 8(1), 91-102.

House, M.R., 1985, Correlation of mid-Palaeozoic ammonoid evolutionary events with global sedimentary perturbations: *Nature*, v. 313, p. 17–22.

House, M.R., 2002, Strength, timing, setting and cause of mid-Palaeozoic extinctions: *Palaeogeography, Palaeoclimatology, Palaeoecology*, v. 181, p. 5–25.

Kędzior, M., Garcia, A. K., Li, M., Taton, A., Adam, Z. R., Young, J. N., & Kaçar, B. (2022). Resurrected Rubisco suggests uniform carbon isotope signatures over geologic time. *Cell Reports*, 39(4), 110726.

Keeley, J. E., & Rundel, P. W. (2003). Evolution of CAM and C<sub>4</sub> carbon-concentrating mechanisms. *International Journal of Plant Sciences*, 164(S3), S55-S77.

Kelly, S.B., 1992, Milankovitch cyclicity recorded from Devonian non-marine sediments: *Terra Nova*, v. 4, p. 578–584.

Lenton, T. M., Daines, S. J., & Mills, B. J. (2018). COPSE reloaded: an improved model of biogeochemical cycling over Phanerozoic time. *Earth-Science Reviews*, 178, 1-28.

Lenton, T.M., Dahl, T.W., Daines, S.J., Mills, B.J.W., Ozaki, K., Saltzman, M.R., and Porada, P., 2016, Earliest land plants created modern levels of atmospheric oxygen: *Proceedings of the National Academy of Sciences of the United States of America*, v. 113, p. 9704–9709.

Leng, M. J., Lamb, A. L., Heaton, T. H., Marshall, J. D., Wolfe, B. B., Jones, M. D., ... & Arrowsmith, C. (2006). Isotopes in lake sediments. In *Isotopes in Palaeoenvironmental Research* (pp. 147-184). Springer, Dordrecht.

Li, Q., Wu, S., Xia, D., You, X., Zhang, H., and Lu, H., 2020, Major and trace element geochemistry of the lacustrine organic-rich shales from the Upper Triassic Chang 7 Member in the southwestern Ordos Basin, China: Implications for paleoenvironment and organic matter accumulation: *Marine and Petroleum Geology*, v. 111, p. 852–867.

Marshall, J.E.A., Brown, J.F., and Astin, T.R., 2011, Recognising the Taghanic Crisis in the Devonian terrestrial environment and its implications for understanding land–sea interactions: *Palaeogeography, Palaeoclimatology, Palaeoecology*, v. 304, p. 165–183.

Marshall, J.E.A., Astin, T.R., Brown, J.F., Mark-Kurik, E., and Lazauskiene, J., 2007, Recognizing the Kačák Event in the Devonian terrestrial environment and its implications for understanding land–sea interactions: *Geological Society Special Publication*, v. 278, p. 133–155.

Marshall, J.E.A., 1996, *Rhabdosporites langii*, *Geminospora lemurata* and *Contagisporites optivus*: an origin for heterospory within the progymnosperms: Review of Palaeobotany and Palynology, v. 93, p. 159–189.

Meyers, P. A. (1994). Preservation of elemental and isotopic source identification of sedimentary organic matter. *Chemical Geology*, 114(3-4), 289-302.

Meyers, P. A. (1997). Organic geochemical proxies of paleoceanographic, paleolimnologic, and paleoclimatic processes. *Organic Geochemistry*, 27(5-6), 213-250.

Meyers, P. A. (2003). Applications of organic geochemistry to paleolimnological reconstructions: a summary of examples from the Laurentian Great Lakes. *Organic Geochemistry*, 34(2), 261-289.

Mariotti, A., Germon, J. C., Leclerc, A., Catroux, G., & Letolle, R. (1982). Experimental determination of kinetic isotope fractionation of nitrogen isotopes during denitrification. *Stable Isotopes*, 459-464.

Marshall, J E A & Hewett, T, 2003, Devonian, in Evans, D., Graham, C., Armour, A. & Bathurst, P. ed., *The Millennium Atlas*, London, Geological Society.

Meyer-Berthaud, B., Scheckler, S.E., and Wendt, J., 1999, *Archaeopteris* is the earliest known modern tree: *Nature*, v. 398, p. 700–701.

Meyer-Berthaud, B., Soria, A., and Decombeix, A.-L., 2010, The land plant cover in the Devonian: a reassessment of the evolution of the tree habit: Geological Society Special Publication, v. 339, p. 59–70.

McLennan, S.M., 2001, Relationships between the trace element composition of sedimentary rocks and upper continental crust: trace element composition and upper continental crust: *Geochemistry, Geophysics, Geosystems: G(3)*, v. 2, doi:10.1029/2000gc000109.

Morris, J.L. et al., 2015, Investigating Devonian trees as geo-engineers of past climates: linking palaeosols to palaeobotany and experimental geobiology: *Palaeontology*, v. 58, p. 787–801.

Müller, P. J. (1977). CN ratios in Pacific deep-sea sediments: Effect of inorganic ammonium and organic nitrogen compounds sorbed by clays. *Geochimica et Cosmochimica Acta*, 41(6), 765-776.

Orem, W. H., Burnett, W. C., Landing, W. M., Lyons, W. B., & Showers, W. (1991). Jellyfish Lake, Palau: Early diagenesis of organic matter in sediments of an anoxic marine lake. *Limnology and Oceanography*, 36(3), 526-543.

Pan, Y., Huang, Z., Li, T., Guo, X., Xu, X., and Chen, X., 2020, Environmental response to volcanic activity and its effect on organic matter enrichment in the Permian Lucaogou Formation of the Malang Sag, Santanghu Basin, Northwest China: *Palaeogeography, Palaeoclimatology, Palaeoecology*, v. 560, p. 110024.

Pawlik, Ł., Buma, B., Šamonil, P., Kvaček, J., Gałazka, A., Kohout, P., & Malik, I. (2020). Impact of trees and forests on the Devonian landscape and weathering processes with implications to the global Earth's system properties-A critical review. *Earth-Science Reviews*, 205, 103200.

Percival, L. M. E., Marynowski, L., Baudin, F., Goderis, S., De Vleeschouwer, D., Rakociński, M., ... & Claeys, P. (2022). Combined Nitrogen - Isotope and Cyclostratigraphy Evidence for Temporal and Spatial Variability in Frasnian-Famennian Environmental Change. *Geochemistry, Geophysics, Geosystems*, v. 23(5).

Percival, L. M. E., Bond, D. P. G., Rakociński, M., Marynowski, L., Hood, A. V. S., Adatte, T., ... & Föllmi, K. B. (2020). Phosphorus-cycle disturbances during the Late Devonian anoxic events. *Global and Planetary Change*, 184, 103070.

Peters, K. E., Sweeney, R. E., & Kaplan, I. R. (1978). Correlation of carbon and nitrogen stable isotope ratios in sedimentary organic matter 1. *Limnology and Oceanography*, 23(4), 598-604.

Royer, D. L. (2014). Atmospheric CO<sub>2</sub> and O<sub>2</sub> during the Phanerozoic: Tools, patterns, and impacts. *Treatise on Geochemistry (Second Edition)*, 6.

Retallack, G. J., & Huang, C. (2011). Ecology and evolution of Devonian trees in New York, USA. *Palaeogeography, Palaeoclimatology, Palaeoecology*, 299(1-2), 110-128.

Royer, D. L. (2014). Atmospheric CO<sub>2</sub> and O<sub>2</sub> during the Phanerozoic: Tools, patterns, and impacts. *Treatise on Geochemistry (Second Edition)*, 6.

Sage, R. F. (2004). The evolution of C<sub>4</sub> photosynthesis. *New Phytologist*, 161(2), 341-370.

Schubert, C. J., & Calvert, S. E. (2001). Nitrogen and carbon isotopic composition of marine and terrestrial organic matter in Arctic Ocean sediments: implications for nutrient utilization and organic matter composition. *Deep Sea Research Part I: Oceanographic Research Papers*, 48(3), 789-810.

Schubert, B. A., & Jahren, A. H. (2012). The effect of atmospheric CO<sub>2</sub> concentration on carbon isotope fractionation in C<sub>3</sub> land plants. *Geochimica et Cosmochimica Acta*, 96, 29-43.

Smart, M. S., Filippelli, G. M., Gilhooly, W.P., Marshall, J.E.A. & Whiteside, J. H., (2022a). Enhanced terrestrial nutrient release during the Devonian emergence and

expansion of forests: Evidence from lacustrine phosphorus and geochemical records.  
GSA Bulletin. In Press.

Smart, M. S., Filippelli, G. M., Gilhooly, W.P., Marshall, J.E.A. & Whiteside, J. H.,  
(2022b). Land plant evolution and volcanism led to the Late Devonian mass extinction.  
Communications Earth and Environment. Submitted.

Sollins, P., Spycher, G., & Glassman, C. A. (1984). Net nitrogen mineralization from  
light-and heavy-fraction forest soil organic matter. *Soil Biology and Biochemistry*, *16*(1),  
31-37.

Stein, W.E. et al., 2020, Mid-Devonian *Archaeopteris* roots signal revolutionary change  
in earliest fossil forests: *Current Biology: CB*, v. 30, p. 421- 431.e2.

Stein, W.E., Berry, C.M., Hernick, L.V., and Mannolini, F., 2012, Surprisingly complex  
community discovered in the mid-Devonian fossil forest at Gilboa: *Nature*, v. 483, p. 78–  
81.

Stephenson, M. H., Leng, M. J., Michie, U., & Vane, C. H. (2006). Palaeolimnology of  
Palaeozoic lakes, focusing on a single lake cycle in the Middle Devonian of the Orcadian  
Basin, Scotland. *Earth-Science Reviews*, *75*(1-4), 177-197.



Tang, L., Song, Y., Pang, X., Jiang, Z., Guo, Y., Zhang, H., Pan, Z., and Jiang, H., 2020, Effects of paleo sedimentary environment in saline lacustrine basin on organic matter accumulation and preservation: A case study from the Dongpu Depression, Bohai Bay Basin, China: *Journal of Petroleum Science & Engineering*, v. 185, p. 106669.

Tipple, B. J., & Pagani, M. (2010). A 35 Myr North American leaf-wax compound-specific carbon and hydrogen isotope record: Implications for C<sub>4</sub> grasslands and hydrologic cycle dynamics. *Earth and Planetary Science Letters*, 299(1-2), 250-262.

Troughton, J. H., & Card, K. A. (1975). Temperature effects on the carbon-isotope ratio of C<sub>3</sub>, C<sub>4</sub> and Crassulacean-acid-metabolism (CAM) plants. *Planta*, 123(2), 185-190.

Vosoughi Moradi, A., Sarı, A., and Akkaya, P., 2016, Geochemistry of the Miocene oil shale (Hançili Formation) in the Çankırı-Çorum Basin, Central Turkey: Implications for Paleoclimate conditions, source–area weathering, provenance and tectonic setting: *Sedimentary Geology*, v. 341, p. 289–303.

Wan, Z., Algeo, T. J., Gensel, P. G., Scheckler, S. E., Stein, W. E., Cressler III, W. L., ... & Sauer, P. E. (2019). Environmental influences on the stable carbon isotopic composition of Devonian and Early Carboniferous land plants. *Palaeogeography, Palaeoclimatology, Palaeoecology*, 531, 109100.

Wei, W., and Algeo, T.J., 2020, Secular variation in the elemental composition of marine shales since 840 Ma: Tectonic and seawater influences. *Geochimica et Cosmochimica Acta*, 287, pp.367-390.

Wilson, A. O. (2012). A high-resolution record of environmental and climatic change in a lacustrine sequence from the Devonian Orcadian Basin, Scotland (Doctoral dissertation, University of Aberdeen).

Wong, W. W., & Sackett, W. M. (1978). Fractionation of stable carbon isotopes by marine phytoplankton. *Geochimica et Cosmochimica Acta*, 42(12), 1809-1815.

Xu, H., Liu, B., and Wu, F., 2010, Spatial and temporal variations of Rb/Sr ratios of the bulk surface sediments in Lake Qinghai: *Geochemical Transactions*, v. 11, p. 3.

Yamaguchi, K. E., Oguri, K., Ogawa, N. O., Sakai, S., Hirano, S., Kitazato, H., & Ohkouchi, N. (2010). Geochemistry of modern carbonaceous sediments overlain by a water mass showing photic zone anoxia in the saline meromictic Lake Kai-ike, southwest Japan: I. Early diagenesis of organic carbon, nitrogen, and phosphorus. *Palaeogeography, Palaeoclimatology, Palaeoecology*, 294(1-2), 72-82.

Young, J. N., Rickaby, R. E. M., Kapralov, M. V., & Filatov, D. A. (2012). Adaptive signals in algal Rubisco reveal a history of ancient atmospheric carbon dioxide.

Philosophical Transactions of the Royal Society B: Biological Sciences, 367(1588), 483-492.

## CHAPTER 5. CONCLUSIONS AND FUTURE STUDY

### 5.1. Land Plant Evolution as an Extinction Mechanism

When embarking on this study, the goal was to attribute the evolution and expansion of land plants as an extinction mechanism for the biotic crises in the Mid-to Late Devonian, confirming the theory first suggested by Algeo et al. (1995). As is often the case in studies involving deep time, the results were not indisputably definitive. Investigations here into whether or not distinct phosphorus (P) weathering events occurred in the Devonian clearly reveal the existence of such events across space and time, from the Devonian Basin in East Greenland to the Orcadian Basin and from the Eifelian to the Famennian. Furthermore, at each study site internal lacustrine geochemical cycling was unexpectedly similar to that which occurs in modern lacustrine systems. Orbitally driven climatic changes provoked expected geochemical responses. And while it was hypothesized that land plant expansion was episodic (and the results presented here suggest that was indeed the case), it was not necessarily expected that their expansion would be tied to orbitally driven climate changes such as during the Kačák Event or initiated by atmospheric changes induced by large scale volcanism during the Kellwasser Event. Nevertheless, it appears that each regional expansion of land plants had an external catalyst. As already noted, extinction events are complex biological calamities and it is only on rare occasions in Earth's past that a significant extinction event can be attributed to a single kill mechanism (i.e., the Cretaceous-Paleogene, or K-Pg, extinction). While geochemical modeling revealed that the measured P export recorded at Heintzbjerg during the Kellwasser Event was sufficient to cause widespread anoxia when

scaled globally, the timing disparity between the initiation of the extinction pulses and the P weathering pulses would seem to rule out land plant expansion as a sole kill mechanism. Certainly in the case of the Kellwasser Event, the extinction pulses were a timely combination of factors, with nutrients mobilized from land plant expansion perhaps delivering the geochemical *coup de grâce*. It would seem likely that each of the Devonian marine extinctions were similarly multifaceted. This would be a reasonable conclusion were it not for the fact that the Kellwasser Event was a massive extinction and considered one of the “Big Five” in the Paleozoic. Perhaps an event of that magnitude required multiple vectors to achieve criticality, but that does not necessarily have to be true for smaller extinctions such as the Choteč, Kačák or Taghanic extinctions. Thus, while this body of work provides strong evidence implicating land plants in the biotic crises of the Devonian, it does not establish them as a definitive extinction mechanism and leaves still more questions that will require further investigations.

## 5.2. Future Study

This project has shown the viability of using lacustrine analyses to track terrestrial nutrient export. This has implications for numerous scientific questions in deep time, but more immediately, provides a blueprint for others to repeat this study design in other locations to address the root hypothesis regarding land plant involvement in Devonian biotic crises. While analyses here were conducted at multiple sites at varying geographic locations, the sole focus on Euramerica is an unfortunate limitation. Additional lakes from Gondwana and sites in Russia and China would allow global comparison and perhaps provide crucial supporting evidence to the hypotheses advanced here.

While the study design presented here is geochemically robust, no study can be considered perfect in its design or considerations. While total P has been effectively combined with other proxies to make a strong case for land plant derived nutrient weathering events, the addition of sequential extraction techniques to determine the relationship between various P fractions would allow further analysis of P source and behavior. For example, during the early stages of landscape evolution, it would be expected that the dominant form of P weathered from terrestrial landscapes would be the mineral phase and as landscapes stabilize, the readily available mineral form would be used up and a transition to organic and occluded forms would take place (Filippelli, 2002). Sequential extraction could be utilized in the lakes studied here to further support the conclusions reached and of possible, should be used in future studies. Along the same lines, there are some shortcomings to utilizing total nitrogen (N) as an approximation for organic N (see Ch. 4). These shortcomings introduce uncertainty regarding interpretations of the C/N ratios presented here. Future studies should endeavor to determine organic N for use in C/N ratios in lieu of total N.

Finally, throughout the course of this project it became apparent that some sample sequences were far more valuable than others. In general, the most extensive sequences were the most informative. This was not universally the case, however, as the Hoxa Head sequence spanned 2.1 Myr and lacked an obvious P weathering event and the Ella Ø sequence spanned just 100 kyr and captured a significant P weathering event. Future studies would benefit from adopting a broad sampling strategy which would ideally cover a continuous sequence with > 800 kyr worth of record. This would be advantageous for a number of reasons. First, the longer the sequence, the more likely the analyst is to capture

a nutrient event (though it is still possible to miss it entirely as was the case at Hoxa Head). Second, 800 kyr is approximately two long eccentricity cycles. This would most easily allow the identification of Milankovitch driven climatic fluctuations. A corollary benefit is that future investigators would be able to use astrochronology in order to establish a relative age of the sequence and thus determine sedimentation and P accumulation rates. This would only truly be possible with the Hoxa Head and Heintzbjerg sequences presented here. The duration of Ella Ø was insufficient to capture the long eccentricity modulations, Heggli Ber was not continuous nor was it long enough to capture the long eccentricity modulations and Genies was not continuous.

Combining the three suggestions presented above would address the limitations of the current body of work whilst furthering the Algeo et al. (1995) hypothesis. By addressing these shortcomings, it is this author's opinion that we will finally be able to definitively determine whether land plants initiated the Choteč, Kačák and Taghanic extinctions.

### 5.3. References

Algeo, T. J., Berner, R. A., Maynard, J. B., & Scheckler, S. E., 1995, Late Devonian oceanic anoxic events and biotic crises: "rooted" in the evolution of vascular land plants: *GSA Today*, v. 5, p. 45–66.

Filippelli, G.M., 2002, The Global Phosphorus Cycle: Reviews in Mineralogy and Geochemistry, v. 48, p. 391–425.

APPENDIX A: ELEMENTAL CORRELATIONS BY SAMPLE LOCATION AND LAKE CYCLE

Lake/ Section	n	P vs Ti	P vs Al	P vs Fe	P vs Ca	P/Ti vs C <sub>org</sub>	P/Ti vs P Accum. Rate	Ti vs Al
<b>Geanies</b>								
20	3	-0.998, 0.0401	+0.212, 0.864	+0.090, 0.9429	-0.652, 0.5480	-0.836, 0.3698	+0.993, 0.0244	+0.897, 0.2909
19	10	+0.768, 0.0095	+0.804, 0.005	+0.876, 0.0009	-0.840, 0.0024	+0.751, 0.0124	-0.058, 0.8737	+0.951, <0.0001
18	7	+0.402, 0.3717	+0.728, 0.0636	+0.730, 0.0626	-0.563, 0.1880	+0.571, 0.1803	-0.0242, 0.6015	+0.594, 0.1599
17	9	+0.643, 0.0618	+0.841, 0.0045	+0.949, <0.0001	-0.063, 0.8723	+0.016, 0.9664	-0.0174, 0.6550	+0.366, 0.3332
16	19	+0.779, <0.0001	+0.624, 0.0043	+0.620, 0.0047	-0.232, 0.3402	+0.350, 0.1455	+0.047, 0.8491	+0.964, <0.0001
15	6	+0.973, 0.0011	-0.356, 0.4884	-0.376, 0.4624	+0.240, 0.6480	+0.591, 0.2163	+0.257, 0.6234	+0.930, 0.0082
14	24	+0.627, 0.001	+0.819, <0.0001	+0.866, <0.0001	-0.333, 0.1122	+0.258, 0.2229	-0.027, 0.9005	+0.670, 0.0004
13	6	-0.451, 0.3694	+0.656, 0.1573	+0.097, 0.8555	+0.273, 0.6005	+0.212, 0.6863	+0.428, 0.3977	+0.830, 0.0433
12	19	+0.586, 0.0083	+0.771, 0.0001	+0.569, 0.0111	-0.920, 0.6005	-0.345, 0.1487	+0.188, 0.4410	+0.941, <0.0001
11	17	-0.002, 0.9946	+0.311, 0.224	-0.217, 0.4036	-0.620, 0.0083	-0.067, 0.7985	+0.386, 0.1261	+0.707, 0.0015
10	17	+0.839, <0.0001	+0.875, <0.0001	+0.826, <0.0001	-0.981, <0.0001	+0.037, 0.8891	-0.513, 0.0353	+0.963, <0.0001
9	14	+0.953, <0.0001	+0.917, <0.0001	+0.740, 0.0011	-0.981, <0.0001	-0.316, 0.2325	-0.569, 0.0216	+0.990, <0.0001
All	151	+0.768, <0.0001	+0.657, <0.0001	+0.624, <0.0001	-0.560, <0.0001	+0.132, 0.1029	-0.284, 0.0004	+0.920, <0.0001
<b>Hoxa Head</b>								
38	5	-0.223, 0.7184	+0.828, 0.0835	-0.677, 0.2093	-0.916, 0.0289	-0.914, 0.0300	+0.654, 0.2314	+0.845, 0.0717
37	2	N.A.†	N.A.†	N.A.†	N.A.†	N.A.†	N.A.†	N.A.†
36	2	N.A.†	N.A.†	N.A.†	N.A.†	N.A.†	N.A.†	N.A.†
35	5	0.446, 0.4513	+0.601, 0.2841	+0.421, 0.4807	-0.817, 0.0915	-0.030, 0.9617	+0.417, 0.4851	+0.847, 0.0704
34	6	0.839, 0.0369	+0.783, 0.0655	+0.900, 0.0146	-0.434, 0.3903	+0.217, 0.6794	-0.657, 0.1564	+0.929, 0.0073
33	10	-0.493, 0.1476	-0.064, 0.8515	+0.031, 0.9289	-0.383, 0.2457	-0.328, 0.3254	+0.626, 0.0394	+0.685, 0.0201
32	9	-0.382, 0.31	+0.608, 0.1101	+0.814, 0.014	-0.851, 0.0074	-0.719, 0.0443	+0.802, 0.0166	+0.723, 0.0429
31	7	-0.253, 0.5846	+0.446, 0.316	+0.544, 0.2067	-0.642, 0.1204	-0.881, 0.0089	+0.571, 0.1808	+0.704, 0.0774
30	3	0.516, 0.6548	+0.434, 0.7141	-0.463, 0.6934	-0.928, 0.2429	-0.911, 0.2713	-0.266, 0.8283	+0.994, 0.0686
29	5	0.027, 0.9653	+0.111, 0.8596	+0.281, 0.647	-0.104, 0.8678	-0.056, 0.9294	+0.167, 0.7883	+0.666, 0.2195
28	10	0.149, 0.6809	+0.526, 0.1184	+0.582, 0.0779	-0.429, 0.2162	-0.710, 0.0215	+0.145, 0.6902	+0.780, 0.0078
27	4	0.289, 0.7112	+0.976, 0.0239	+0.991, 0.0095	-0.952, 0.0485	+0.310, 0.6897	+0.881, 0.1194	+0.892, 0.1084
26	2	N.A.†	N.A.†	N.A.†	N.A.†	N.A.†	N.A.†	N.A.†
25	3	0.977, 0.1381	+0.992, 0.0799	+0.468, 0.6902	+0.959, 0.1827	+0.866, 0.3338	-0.899, 0.2885	+0.990, 0.0901
24	12	0.269, 0.3983	+0.774, 0.0031	+0.878, 0.0002	-0.760, 0.0042	+0.022, 0.9454	+0.170, 0.5966	+0.448, 0.1445
23	8	-0.043, 0.9199	-0.105, 0.8038	-0.247, 0.5555	-0.010, 0.9821	+0.291, 0.4852	+0.782, 0.0219	+0.823, 0.012



<b>22</b>	3	-0.987, 0.1028	-0.532, 0.643	-0.146, 0.9068	-0.137, 0.9124	-0.688, 0.5166	+0.988, 0.0997	+0.513, 0.6572
<b>21</b>	4	0.446, 0.5543	+0.548, 0.4521	+0.681, 0.3186	+0.101, 0.8986	+0.187, 0.813	-0.286, 0.714	+0.950, 0.0500
<b>20</b>	4	0.016, 0.984	+0.792, 0.2085	+0.934, 0.0661	-0.864, 0.1361	-0.584, 0.4165	+0.597, 0.403	+0.882, 0.1184
<b>19</b>	5	0.606, 0.2787	-0.114, 0.8554	-0.468, 0.4263	+0.319, 0.6012	-0.352, 0.5614	-0.125, 0.8409	+0.411, 0.4917
<b>18</b>	8	0.678, 0.0646	+0.900, 0.0023	+0.884, 0.0036	-0.800, 0.0172	-0.286, 0.4924	-0.084, 0.8438	+0.950, 0.0003
<b>All</b>	117	-0.007, 0.9363	+0.197, 0.0335	+0.249, 0.0068	-0.300, 0.001	-0.086, 0.3555	+0.415, <0.0001	+0.781, <0.0001
<b><u>Ella Ø</u></b>								
<b>1</b>	13	+0.016, 0.9588	+0.510, 0.0751	+0.660, 0.0140	+0.640, 0.0189	+0.320, 0.2921	+0.800, 0.0010	+0.870, <0.0001
<b><u>Hegglie Ber</u></b>								
<b>3</b>	1	N.A.†	N.A.†	N.A.†	N.A.†	N.A.†	N.A.†	N.A.†
<b>2</b>	4	-0.530, 0.4709	-0.640, 0.3599	+0.504, 0.4964	+0.370, 0.6335	+0.970, 0.0298	+0.932, 0.0682	+0.970, 0.0339
<b>1</b>	4	-0.212, 0.7878	-0.331, 0.6690	+0.506, 0.4936	-0.300, 0.7010	+0.099, 0.9012	+0.430, 0.5835	+0.820, 0.1834
<b>All</b>	9	-0.467, 0.2054	-0.552, 0.1232	-0.070, 0.8575	-0.503, 0.1680	+0.921, 0.0004	+0.880, 0.0018	+0.983, <0.0001
<b><u>Heintzbjerg</u></b>								
<b>Famennian</b>	27	+0.238, 0.2326	+0.352, 0.0716	+0.478, 0.0116	-0.540, 0.2874	+0.484, 0.0106	*	+0.872, <0.0001
<b>UKW</b>	40	-0.107, 0.5094	-0.194, 0.2304	-0.078, 0.6310	+0.014, 0.9300	-0.200, 0.2167	+0.142, 0.4467	+0.500, 0.0013
<b>Midnatspas</b>	21	-0.440, 0.0457	+0.120, 0.6033	+0.370, 0.0991	-0.220, 0.3376	-0.365, 0.2167	-0.491, 0.0239	+0.805, <0.0001
<b>LKW</b>	17	-0.163, 0.5311	-0.248, 0.3379	-0.380, 0.1374	+0.196, 0.4513	+0.165, 0.5272	*	+0.919, <0.0001
<b>All</b>	105	-0.104, 0.2907	-0.101, 0.3061	+0.025, 0.8000	-0.061, 0.4513	+0.021, 0.8305	+0.270, 0.0566	+0.690, <0.0001

*Note:* Correlations noted as r values (+/-) followed by *P*-value performed for each lake cycle, or significant division within the sample set in the case of Heintzbjerg, as well as for the sequence.

\* *P* accumulation rate could not be calculated for this portion of the sequence.

† N.A. denotes lakes where correlation was not possible due to insufficient data points.

APPENDIX B: PHOSPHORUS ACCUMULATION RATES

	Sed. Rate (cm kyr <sup>-1</sup> )	P Accum. Rate (μmol cm <sup>-2</sup> kyr <sup>-1</sup> )	Notes
Heintzbjerg, Greenland (Famennian)	219-250	393-2,075	Post-UKW landscape stabilization.
Heintzbjerg, Greenland (UKW)	218-239	692-5,700	UKW nutrient pulse (warm/wet, possibly high CO <sub>2</sub> climate). Land plant spread/proliferation.
Heintzbjerg, Greenland (Midnatspas)	14-109	28-532	Stable landscape (arid climate).
Heintzbjerg, Greenland (LKW)	11-206	64-1,540	LKW nutrient pulse (warm/wet climate). Episodic land plant spread/spread in drainage basin.
Anderson Pond, Tennessee, U.S.A. (stabilized landscape)	N/A	100	Mature/stable landscape analogue.
Anderson Pond, Tennessee, U.S.A. (post-glacial retreat)	N/A	3,800	Terrestrial nutrient pulse following plant colonization. Young landscape analogue.
Jackson Pond, Kentucky, U.S.A. (stabilized landscape)	N/A	200	Mature/stable landscape analogue.
Jackson Pond, Kentucky, U.S.A. (post-glacial retreat)	N/A	1,700	Terrestrial nutrient pulse following plant colonization. Young landscape analogue.
Dry Lake, California, U.S.A (stabilized landscape)	N/A	200	Mature/stable landscape analogue.
Dry Lake, California, U.S.A (post- glacial retreat)	N/A	7,000-11,000	Terrestrial nutrient pulse following plant colonization. Young landscape analogue.
St. Lawrence Seaway	200	1,100-8,000	Comparable to Heintzbjerg UKW interval. Likely heavily influenced by detrital nutrient flux. Likely impacted by modern anthropogenic nutrient loading.
North Carolina Margin	60	810-830	Comparable to Heintzbjerg Midnatspas interval. Reflective of generally stable/mature landscape.
Peru Margin	160-360	770-1800	Comparable to Famennian interval. Reflective of generally stable/mature landscape.

Data from Heintzbjerg compared with Holocene and modern analogues with respect to sedimentation rate (where available) and phosphorus accumulation rate. The Heintzbjerg data is divided into four sections: LKW, Midnatspas, UKW and Famennian. The LKW and UKW are considered “young” landscapes (newly colonized by land plants and are analogous to the post-glacial retreat landscapes at Anderson Pond, Jackson Pond and Dry Lake (Filippelli and Souch, 1999). The Midnatspas and Famennian sections are considered stable landscapes and are thus comparable with mature/stable Holocene landscapes at Anderson Pond, Jackson Pond and Dry Lake. St. Lawrence Seaway, North Carolina Margin and Peru Margin (Filippelli, 1997) are modern examples with varying sedimentation rates and phosphorus accumulation rates used to illustrate that the range of Devonian values is not unprecedented in either modern or Holocene analogues.

## CURRICULUM VITAE

### **Matthew Stephen Smart**

#### **Education**

- Ph.D., Applied Earth Sciences with a minor in Geographic Information Systems (GIS), Indiana University degree earned at Indiana University-Purdue University Indianapolis (December 2022)
- B.S., Oceanography (with Honors), earned at the United States Naval Academy (May 2007)

#### **Honors, Awards, Fellowships Research and Training Experience**

- Joint Service Commendation Medal, United States Navy (2020)
- Joint Service Commendation Medal, United States Navy (2019)
- Geological Society of America Graduate Student Research Grant (2018)
- Indiana University Purdue University Indianapolis University Fellow (2015-2016)
- Navy Commendation Medal, United States Navy (2015)
- Honor-Graduate, Basic Oceanography Officer Accession Training, United States Navy (2013)
- Navy Recruiting District Portland Officer Recruiter of the Quarter, United States Navy (2013)
- Rear Admiral Herbert E. Schondland Award for Excellence in Damage Control, United States Navy (2010)

- Professor Emeritus Jerome Williams Oceanography Research Paper Award, United States Naval Academy (2007)

### **Professional Experience**

- Indiana University Purdue University Indianapolis, Department of Earth Sciences Research and Teaching Assistant (2015-2022)
- Meteorology and Oceanography Watch Officer, United States Strategic Command, United States Navy Reserve (2020-2022)
- United States State Department Diplomacy Lab Researcher (2020)
- Geological Society of America Annual Meeting Technical Session Chair (2020)
- Philosophical Transactions of the Royal Society A Referee (2020)
- Meteorology and Oceanography Watch Officer, North American Aerospace Defense Command – United States Northern Command, United States Navy Reserve (2015-2020)
- United States State Department Diplomacy Lab Researcher (2015)
- Meteorology and Oceanography Officer, United States Navy Active Duty (2007-2015)
- Naval Research Laboratory Stennis Space Center Summer Internship (2007)
- Los Alamos National Laboratory Summer Internship (2005)

### **Professional Presentations**

- Smart, M. S., Filippelli, G. M., Gilhooly, W., Vander Pas, B. E., Marshall, J. E. A. & Whiteside, J. H. (2022). Implicating land plant expansion in the Kačák Event:

incorporating nitrogen isotopes in a Devonian lacustrine record. In Astrobiology Science Conference, Atlanta, GA, 2022. AGU.

- Smart, M. S., Filippelli, G. M., Gilhooly, W., Vander Pas, B. E., Marshall, J. E. A. & Whiteside, J. H. (2022). Implicating land plant expansion in the Kačák Event: incorporating nitrogen isotopes in a Devonian lacustrine record. In Geological Society of America North-Central/Southeastern Joint Section meeting. GSA, Cincinnati, OH, 2022.
- Smart, M. S., Filippelli, G. M., Gilhooly III, W., Marshall, J. E. A., & Whiteside, J. H. (2021). A multi-proxy analysis of Devonian lacustrine systems: insights into geochemical cycling and potential global implications. In AGU Fall Meeting, New Orleans, LA, 2021.
- Smart, M.S., Reinhard, C.T., Ozaki, K., Marshall, J. E. A., & Whiteside, J. H., Gilhooly III, W.P., Filippelli, G.M. (2021). Modeling global biosphere response to enhanced riverine nutrient delivery during the Late Devonian Kellwasser Event. In AGU Fall Meeting, New Orleans, LA, 2021.
- Smart, M. S., Filippelli, G. M., Gilhooly III, W., Marshall, J. E. A., & Whiteside, J. H. (2021). A multi-proxy analysis of Devonian lacustrine systems: insights into geochemical cycling and potential global implications. In Midwest Geobiology Conference, 2021.
- Smart, M.S., Reinhard, C.T., Ozaki, K., Marshall, J. E. A., & Whiteside, J. H., Gilhooly III, W.P., Filippelli, G.M. (2021). Modeling global biosphere response to enhanced riverine nutrient delivery during the Late Devonian Kellwasser Event. In Goldschmidt Online, Lyon, France, 2021.

- Smart, M. S., Filippelli, G. M., Gilhooly III, W., Marshall, J. E. A., & Whiteside, J. H. (2021). Tracking Phosphorus Across the Kellwasser Event: A Nutrient Profile from Euramerica. In *Trigger Factors of the Evolution of the Organic World*, Syktyvkar, Russia, 2021.
- Bailey, R.A., Orr, I.S., Rui, L., Smart, M. S., Wood, L.R. & Filippelli, G. M. (2021). Climate Change impacts on the Kavango–Zambezi Transfrontier Conservation Area, Africa. In U.S. State Department Diplomacy Lab, 2021.
- Smart, M., & Marshall, J. E. A. (2020, October). T66. Reconstructing Events of the Late Devonian: Fossil and Rock Record Insights into a Dynamic Biosphere II. In *GSA 2020 Connects Online*. GSA.
- Smart, M. S., Filippelli, G. M., Gilhooly III, W., Marshall, J. E. A., & Whiteside, J. H. (2020). Tracking Phosphorus Across the Kellwasser Event: A Nutrient Profile from Euramerica. In *GSA 2020 Connects Online*, 2020.
- Smart, M. S., Filippelli, G. M., Gilhooly III, W., & Whiteside, J. H. (2019). Decoding Devonian Mass Extinctions: New Evidence Linking Land Plant Expansion to Marine Anoxia. In *AGU Fall Meeting, 2019*, PP54A-07.
- Smart, M. S., Filippelli, G. M., Gilhooly III, W., & Whiteside, J. H. (2019). Decoding Devonian Mass Extinctions: New Evidence Linking Land Plant Expansion to Marine Anoxia. In *GSA Annual Meeting, 2019*.
- Smart, M. S., Filippelli, G. M., Gilhooly III, W., & Whiteside, J. H. (2019). Decoding Devonian Mass Extinctions: New Evidence Linking Land Plant Expansion to Marine Anoxia. In *Midwest Geobiology Conference, 2019*.

- Smart, M. S., Filippelli, G. M., Gilhooly, W., & Whiteside, J. H. (2019, June). The Devonian Plant Revolution: Roots, Weathering and the Impact on Global Biogeochemical Cycling. In 2019 Astrobiology Science Conference. AGU.
- Smart, M. S., Filippelli, G. M., Gilhooly III, W., & Whiteside, J. H. (2018). The Devonian plant revolution: roots, weathering and the impact on global biogeochemical cycling. In AGU Fall Meeting, 2018, EP42A-03.
- Agrios, L., Ahmed, M., Fouskas, F., Goss, S., Holper, K., Perello, M., Phelps, C., Rollings, A., Smart, M. S., & Filippelli, G. M. (2016). Freshwater Security in the Arctic. In U.S. State Department Diplomacy Lab, 2016.

### **Publications**

- Smart, M.S., Filippelli, G.M., Gilhooly III, W.P., Marshall, J.E.A, & Whiteside, J.H. (In press). Enhanced terrestrial nutrient release during the Devonian emergence and expansion of forests: Evidence from lacustrine phosphorus and geochemical records. GSA Bulletin.
- Smart, M.S., Filippelli, G.M., Gilhooly III, W.P., Ozaki, K., Reinhard, C.T., Marshall, J. E. A., & Whiteside, J. H., (Submitted). Land plant evolution and volcanism led to the Late Devonian mass extinction. Communications Earth and Environment.
- Smart, M.S., Filippelli, G.M., Gilhooly III, W.P., Vander Pas, B.E., Marshall, J.E.A, & Whiteside, J.H. (In preparation). Linking land plant expansion to episodic anoxia in a Devonian lake.